PHOTOSENSITIVITY, GRATING STRENGTH AND THERMAL ENDURANCE OF FIBRE BRAGG GRATINGS

DINUSHA SERANDI GUNAWARDENA

INSTITUTE OF GRADUATE STUDIES
UNIVERSITY OF MALAYA
KUALA LUMPUR

2016

PHOTOSENSITIVITY, GRATING STRENGTH AND THERMAL ENDURANCE OF FIBRE BRAGG GRATINGS

DINUSHA SERANDI GUNAWARDENA

THESIS SUBMITTED IN FULFILMENT OF THE REQUIREMENTS FOR THE DEGREE OF DOCTOR OF PHILOSOPHY

INSTITUTE OF GRADUATE STUDIES
UNIVERSITY OF MALAYA
KUALA LUMPUR

2016

UNIVERSITY OF MALAYA

ORIGINAL LITERARY WORK DECLARATION

Name of Candidate: DINUSHA SERANDI GUNAWARDENA

Registration/Matric No: HHE130004

Name of Degree: DOCTOR OF PHILOSOPHY

Title of Thesis: PHOTOSENSITIVITY, GRATING STRENGTH AND THERMAL ENDURANCE OF FIBRE BRAGG GRATINGS

Field of Study: PHOTONICS ENGINEERING

I do solemnly and sincerely declare that:

(1) I am the sole author/writer of this Work;
(2) This Work is original;
(3) Any use of any work in which copyright exists was done by way of fair dealing and for permitted purposes and any excerpt or extract from, or reference to or reproduction of any copyright work has been disclosed expressly and sufficiently and the title of the Work and its authorship have been acknowledged in this Work;
(4) I do not have any actual knowledge nor do I ought reasonably to know that the making of this work constitutes an infringement of any copyright work;
(5) I hereby assign all and every rights in the copyright to this Work to the University of Malaya ("UM"), who henceforth shall be owner of the copyright in this Work and that any reproduction or use in any form or by any means whatsoever is prohibited without the written consent of UM having been first had and obtained;
(6) I am fully aware that if in the course of making this Work I have infringed any copyright whether intentionally or otherwise, I may be subject to legal action or any other action as may be determined by UM.

Candidate's Signature Date:

Subscribed and solemnly declared before,

Witness's Signature Date:

Name:

Designation:

ABSTRACT

Fibre Bragg gratings (FBGs) are wavelength selective fibre structures composed of periodic refractive index changes which occur in the fibre core due to high intensity UV irradiation. FBGs are considered to be the backbone of optical fibre technology. Thus, the main goal of this thesis is to conduct a comprehensive investigation on the photosensitivity, the grating strength and the thermal endurance of fibre Bragg gratings.

This thesis elaborates on the photosensitivity and thermal properties of a new type of optical fibre known as gallosilicate fibre. Gallosilicate fibre provides enhanced photosensitivity compared to the widely used germanosilicate fibre when exposed to 193 nm ArF excimer laser at low UV fluence levels. In addition, these fibres consisting of a single dopant with a concentration as a low as 5 wt%, possess high temperature grating regeneration characteristics, thereby making them potential candidates for high temperature resistant gratings.

One of the prime intentions of this thesis is to propose a mathematical model in order to explain the formation of the grating structure in photosensitive germanosilicate fibres by using a combination of KrF excimer laser and phase-mask. The growth characteristics of these two local refractive index changes are compared and represented by a single characteristic function. Since grating and interference visibilities are the two key parameters which influence the grating strength of an FBG, a new measurement technique is introduced to estimate the interference visibility. Another technique, which is based on the bent-spectral analysis method is also proposed for precise determination of the grating visibility of an FBG. The grating visibility is estimated with the aid of a simple mathematical expression by varying “ac” and “dc” coupling coefficients at different bending radii. The effect of the decreasing bending radius on the Bragg Transmission Depth (BTD), and both the “ac” and “dc” coupling coefficients are thoroughly explored.

Moreover, the influence of the degradation of coupling coefficients on the centre wavelength shift is investigated. The accuracy of the model proposed is verified with experimental results.

The main contribution of this thesis is the investigation of thermally induced reversible effect present in gratings inscribed in PS 1250/1500 fibre. The grating strength of a grating with prolonged thermal endurance is characterised over a time period of a thousand years over a temperature range of 200 °C to 400 °C. A noteworthy increment in the grating reflectivity is observed during annealing at 425 °C, deviating from the general thermal decay behaviour of an FBG. A comprehensive investigation is carried out on both stepwise and continuous annealing procedures which indicate a similar trend in the accelerated ageing characteristics when analysed with respect to the demarcation energy (E_d) domain. Finally, the salient features of alteration in the temperature ramping rates, on the grating strength is analysed in detail by performing thermal annealing procedures on three different types of Bragg gratings where a comparative exploration is carried out.

ABSTRAK

Parutan Fibre Bragg (FBGs) iahlah struktur serat panjang gelombang terpilih di mana teras gentiannya mempunyai indeks biasan berkala yang dihasilkan dengan penyinaran UV berintensiti tinggi. FBGs dianggap sebagai tulang belakang kepada teknologi gentian optik. Oleh itu, matlamat utama tesis ini adalah untuk menjalankan siasatan menyeluruh mengenai kefotopekaan, kekuatan parutan dan ketahanan haba parutan serat Bragg.

Tesis ini menghuraikan kefotopekaan dan sifat haba jenis serat optik baru yang dikenali sebagai gentian gallosilikat. Gentian gallosilikat menunjukkan peningkatan dalam kefotopekaan berbanding gentian germanosilika yang lebih umum digunakan apabila terdedah kepada 193 nm excimer laser ArF pada tahap fluence UV yang rendah. Di samping itu, gentian ini mempunyai pendopan tunggal dengan kepekatan serendah 5wt% dan mempunyai suhu pertumbuhan semula yang tinggi. Ciri-ciri itu menjadikan mereka calon-calon yang berpotensi untuk parutan tahan suhu tinggi.

Salah satu tujuan utama karya ini adalah untuk mencadangkan satu model matematik untuk menerangkan pembentukan struktur parutan dalam gentian germanosilikat fotopeka dengan menggunakan gabungan KrF excimer laser dan mask-fasa. Ciri-ciri pertumbuhan kedua-dua perubahan indeks biasan tempatan dibandingkan dan diwakili oleh satu fungsi cirian. Oleh sebab parutan dan *visibility* interferens adalah dua parameter utama yang mempengaruhi kekuatan parutan FBG, teknik pengukuran baru untuk menganggarkan jarak penglihatan gangguan diperkenalkan. Satu lagi teknik pengukuran, yang berasaskan kaedah analisis bengkok spektrum juga dicadangkan untuk penentuan tepat penglihatan parutan FBG. *Visibility* parutan dianggarkan dengan bantuan ungkapan matematik yang mudah dengan mengubah “ac” dan “dc” pekali gandingan pada jejari lenturan yang berbeza. Kesan radius lenturan yang semakin berkurangan pada *Bragg Transmission Depth* (BTD), dan kedua-dua “ac” dan “dc” pekali gandingan diterokai

dengan teliti. Selain itu, pengaruh degradasi pekali gandingan pada peralihan pusat panjang gelombang disiasat. Ketepatan model yang dicadangkan itu telah disahkan dengan keputusan eksperimen.

Sumbangan utama tesis ini adalah penyiasatan haba kesan berbalik disebabkan di dalam parutan tertulis pada PS 1250/1500 serat. Ciri-ciri kekuatan parutan parutan dengan ketahanan haba yang dilanjutkan sepanjang tempoh masa seribu tahun pada suhu di antara 200 °C hingga 400 °C juga dicirikan. Satu perubahan ketara dalam kenaikan pemantulan parutan semasa penyepuhlindapan pada suhu 425 °C adalah diperhatikan menyeleweng daripada ciri-ciri umum pereputan haba FBG. Satu penyiasatan secara menyeluruh dengan kedua-dua prosedur penyepuhlindapan iaitu cara langkah demi langkah dan cara berterusan telah dijalankan, keputusan mereka menunjukkan trend yang sama dalam ciri-ciri penuaan dipercepatkan apabila dianalisis berkenaan dengan domain tenaga penandaan (E_d). Akhir sekali, ciri-ciri utama perubahan dalam suhu yang ramping kadar, kekuatan parutan dianalisis secara terperinci dengan menjalankan prosedur penyepuhlindapan terma ke atas tiga jenis parutan Bragg di mana penerokaan perbandingan dijalankan.

ACKNOWLEDGEMENTS

First and foremost, I would like to express my sincere gratitude to my supervisor Dr. Kok-Sing Lim for all his advices and for being a great source of guidance throughout my Ph.D. studies. It has been a great pleasure to be his Ph.D. student. His perseverance, enthusiasm and passion for research are truly inspirational. Also, I would like to extend my gratitude and appreciation to Distinguished Professor Harith Ahmad for his continuous assistance and remarkable skill of supervision. Being a part of his research group was an absolute honour. Special thanks to my external supervisor Professor Amin Malekmohammadi for his tireless support in refining and improving my research articles.

Furthermore, I acknowledge the dean and deputy dean of the Institute of Graduate studies for their strategic direction in maintaining research excellence. I am ever grateful to my colleagues, collaborators and members of the Photonics Research Centre who have helped me in many ways throughout these years. Special thanks to Man-Hong Lai for all the fruitful discussions and always sharing his outstanding physical intuition. My deepest gratitude to Yen-Sian Lee for his amazing attitude and kind support in numerous ways in the laboratory. I gratefully acknowledge the Bright Sparks Unit, Photonics Research Centre, IGS and University of Malaya for the financial support, excellent research facilities and the peaceful research atmosphere.

My sincere appreciation to my best friend, Ayeshath Iqbal for her incredible amount of patience, for always lending a listening ear throughout these years and for her tremendous moral support whenever I faced any difficulty. Finally, my heartfelt gratitude goes to my parents, Gamini and Chitrangani Gunawardena and my sister, Neranja Upeshika Gunawardena for their unconditional love, countless advices and continuous encouragement in achieving my goals. Their blessings will always be a valuable asset to me in my life.

May the force be with all of you!

TABLE OF CONTENTS

LIST OF FIGURES

LIST OF TABLES

LIST OF SYMBOLS AND ABBREVIATIONS

ASE	:	Amplified Spontaneous Emission
BTD	:	Bragg Transmission Depth
CCG	:	Chemical Composition Grating
CW	:	Continuous Wave
DBR	:	Distributed Bragg Reflector
EDFA	:	Erbium Doped Fibre Amplifier
FBG	:	Fibre Bragg Grating
GODC	:	Germanium-Oxygen Defficiency Centre
ICC	:	Integrated Coupling Coefficient
LPG	:	Long Period Grating
MCVD	:	Modified Chemical Vapour Deposition
NA	:	Numerical Aperture
NBOHC	:	Non-Bridging Oxygen Hole Centres
NICC	:	Normalised Integrated Coupling Coefficient
NODV	:	Neutral Oxygen Di-vacancy
NOMV	:	Neutral Oxygen Monovacancy
OSA	:	Optical Spectrum Analyser
PS	:	Photosensitive
RFBG	:	Regenerated Fibre Bragg Grating
SG	:	Seed Grating
SMF	:	Single Mode Fibre
TFBG	:	Tilted Fibre Bragg Grating
UV	:	Ultra Violet
WDM	:	Wavelength Division Multiplexing

LIST OF APPENDICES

Appendix A:

CHAPTER 1: INTRODUCTION

This section intends to provide a general understanding about fibre Bragg gratings (FBGs) to the readers who are less familiar with their structure, functionality and the significance of photosensitivity, grating strength and thermal endurance of Bragg gratings. It also emphasises the motivation behind the research conducted and presented in this thesis. Furthermore, research objectives and the series of events leading to the evolution of the thesis are outlined as well.

1.1 Background

The increased demand for communication capacity over the past three decades has brought fibre optics into the limelight. One of the prime elements among both active and passive components for optical communication are the fibre Bragg gratings. FBGs have acquired prodigious technological advancements in terms of fabrication techniques, fibre photosensitivity, grating structures and thermal endurance. Emerging as a strong competitor for conventional electrical and electronic sensors, FBGs inherit immense benefits including immunity to electro-magnetic interference, low fabrication cost, high sensitivity and multiplexing capabilities (Kersey et al., 1997). These properties have led to the wide use of FBGs particularly in the telecommunication and sensing industries.

FBGs are wavelength selective elements. Numerous FBG based components, tailored to meet the stringent regulations of telecommunication systems exist. Among them, fibre lasers, loss filters for gain equalisation, dispersion compensators, narrow band reflectors for wavelength-division-multiplexing (WDM) and add-drop filters all of which play a significant role (Kashyap, 1999). FBGs suitable for operations at temperatures well above the standard telecommunication conditions are crucial in the development of fibre based temperature sensors. Hence, the thermal characteristics of FBGs have been comprehensively investigated in many research studies (Chen & Herman, 2003; Erdogan, Mizrahi, Lemaire, & Monroe, 1994).

Bragg gratings are axially variable refractive index structures inscribed in the core of an optical fibre through the usage of intense periodic ultraviolet irradiation. Photosensitive dopants in the preform and hence the drawn fibres are the key factors responsible for the formation of the grating structure by means of UV-induced index change. The photosensitive response of an optical fibre may significantly vary based on the type of dopant, prior treatment of the fibre, UV irradiation wavelength, UV laser intensity and several other factors. Furthermore, implementation of effective grating characterisation techniques at an early stage of research study is useful in obtaining accurate measurements of the grating structure which also reflects on the stability and repeatability of experimental procedures.

The type of the grating and the process of refractive index modification are vital when employing FBGs as temperature sensors for high temperature applications. Different approaches, for instance, tailoring the glass composition to improve the temperature resistivity (Butov, Dianov, & Golant, 2006), process of hyper-sensitisation (Åslund & Canning, 2000) and formation of type II and type IIa gratings using femtosecond lasers (Archambault, Reekie, & Russell, 1993a; Groothoff & Canning, 2004) have been used to accommodate FBGs in high temperature environments. In the recent years, a new type of thermal resistant grating referred to as a regenerated fibre Bragg grating (RFBG) has been reported (Bandyopadhyay, Canning, Stevenson, & Cook, 2008). Such gratings have proven to be stable and robust for operations under extreme temperature conditions. Prediction of grating life time is another important criteria which provides information about the durability of a specific grating. This is useful when employing them in fibre based devices for efficient functioning in the long run.

1.2 Motivation

A number of dopants have been used in optical fibres over the past few decades for photosensitivity enhancement and efficient fabrication of FBGs. Nevertheless, it is prudent to explore alternative materials to enhance fibre photosensitivity in terms of simple fabrication with the incorporation of low dopant concentration and a single absorption band that is compatible with the irradiation wavelength and photosensitive to low UV fluence levels. In addition, grating and interference visibilities are two important parameters which have a direct influence on the grating strength. The grating strength and reflectivity of a particular FBG rely on the "ac" coupling coefficient, which is associated with the grating visibility (Erdogan, 1997). Despite the high UV fluence applied in the grating inscription process, the growth of grating reflectivity may be rather slow due to the poor interference visibility (Huebner, Svalgaard, Gruener-Nielsen, & Kristensen, 1997). Thus, it would be beneficial to acquire details about the interference and grating visibilities of a particular FBG, as it would provide accurate information about the grating strength of the fibre.

The other factor that also motivated this research study was the need to provide the visibility values for the users who employ commercial FBGs in various applications. Awareness about these details allow optimisation of the grating inscription system, resulting in the acquisition of efficient and quality FBGs with enhancing photosensitivity capabilities. Moreover, it prevents excessive UV irradiation which would weaken the fibre glass strength.

Many of the research studies often focus on RFBGs fabricated in Germanium-doped (Ge) optical fibres, whereas only a few have revealed the existence of RFBGs in non-Ge-doped optical fibres (Yang, Qiao, Das, & Paul, 2014). Hence, these RFBGs are attracting the attention of the research community. Thus, the development of optical fibres with new glass compositions which consist of a single dopant with high photosensitivity characteristics together with high temperature sustainability is essential and provides the opportunity to be used as alternatives to the existing RFBGs.

In a RFBG, the low reflectivity and the complete erasure of the seed grating are considered as draw-backs when obtaining detailed information about the grating. Besides, it is imperative to explore new types of enduring gratings with minimum decay in the grating reflectivity and consisting of extended lifetimes which are produced by thermal annealing at a temperature below the transition temperature of the glass, T_g.

1.3 Research Objectives

1. To investigate the photosensitivity of Gallium (Ga) doped optical fibres and the thermal stability of Bragg gratings inscribed in them at elevated temperatures.
2. To study and analyse the grating and interference visibilities of a fibre Bragg grating with increasing UV fluence through the development of a mathematical model and to investigate the influence of them on the spectral properties and grating strength of the FBG.
3. To demonstrate and characterise the grating strength of a thermal enduring grating fabricated based on the thermally induced reversible effect.

1.4 Evolution of the thesis

The research contribution of this thesis is divided into 6 chapters.

Chapter 1 is a short introduction to the thesis which includes a brief background about the significance of FBGs, motivation which led to the investigations carried out in this research study, research objectives and evolution of the thesis.

Chapter 2 focuses on fundamentals and theoretical concepts of FBGs with particular emphasis on coupled-mode theory. In addition, a general classification of different types of grating structures and inscription techniques are outlined as well.

Chapter 3 is an overview of the fibre photosensitivity which describes the photosensitivity mechanisms, currently existing techniques for photosensitivity enhancement and material considerations for the fabrication of photosensitive fibres. Gallium (Ga) is suggested as a new photosensitive dopant and the role of Ga-doped optical fibre during grating inscription is demonstrated. The curve-matching technique and bent-spectral analysis technique are proposed in this chapter for characterisation of the grating strength in terms of interference and grating visibilities.

Chapter 4 is a discussion on the thermal stability and decay characteristics of FBGs. A brief description about various decay models and methods to increase the thermal stability of Bragg gratings is provided. The regeneration characteristics of Ga-doped fibre suitable to withstand high temperature environments are explored and illustrated.

Chapter 5 describes the thermally induced reversible effect focusing on the fabrication of thermal enduring gratings and the prediction of their lifetimes. The grating decay is characterised in the demarcation energy domain. In addition, the effect of different temperature ramping rates during thermal annealing on grating decay is included.

Chapter 6 concludes the thesis with a discussion of different possible applications and implications of the research results presented with possible suggestions for future work based on the research findings of this thesis.

CHAPTER 2: THEORETICAL LITERATURE OF FIBRE BRAGG GRATINGS

This chapter is dedicated to the theory of fibre Bragg gratings (FBGs). Some of the salient features of different types of Bragg gratings, which depend on their various refractive index modulation profiles, are demonstrated. Particularly, a numerical expression for reflectivity is shown as a function of wavelength for Bragg gratings with the use of coupled-mode equations. This chapter also intends to provide a general understanding of the various fabrication techniques involved in grating inscription with specific emphasis on the phase-mask technique.

2.1 Maxwell's Equations

Electromagnetic theory of optics initiates with the introduction of Maxwell's equations. It forms an entire theory of optical propagation phenomena, which explains many known observations on light propagation. The Maxwell's equations which describe the electromagnetic field state:

$$\nabla \times \vec{E} = -\frac{\partial \vec{B}}{\partial t} \tag{2.1}$$

$$\nabla \times \vec{H} = \frac{\partial \vec{D}}{\partial t} + J \tag{2.2}$$

$$\nabla \cdot \vec{D} = \rho \tag{2.3}$$

$$\nabla \cdot \vec{B} = 0 \tag{2.4}$$

where $\vec{E}$, $\vec{H}$ are the electric and magnetic field vectors respectively, $\vec{D}$ and $\vec{B}$ are the electric and magnetic flux densities. J and ρ represent the displacement current and the volume charge density respectively. In the dielectric media of the optical fibre in the absence of free charges, the latter two parameters are null:

$$\begin{cases} J = 0 \\ \rho = 0 \end{cases} \tag{2.5}$$

Through constitutive relations, flux densities and field vectors are correlated.

$$\vec{D} = \varepsilon_0 \vec{E} + \vec{P} \quad (2.6)$$

$$\vec{B} = \mu_0 \vec{H} + \vec{M} \quad (2.7)$$

where $\vec{P}$ and $\vec{M}$ denote the induced electric and magnetic polarizations and ε_0 and μ_0 are scalar quantities representing the permittivity and permeability of free space. Since optical fibres are non-magnetic materials, $\vec{M}$ = 0. Assuming the dielectric media of the fibre is linear, such that

$$\vec{P} = \varepsilon_0 \chi \vec{E} \quad (2.8)$$

where χ denotes the linear susceptibility of the media. This in turn leads to the relation between $\vec{D}$ and $\vec{E}$:

$$\vec{D} = \varepsilon_0 \varepsilon \vec{E} \quad (2.9)$$

where ε = (1+ χ) describes the relative permittivity of the media associated with the refractive index *n* by

$$\varepsilon = n^2 \quad (2.10)$$

2.2 Fibre Bragg gratings

A fibre Bragg grating is composed of a periodic refractive index change localised at the core of the fibre, formed through exposure to intense ultraviolet light. A primary great use of FBGs are their ability for wavelength-selective reflection. When light from a broadband source is coupled into a fibre consisting of an FBG, light with matching wavelengths to the Bragg condition is reflected permitting the rest to transmit along the fibre as shown in Figure 2.1.

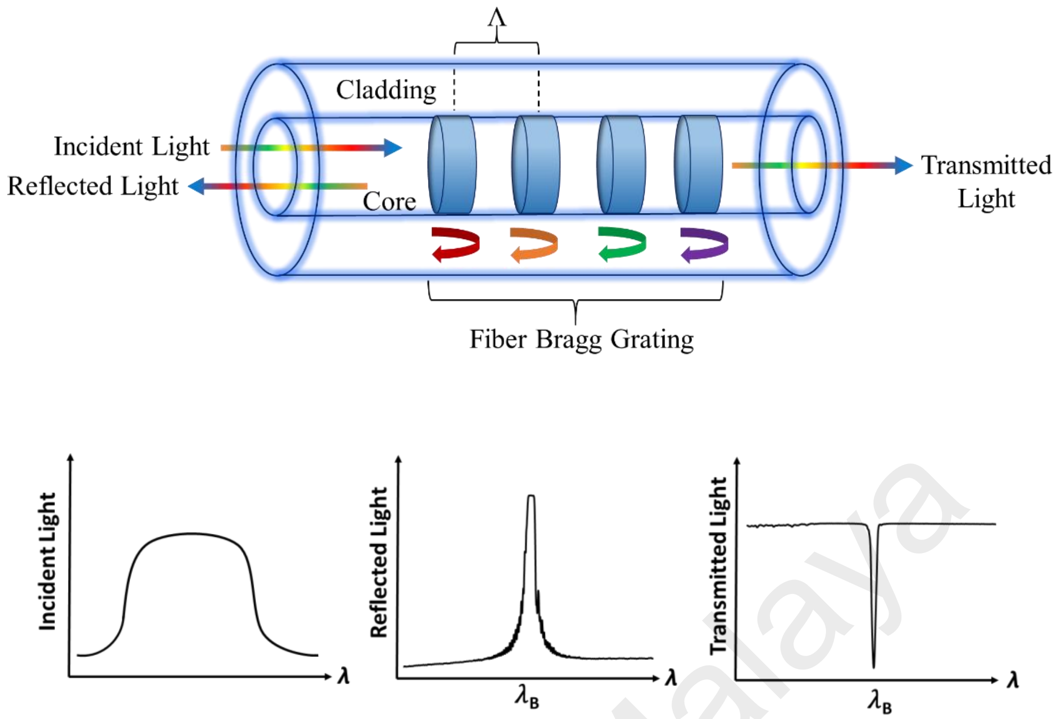

Figure 2.1: Spectral response of fibre Bragg gratings

The perturbation to the effective refractive index, of the guided mode in an optical fibre is given by (Erdogan, 1997)

$$\delta n_{eff}(z) = \overline{\delta n_{eff}}(z)\{1 + \upsilon \cos[\frac{2\pi}{\Lambda} z + \phi(z)]\} \tag{2.11}$$

where $\overline{\delta n_{eff}}$ denotes the "dc" index change which is averaged spatially over the grating period, υ is fringe visibility (also known as grating visibility, v_g) of the index change, Λ the nominal period and $\phi(z)$ denotes the spatially varying phase of the grating along the longitudinal axis of the fibre. The Gaussian index modulation depth may vary along the length of the FBG leading to the formation of an apodised grating. In the scenario where the fibre consists of a step-index profile, an induced index change is formed uniformly across the fibre core. The typical spectral response of a 20 mm long uniform FBG is shown in Figure 2.2 below.

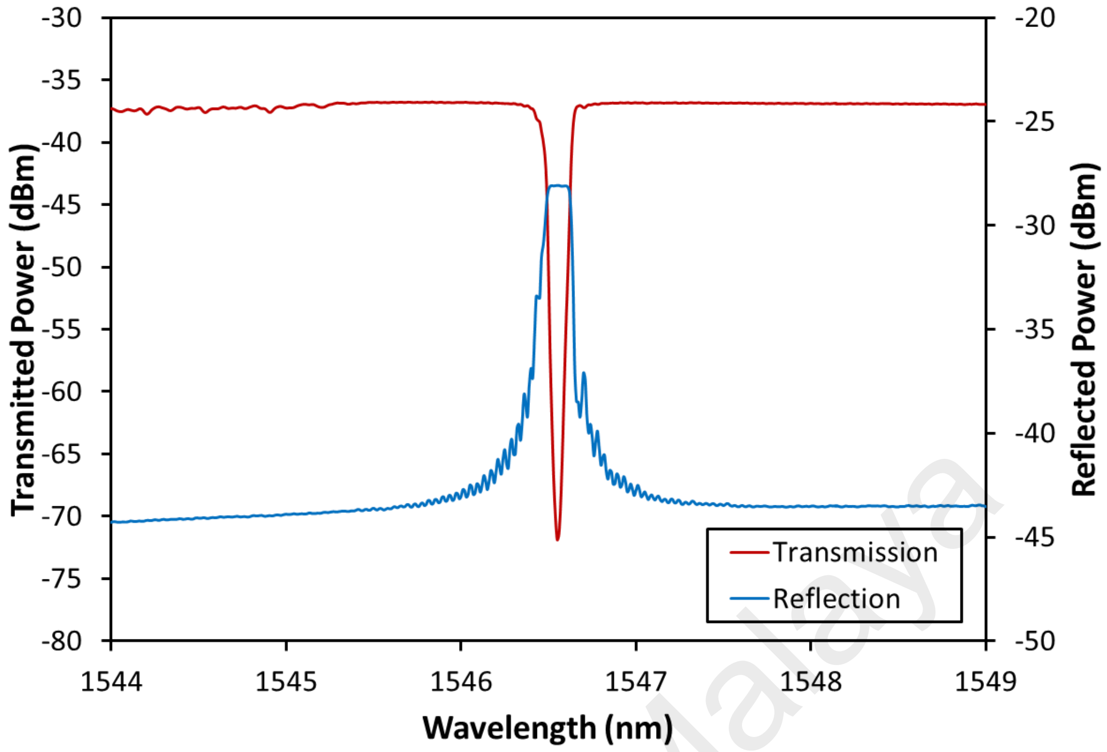

Figure 2.2: Spectral response of a 20 mm long uniform FBG.

2.2.1 Resonant wavelength for grating diffraction

A Bragg grating is an optical diffraction element and its effect on a light wave incident on the grating at an angle θ_1 is represented as

$$n\sin\theta_2 = n\sin\theta_1 + m\frac{\lambda}{\Lambda} \tag{2.12}$$

where θ_2 refers to the angle of the diffracted wave and integer, m the diffraction order (see Figure 2.3).

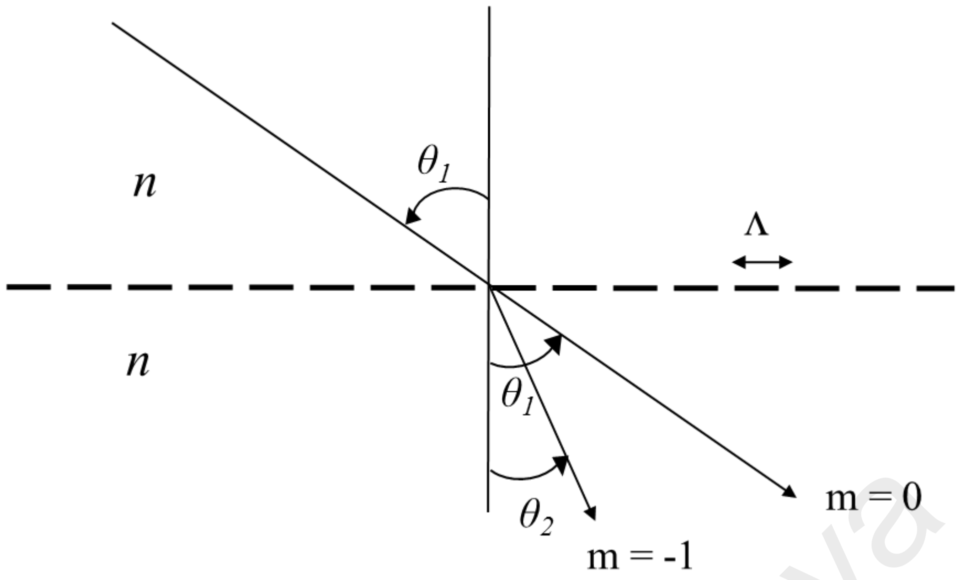

Figure 2.3: Diffraction of a light wave by a grating (Erdogan, 1997).

This equation is only able to anticipate the directions defined by θ_2 where constructive interference is present. It also provides sufficient information in deducing the wavelength where a fibre grating couples light between two modes efficiently.

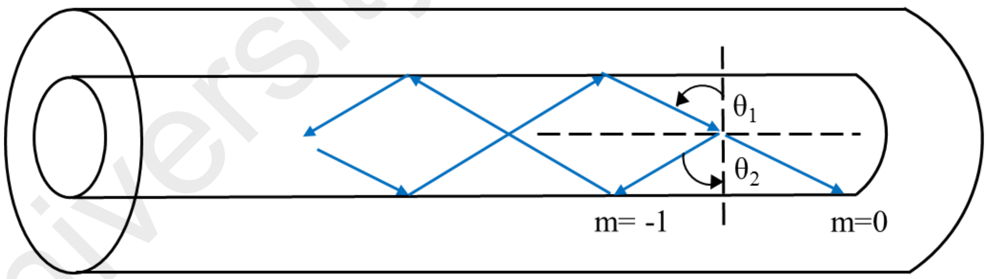

Figure 2.4: Ray-optic illustration of reflection by an FBG (Erdogan, 1997).

The reflection in an FBG is the result of mode coupling between two counter-propagating guided modes in the grating. Figure 2.4 illustrates reflection of a mode with a bounce angle of θ_1 towards the same mode travelling in the reverse direction with a bounce angle of $\theta_2 = -\theta_1$. Since the mode propagation constant β is described as $\beta = (2\pi/\lambda)\ n_{eff}$ where $n_{eff} = n\sin\theta$, Eq. (2.12) can be re-written for the guided mode as

$$\beta_2 = \beta_1 + m\frac{2\pi}{\Lambda} \tag{2.13}$$

In the dominant first order diffraction of a Bragg grating, m = -1. From Eq. (2.13) and through recognition of $\beta_2 < 0$ (negative values indicate modes that propagate in $-z^{th}$ direction) the resonant wavelength for reflection from a mode of index $n_{eff,1}$ into a mode of index $n_{eff,2}$ is represented as

$$\lambda = (n_{eff,1} + n_{eff,2})\Lambda \tag{2.14}$$

In the scenario where the two modes are identical, the resonance condition is achieved at a specific wavelength referred to as the Bragg reflection wavelength and is given by

$$\lambda_B = 2n_{eff}\Lambda \tag{2.15}$$

2.2.2 Coupled-mode theory

Coupled-mode theory is an intuitive model which is often incorporated in the precise modelling of the optical properties of most gratings and other optical fibre components and systems. In the case of an FBG it describes the interaction between modes in the presence of a refractive index perturbation which varies capriciously along the fibre axis. The derivations of coupled-mode equations are discussed in various articles and texts (Erdogan, 1997; Kogelnik & Shank, 1972; Yariv, 1973). It is possible to represent the transverse component of the electric field as a superposition of the ideal modes according to the ideal-mode estimation to coupled-mode theory. They are denoted as j which are also the modes in an ideal waveguide without any grating perturbation. Therefore,

$$\vec{E}_t(x,y,z,t) = \sum_j [A_j(z)\exp(i\beta_j z) + B_j(z)\exp(-i\beta_j z)].\,\vec{e}_{jt}(x,y)\exp(-i\omega t) \tag{2.16}$$

where $A_j(z)$ and $B_j(z)$ denote the respective amplitudes of the j th mode propagating in the $+z$ and $-z$ directions while being subjected to slow variation. The transverse mode fields $\vec{e}_{jt}(x,y)$ explain cladding modes. The modes are orthogonal in an ideal waveguide and therefore, energy exchange does not take place. Hence, the dielectric perturbation causes the modes to be coupled where the amplitudes A_j and B_j of mode j evolve along z axis based on

$$\begin{aligned}\frac{dA_j}{dz} &= i\sum_k A_k(K^t_{kj}+K^z_{kj})\exp[i(\beta_k-\beta_j)z] \\ &+ i\sum_k B_k(K^t_{kj}-K^z_{kj})\exp[-i(\beta_k+\beta_j)z]\end{aligned} \tag{2.17}$$

$$\begin{aligned}\frac{dB_j}{dz} &= -i\sum_k A_k(K^t_{kj}-K^z_{kj})\exp[i(\beta_k+\beta_j)z] \\ &- i\sum_k B_k(K^t_{kj}+K^z_{kj})\exp[-i(\beta_k-\beta_j)z]\end{aligned} \tag{2.18}$$

K^t_{kj} is the transverse coupling coefficient between the modes j and k in Eq. (2.17) and Eq. (2.18). It is given by

$$K^t_{kj}(z) = \frac{\omega}{4}\iint_{\infty} dx\,dy\;\Delta\varepsilon(x,y,z)\,\vec{e}_{kt}(x,y)\,.\,\vec{e}^{\,*}_{jt}(x,y) \tag{2.19}$$

where $\Delta\varepsilon$ is the perturbation to the permittivity and is approximately expressed as $\Delta\varepsilon \approx 2n\delta n$ when $\delta n < n$. The longitudinal coefficient $K^z_{kj}(z)$ is analogous to $K^t_{kj}(z)$. However, this coefficient is generally omitted since usually for fibre modes $K^z_{kj}(z) \ll K^t_{kj}(z)$.

The induced index change of gratings is uniform across the fibre core and is absent outside the core. Therefore, the core index change can be described by $\overline{\delta n}_{co}(z)$. The definition of the two new coefficients is

$$\sigma_{kj}(z) = \frac{\omega n_{co}}{2}\overline{\delta n}_{co}(z)\iint_{core} dx\,dy\,\vec{e}_{kt}(x,y).\vec{e}^{\,*}_{jt}(x,y) \tag{2.20}$$

$$\kappa_{kj}(z) = \frac{\upsilon}{2}\sigma_{kj}(z) \tag{2.21}$$

where σ is the "dc" coupling coefficient and κ is the "ac" coupling coefficient which results in a general coupling coefficient of

$$K_{kj}^{t}(z) = \sigma_{kj}(z) + 2\kappa_{kj}(z)\cos\left[\frac{2\pi}{\Lambda}z + \phi(z)\right] \tag{2.22}$$

In the case of FBGs, the dominant interaction is considered to be the reflection of a mode of amplitude $A(z)$ into an identical counter-propagating mode consisting of an amplitude $B(z)$. Eq. (2.17) and Eq. (2.18) can be further simplified by keeping the terms which include amplitudes of the specific mode and then carrying out synchronus approximation. Eq. (2.18) requires the negligence of terms on the right-hand side of the differential equations since these terms have minimal contribution towards the growth and decay of amplitudes and are dependent on the rapidly oscilating z. The resultant equations are

$$\frac{dR}{dz} = i\hat{\sigma}R(z) + i\kappa S(z) \tag{2.23}$$

$$\frac{dS}{dz} = -i\hat{\sigma}S(z) - i\kappa^{*}R(z) \tag{2.24}$$

where the amplitudes R and S denote $R(z) \equiv A(z)\exp(i\delta z - \phi/2)$ and $S(z) \equiv B(z)\exp(-i\delta z + \phi/2)$. "$\kappa$" refers to the "ac" coupling coefficient defined in Eq. (2.21) and $\hat{\sigma}$ is the general "dc" self-coupling coefficient expressed as

$$\hat{\sigma} = \delta + \sigma - \frac{1}{2}\frac{d\phi}{dz} \tag{2.25}$$

The detuning δ, independent of z for all gratings is given by

$$\begin{aligned}\delta &= \beta - \frac{\pi}{\Lambda} \\ &= \beta - \beta_D \\ &= 2\pi n_{eff}\left(\frac{1}{\lambda} - \frac{1}{\lambda_D}\right)\end{aligned} \tag{2.26}$$

where $\lambda_D \equiv 2n_{eff}\Lambda$ is the design wavelength for a weak grating ($\delta n_{eff} \rightarrow 0$) consisting of a grating period, Λ. When $\delta = 0$, the Bragg condition is met $\lambda = 2n_{eff}\Lambda$. The "dc" coupling coefficient is introduced in Eq. (2.20). The derivative $(1/2)d\phi/dz$ explains the chirp of the grating period and $\phi(z)$ is defined through Eq. (2.11) and Eq. (2.22). An FBG inscribed in single-mode fibre can be described using the relations below:

$$\sigma = \frac{2\pi}{\lambda}\overline{\delta n_{eff}} \tag{2.27}$$

$$\begin{aligned}\kappa &= \kappa^* \\ &= \frac{\pi}{\lambda}\upsilon\overline{\delta n_{eff}}\end{aligned} \tag{2.28}$$

For a grating which is uniform along the z axis, $\overline{\delta n_{eff}}$ is a constant and $d\phi/dz = 0$, and therefore, κ, σ and $\hat{\sigma}$ are also constants. Hence, Eq. (2.23) and (2.24) are referred to as coupled first-order differential equations which contain constant coefficients. The reflectivity of a uniform FBG with length L can be analytically calculated through the assumption of a forward propagating wave incident from $z = -\infty$ [eg: $R(-L/2) = 1$] with the absence of a backward propagating wave for $z \geq L/2$ which is $S(L/2) = 0$. The amplitude and power reflection coefficients are $\rho = S(-L/2)/R(-L/2)$ and $r = |\rho|^2$ respectively, and can be expressed as

$$\rho = \frac{-\kappa\sinh(\sqrt{\kappa^2-\hat{\sigma}^2}L)}{\hat{\sigma}\sinh(\sqrt{\kappa^2-\hat{\sigma}^2}L) + i\sqrt{\kappa^2-\hat{\sigma}^2}\cosh(\sqrt{\kappa^2-\hat{\sigma}^2}L)} \tag{2.29}$$

and

$$r = \frac{\sinh^2(\sqrt{\kappa^2-\hat{\sigma}^2}L)}{\cosh^2(\sqrt{\kappa^2-\hat{\sigma}^2}L) - \dfrac{\hat{\sigma}^2}{\kappa^2}} \tag{2.30}$$

The normalised wavelength is

$$\frac{\lambda}{\lambda_{\max}} = \frac{1}{1+\dfrac{\hat{\sigma}L}{\pi N}} \tag{2.31}$$

where N represents the total amount of grating periods such that $N=L/\Lambda$ and based on the experiment conducted by Erdogan (1997), N = 10000. $\lambda_{\max}$ is the corresponding wavelength at which point the maximum reflectivity occurs. Depending on larger or smaller N, the reflection spectrum would result in a narrower or broader bandwidth respectively, for a specific value of κL.

According to Eq. (2.30), the maximum reflectivity of an FBG is denoted as

$$r_{\max} = \tanh^2(\kappa L) \tag{2.32}$$

which takes place at the wavelength,

$$\lambda_{\max} = (1 + \frac{\overline{\delta n_{eff}}}{n_{eff}})\lambda_D \tag{2.33}$$

or when σ = 0.

2.2.3 Apodisation of FBGs

The reflection spectrum of an FBG consisting of a specific length with uniform Δn_{mod} is accompanied by a series of side lobes at the adjacent wavelengths. Suppression of the reflectivity of these side lobes, (or apodisation of the reflection spectrum) is important in devices where high rejection of the non-resonant light is required (Othonos, 1997). Matsuhara and Hill (1974) have proposed that slow variation of the coupling coefficient along the length of the coupling area can be useful in designing band-rejection filters containing diminished side lobes. They exist due to the variation in the effective refractive index as a result of the induced perturbation during UV irradiation. Apodised gratings are helpful in defining the channels through which transmission of information occurs in optical communication. In WDM systems, side lobes may contribute towards crosstalk between channels. Suppression of these side lobes can be achieved by tailoring the refractive index change along the grating. Various methods have been used in FBG apodisation including the amplitude mask technique (Albert, Hill, Johnson, Bilodeau, & Rooks, 1996), variable diffraction efficiency phase-mask technique (Albert et al., 1995), intrinsic apodisation using UV pulse interferometry (Cortes, Ouellette, & LaRochelle, 1998), moving fibre/phase-mask-scanning beam technique (Cole, Loh, Laming, Zervas, & Barcelos, 1995) and multiple printing of in-fibre gratings (Storøy, Engan, Sahlgren, & Stubbe, 1997). Cole et al. (1995) has demonstrated that grating apodisation can also be obtained by applying dither to the fibre. Furthermore, the study by Stephens et al. (1996) indicates that dithering the phase-mask is a much more relaible procedure compared to that of the fibre and leads to an enhanced mechanical stability of the grating inscription system. This method also allows the addition of a phase shift to the grating.

2.3 Types of fibre Bragg gratings

Several distinct types of FBGs exist and have been widely explored in the literature. The forthcoming sections provide a brief overview on the various structures of Bragg gratings together with some of their applications based on their coupling and growth characteristics during grating inscription. The common Bragg reflector, long period gratings, tilted gratings, chirped gratings, phase-shifted gratings, type I, type II and type IIa gratings are some of them. Furthermore, the photosensitivity and thermal stability characteristics of some of these gratings are discussed in Chapter 3, 4 and 5.

2.3.1 Common Bragg Reflector

The first intra-core fibre grating written with the aid of a “self-induced” writing technique is referred to as the common Bragg reflector (Othonos, 1997). A Bragg reflector can operate as a narrow-band transmission or reflection filter or as a broadband mirror based on other parameters such as grating length and the extent of the induced index change. When combined with other Bragg reflectors, they can be used as bandpass filters.

Bragg reflectors are considered to be outstanding candidates for strain and temperature sensing devices due to their wavelength encoded detection which eliminates problems caused by the fluctuations in the amplitude or intensity in other fibre sensors. As a result of the specific wavelength-encoded signature, a sequence of Bragg reflectors can be inscribed in the same fibre where each of them exhibit a separate Bragg resonance signal (Othonos, 1997). This arrangement is useful in wavelength division multiplexing or quasi distributed sensing applications (Morey, Dunphy, & Meltz, 1992) and can be further used as components in semiconductor or tuneable lasers (Ball & Morey, 1991; Ball, Morey, & Glenn, 1991; D'Amato & Dunphy, 1992). Ball and Morey (1992) has elaborated on a continuously tuneable single-mode erbium fibre laser. The capability to continuously tune with the exception of mode hopping has been obtained by uniformly stretching both the gratings and the fibre enclosed. Fibre lasers based on Bragg gratings are also beneficial as sensors. In this scenario, the Bragg reflector facilitates dual purposes, as the tuning element and the sensor (Othonos, Alavie, Melle, & Karr, 1993).

2.3.2 Long period gratings (LPGs)

Long period gratings consist of a grating period typically in the order of 100 μm and have been initially demonstrated by Vengsarkar et al. (1996) where the LPGs have been fabricated using an amplitude mask. These gratings couple the guided core mode and the cladding modes that are co-propagating in the fibre. In the process, light may be lost owing to absorption and scattering. LPGs can serve as loss filters for gain equalisation in Erbium-doped fibre amplifier (EDFA). Furthermore, a number of coatings exist for LPGs which can improve or even initiate sensitivity to some external physical or chemical influences (James & Tatum, 2003; Pilla et al., 2005; Smietana, Korwin-Pawlowski, Bock, Pickrell, & Szmidt, 2008; Sun, Li & Liu, 2005). Due to the long period of the grating, LPGs can be successfully created with the aid of point by point writing using heat or UV exposure. In order to locally heat the fibre, a CO_2 laser or an electric arc discharge can be used (Dianov, Karpov et al., 1997).

2.3.3 Tilted gratings

In standard FBGs, the change in the refractive index occurs uniformly across the width of the fibre. By tilting fringes (or blazing) of Bragg gratings at an angle to the optical axis, light can be coupled out from the fibre core to the backward propagating radiation modes. These loss gratings are generally known as slanted gratings or tilted FBGs (TFBGs) (Figure 2.5). The tilted angle of a TFBG affects the reflected wavelength as well as the bandwidth (Kashyap, 1999). Such gratings are useful in refractive index measurements (Caucheteur, Wuilpart, Chen, Megret, & Albert, 2009). Furthermore, they are useful for gain equalisation of EDFAs (Riant, 2002). Another intriguing application of tilted gratings is in mode conversion. The periodic refractive-index perturbation induced along the fibre length consists of a periodicity which connects the mismatch in momentum among the modes. This permits phase-matched coupling between selected modes, resulting in the production of a mode converter. Various grating periods can be used for mode conversion at various wavelengths (Othonos, 1997). A mode conversion efficiently carried out between forward propagation modes, LP_{01} and LP_{11} has been studied by Hill, Bilodeau, Malo, and Johnson (1991).

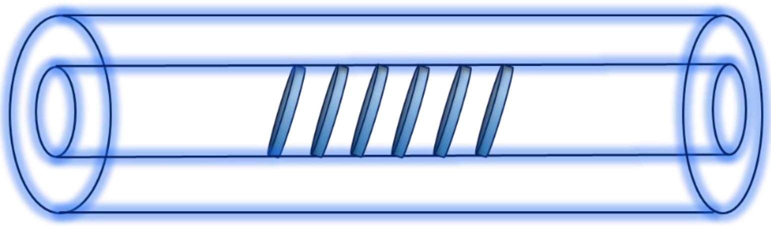

Figure 2.5: Schematic diagram of a tilted grating.

2.3.4 Chirped gratings

A chirped grating possesses a monotonically varying grating period along its length (see Figure 2.6) and can be achieved by axially altering either the period of the grating or the refractive index of the fibre core or both. Varying the amplitude of the Δn_{mod} profile or tapering the grating length region of the fibre leads to a change in the average refractive index (Byron, Sugden, Bricheno, & Bennion, 1993). These type of gratings typically exhibit a broad spectral response reflecting wavelengths associated with the range of grating periods along the length of the grating. Various fabrication techniques are used in the inscription of chirped gratings (Byron et al., 1993; Hill et al., 1994; Kashyap, McKee, Campbell, & Williams, 1994; Martin, Lauzon, Thibault, & Ouellette, 1994; Sugden, Bennion, Molony, & Copner, 1994). A simple and a repeatable method for chirped grating fabrication relies on the phase-mask where a step chirp is used to approximate the linear chirp (Othonos, 1997). These chirped gratings are used in compensation for the scattering in communication networks and for intra-grating sensing (Nand, 2007). Furthermore, broadband chirped FBGs are used for pump rejection and for recycling unabsorbed pump light from an EDFA (Farries, Radgale, & Reid, 1992). A recent study has demonstrated the fabrication of chirped broadband FBGs using ultrafast laser inscription process (Antipov et al., 2016). In addition, Markowsky, Jedrzejewski, and Osuch (2016) have conducted a theoretical analysis of double chirp effect in tapered and linearly chirped FBGs.

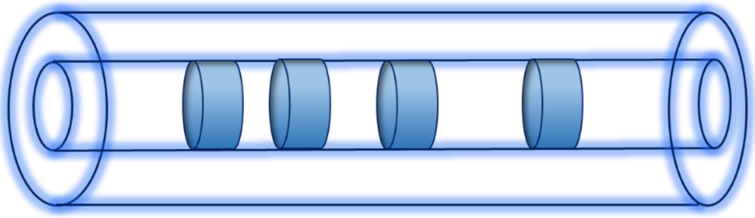

Figure 2.6: Schematic diagram of a chirped grating.

2.3.5 Phase-shifted gratings

Phase-shifted gratings have a discontinuity in the phase along the periodic grating structure. The phase shift separates the grating into two, which results in two Bragg gratings. These gratings are out of phase with each other and act as a wavelength-selective Fabry-Perot resonator. The phase shift results in the production of a narrow transmission resonance at a specific wavelength inside the bandwidth of the grating which is verified with reference to the amplitude and the position of the phase shift (Erdogan, 1997). There are several different approaches for the production of phase-shifted gratings. Canning and Sceats (1994) have fabricated phase-shifted gratings using a UV post processing technique. Several other studies have demonstrated fabrication of phase-shifted gratings by other means such as etching the centre of pre-fabricated FBGs (Iadicicco, Campopiano, Paladino, Cutolo, & Cusano, 2007), phase-mask shift at half of its period throughout FBG inscription procedure (Stepanov, Canning, & Brodzeli, 1999) or merely by use of a phase-shifted phase-mask (Kashyap et al., 1994).

2.3.6 Classification by growth characteristics

Gratings can be categorised based on their growth characteristics during the inscription process. Surface relief gratings based on surface corrugation or modification of the cladding closer to the fibre core have been used in some applications even prior to the finding of photosensitivity in optical fibres. These gratings can generally be produced using etching or polishing processes (Rowe, Bennion, & Reid, 1987). In this section, Bragg gratings are classified into three categories of type I, type II and type IIa gratings. The type of the final grating relies on the initial grating inscription conditions and the properties of the respective fibre.

2.3.6.1 Type I gratings

Type I gratings are the most widely employed gratings, formed under moderate irradiation intensities and are characterised by their monotonous growth pattern. The spectral response of a uniform type I FBG is previously indicated in Figure 2.2. The reflection spectrum of the grating is corresponds to the transmission spectrum which indicates a lossless or negligible loss system due to absorption or reflection into the fibre cladding. Hence, this is an important feature of Type I FBGs. In addition, it is possible to erase type I gratings at relatively low temperatures, around 200 °C. However, they can effectively operate over a temperature range of -40 to +80 °C.

2.3.6.2 Type II gratings

Type II gratings, also referred to as optically damaged gratings have been initially described in an experiment conducted to investigate the link between the pulse energy and the grating strength where the refractive index change has been predicted from the reflection spectrum with the aid of coupled mode theory (Archambault et al., 1993a). These gratings are produced when the energy of the inscription beam is raised above 30 mJ (Archambault, Reekie, & Russell, 1993b). This causes physical damage to a particular side of the fibre core. When examined under an optical microscope a damaged track has been revealed in the core-cladding interface, a typical characteristic of this type of grating (Islam et al., 2016). The fact that the damage is restricted to one side of the fibre core indicates that the majority of the UV light has been absorbed locally.

Since the definite threshold is accompanied by a higher change in the Δn_{mod}, gratings with high reflectivity characteristics can be inscribed using a single laser pulse. Saturation of the refractive index modulation at a value of 3×10^{-3} is observed when the pulse energy exceeds 40-60 mJ (Kashyap, 1999). Energy in the range of 50-60 mJ is capable of destroying the optical fibre. A type II grating generally possesses a broad reflection spectrum where irregularity can be observed over the whole of the spectral profile owing to non-uniformity in the laser beam profile that are magnified strongly by the highly nonlinear response mechanism of the glass core (Grattan & Meggitt, 2000). Spatial filtering of the beam allows generation of gratings with improved reflection profiles but with a decreased grating reflectivity (Archambault, 1994). Type II gratings pass wavelengths longer than λ_B. As in the case for etched or relief FBGs (Russell & Ulrich, 1985), shorter wavelengths are strongly coupled into the cladding.

Investigations regarding thermal stability of type II gratings indicate that they are extremely stable at elevated temperatures (Archambault et al., 1993a). Decay of the grating reflectivity is not visible at 800 °C over a time period of 24 hours. However, near 1000 °C most of the grating gradually extinguishes demonstrating that the localised fusion has been thermally wiped away. This superior temperature stability of type II gratings is beneficial for sensing applications in extreme temperature environments.

2.3.6.3 Type IIa gratings

Type IIa gratings possess similar spectral characteristics to those of Type I gratings but have different thermal stability levels (Pal, 2006). Due to the various mechanisms involved with the inscription of these gratings there are some significant characteristics which can be observed under dynamic conditions during initial fabrication or thermal annealing of the gratings. Type IIa gratings can be generated at low power densities or after long exposure using pulsed lasers (Xie et al., 1993). They generally consist of a characteristic rollover in the index growth during grating fabrication and can be tuned to be thermally stable up to 800 °C for short term usage (Groothoff & Canning, 2004). Bragg gratings of Type IIa are generally present in pristine fibres with a highly germanium-doped core (≥ 20 mol. % GeO_2) when exposed to UV irradiation. Here photosensitivity is present due to the dilation of the glass network which results in a decrease in the index in the irradiated regions (Ky, Limberger, Salathé, Cochet, & Dong, 2003). The reverse shift of Bragg wavelength compared to the original starting point demonstrating a decrease in the average refractive index, results in the formation of a negative index grating.

The negative component as well as the fact that the grating is formed below the damage threshold are important features of Type IIa gratings (Canning, 2008). Based on the applied tension and other parameters, the magnitude of the negative component differs. Even though full stress relief has not been noticed, it has been reported that type IIa gratings are linked with the diminished axial stress (Ky et al., 2003). Poignant et al. (1997) has demonstrated that the presence of H_2 results in a significant variation in the inscription properties of Type IIa gratings. Fabrication of Type IIa thermally regenerated gratings on highly Ge-doped photosensitive fibre using 248 nm nano-second laser pulses has been reported by Lindner et al. (2009). In addition, a recent study has reported about the production of a type IIa RFBG using the thermal activation process at 600 °C in Ge/B co-doped fibre (Cheong, Chong, Chong, Lim, & Ahmad, 2014). The improved thermal stability of Type IIa gratings in comparison to the type I gratings is a valuable advantage of these gratings especially when exposed to high ambient temperatures.

2.4 Grating inscription techniques

2.4.1 Fabrication of the original Hill grating

In 1978, Hill and co-workers from the Canadian Communication Research Centre (CRC) revealed the first observation of photosensitivity of optical fibre and the generation of permanent Bragg gratings in an optical fibre (Hill, Fujii, Johnson, & Kawasaki, 1978). This was achieved through exposure of a segment of germanosilicate optical fibre to intense coherent counter propagating light from an argon-ion laser at a wavelength of 488 nm. Afterwards, an increase in the intensity of the reflected light was observed where majority of the probe light was reflected back from the optical fibre creating a narrow Bragg grating across the 1 m long fibre. This grating is referred to as the “Hill Grating” or “internally written grating”. The “photosensitivity” phenomenon was used to explain the growth in intensity of the back reflected light which also enables the creation of an index grating. The fabricated Bragg grating consisted of 90% grating reflectivity with a bandwidth of less than 200 MHz at the argon-ion laser wavelength. Since the reflected light from the gratings possess a wavelength the same as the wavelength used to inscribe the grating, this method can be used for applications which use wavelengths at or near the inscription wavelength.

2.4.2 Interferometric technique

The initial external writing method on FBGs, interferometric method was revealed by Meltz, Morey, and Glenn (1989) in photosensitive fibre. During this process, an interferometer was deployed which divided the incoming UV light into two beams, and a subsequent recombination of them occurred which led to the creation of an interference pattern. A photosensitive fibre was exposed to this fringe pattern in order to induce a Δn_{mod} in the fibre core. FBGs have been inscribed with the aid of both amplitude splitting and wave-front-splitting interferometers (Hill & Meltz, 1997). Therefore, the following sections are devoted to the examination of two different types of interferometers.

2.4.2.1 Amplitude-splitting interferometer

As shown in Figure 2.7, the amplitude-splitting interferometer goes through a process in which the UV light is separated by a beam splitter into two beams with equivalent intensity which are subsequently recombined after propagation over various optical passages. This creates an interference pattern at the core of the optical fibre. The interfering beams are focused perpendicularly to the fibre axis with the aid of cylindrical lenses placed inside the interferometer to generate a fine line which are aligned with the core of the fibre. This improves grating inscription by producing high intensities at the core of the fibre. The period of the Bragg grating Λ, is presented by:

$$\Lambda = \frac{\lambda_{UV}}{2\sin\varphi} \tag{2.34}$$

where λ_{UV} denotes the UV irradiation wavelength and φ the half angle between the intersecting UV beams (Othonos, 1997). Λ is identical to the fringe pattern of interference (Hill & Meltz, 1997). Considering the Bragg condition in Eq. (2.15), the Bragg resonance wavelength λ_B can be represented as

$$\lambda_B = \frac{n_{eff}\lambda_{UV}}{\sin\varphi} \tag{2.35}$$

From Eq. (2.35) it is observed that the λ_B can be conveniently tuned by altering φ or λ_{UV}. The ability to write Bragg gratings at different wavelengths through simple alteration of the angle of intersection between the UV beams, was considered to be an important benefit of this technique. It also provides flexibility in the decision of the grating length when adjusting the bandwidth of the grating. The main drawback of this method is its sensitivity towards mechanical vibrations (Kashyap, 1999).

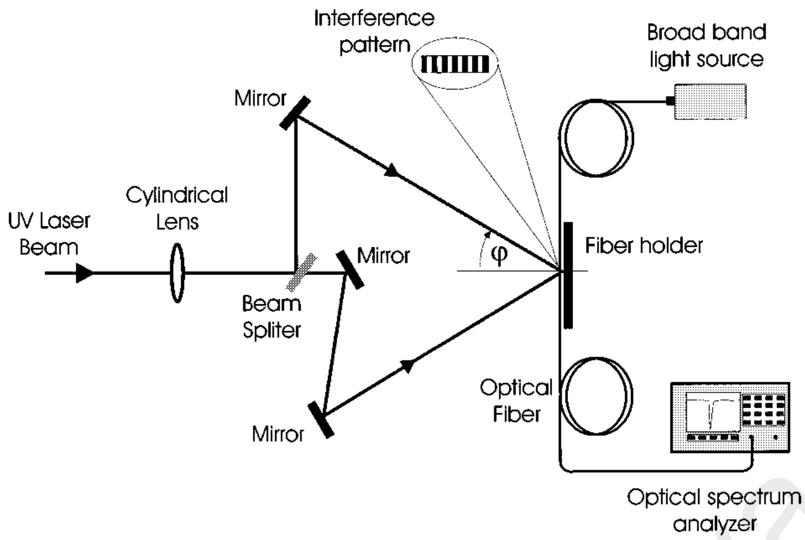

Figure 2.7: Experimental setup of the amplitude-splitting interferometer for grating fabrication (Othonos, 1997).

The incorporation of a laser source with good spectral and temporal coherence including exceptional output power stability is helpful in the production of high quality FBGs (Sang, Chu, Yu, & Lai, 2006).

2.4.2.2 Wave-front-splitting interferometer

Wave-front-splitting interferometers have more benefits compared to the amplitude-splitting interferometers even though they are less popular when compared with the latter. Prism interferometer (Eggleton, Ahmed, Liu, Krug, & Poladian, 1994; Kashyap, Armitage, Wyatt, Davey, & Williams, 1990) and Lloyd's interferometer (Limberger et al., 1993) are examples of wave-front-splitting interferometer used for FBG fabrication in optical fibre. In these two scenarios, the period of the interference pattern relies on the angle of incidence between the prism and the beam or on the angle between the mirror and the beam. The increase in the angle of intersection results in an increase in the variation between the path lengths of the beams. Hence, the coherence length restricts the tuneability of the λ_B (Othonos, 1997). A major advantage of this particular type of interferometer is that it requires the use of only a single optical component, thereby considerably reducing the susceptibility to mechanical vibrations. The wave-front distortion induced by air currents and temperature variation between the two interfering beams is reduced by the limited distance, over which the UV beams separate (Othonos, 1997). Moreover, the angle of intersection can be changed through easy rotation of this convention, in order to tune the Bragg wavelength.

2.4.3 Mask image projection

High-resolution mask projection has been introduced for FBG fabrication in optical fibre using excimer laser irradiation (Mihailov & Gower, 1994). A transmission mask that consists of a sequence of UV opaque line spaces is used to create a periodic beam for grating inscription in optical fibres (Mihailov & Gower, 1994). A multi-component fused silica high-resolution system with a demagnification of 10:1 is used to image the transmitted beam onto the fibre core. The mask-imaging method has been useful in the inscription of gratings having grating periods of 1, 2, 3, 4, 5 and 6 µm on Ge-doped single-mode fibre. The simplicity of the system allows a flexible recording of the coarse period gratings by mask-imaging exposures. A simple alteration of the mask provides the possibility to fabricate more complex grating structures such as blazed, chirped, etc (Ivanov, 2004).

2.4.4 Point-by-point technique

In the point-by-point inscription technique (Malo, Hill, Bilodeau, Johnson, & Albert, 1993) as shown in Figure 2.8, refractive index change is induced one step at a time along the fibre core. A single pulse of the UV beam from an excimer laser is focused onto the fibre at a specific point after passing through a narrow slit. This results in a local increase in the refractive index in the exposed region. Then the fibre is translated along the fibre axis by a particular distance Λ, which corresponds to the grating period. The procedure is repeated until the required grating length is reached. The flexibility provided in altering the parameters of the Bragg grating is considered as the prime advantage of this technique. This includes the variation of grating length, pitch and modulation intensity. In addition, this method also permits the fabrication of spatial-mode converters (Hill et al., 1990) and polarisation-mode converters or rocking filters (Hill et al., 1991) which consist of grating periods which span from tens of micrometres to tens of millimetres. The relatively long time consumed during the step-by-step process and the high cost of the translation stage with sufficient resolution are some of the disadvantages of this method. Due to the occurrence of small errors in the grating spacing as a result of the thermal effects or fluctuations in the strain characteristics of the fibre, the gratings are limited to much shorter lengths.

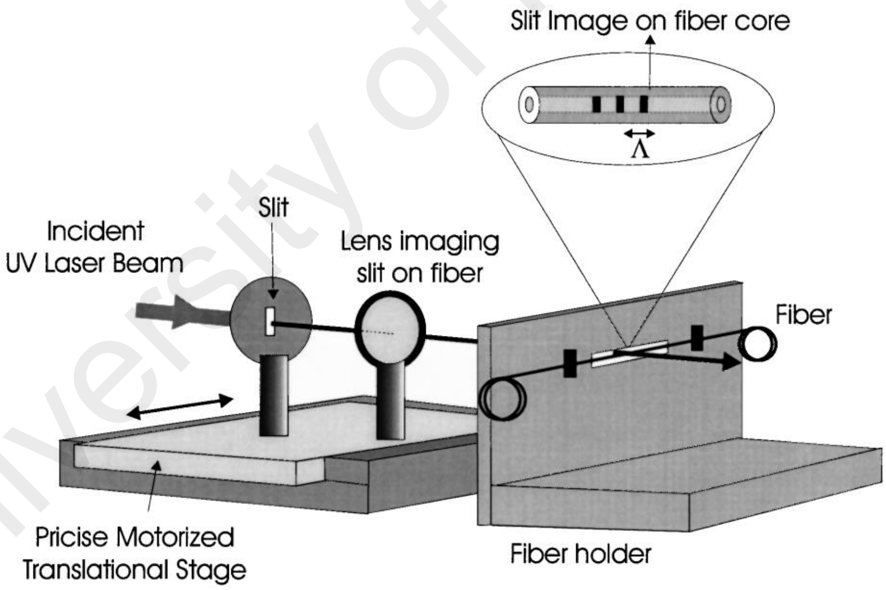

Figure 2.8: Experimental setup for point-by-point fabrication technique (Othonos, 1997).

2.4.5 Phase-mask technique

The phase-mask technique is one of the widely used inscription methods for gratings in optical fibres (Anderson, Mizrahi, Erdogan, & White, 1993a; Hill, Malo, Bilodeau, Johnson, & Albert, 1993). A phase-mask can be created either holographically or by electron-beam lithography (Anderson, Mizrahi, Erdogan, & White, 1993b). The absence of the stitching error in the grating pattern on the mask, is an advantage of the holographic method compared to the electron-beam lithography method (Albert, Theriault, et al., 1996). However, complex patterns such as quadratic chirps can be inscribed into the masks produced using electron beams. The phase-mask technique occupies a diffractive optical element which spatially modulates the UV writing beam. In ideal conditions, the period of a phase-mask Λ_{pm}, is twice the period of a grating Λ (Kashyap, 1999) and can be represented as:

$$\Lambda_{pm} = 2\Lambda \tag{2.36}$$

The period of the etched grooves and the etched depth are considered to be key features of a phase-mask. FBGs are produced through the diffraction of UV light into several orders, $m = 0, \pm 1, \pm 2, \ldots$ The incident and the diffracted orders meet the general diffraction equation

$$\Lambda_{pm} = \frac{m\lambda_{UV}}{\sin\theta_m - \sin\theta_i} \tag{2.37}$$

where Λ_{pm} is the phase-mask period, θ_m the angle of the diffracted order, λ_{UV} the irradiation wavelength and θ_i the angle of incident UV beam. When an optical fibre is placed near or in contact with the phase-mask, the superposition of the diffraction orders near the phase-mask surface produces an interference pattern leading to the inscription of Bragg gratings. A maximum visibility is attained when the zeroth order diffraction is suppressed to a minimum intensity while the +1 and -1 orders consist of identical maximum intensity or when the transmitted beam and -1 order beam consist of identical maximum intensity.

FBG inscription using these two methods for normal incident conditions was demonstrated by (Hill et al., 1993) and for non-normal conditions by (Anderson et al., 1993a). Nevertheless, comparatively the usage of a phase-mask at normal incident conditions is more convenient. Under normal incident conditions, the zero order beam intensity can be minimised by adjusting the depth of the phase-mask grooves *d*, in such a way that the UV light obtains a π phase shift between the air and silica transmission pathways which results in

$$\frac{2\pi}{\lambda_{UV}}(n_{slc}-1)d=\pi \tag{2.38}$$

where n_{slc} denotes the refractive index of silica at the UV inscription wavelength. The zero order will be nulled for the design wavelength λ_{UV}, in the scenario where the depth *d*, of the phase-mask grooves satisfy Eq. (2.38). The alteration in the wavelength of the laser source requires the employment of a different phase-mask.

The involvement of a phase-mask greatly reduces the complications in an FBG inscription system. The usage of a single optical element gives a simple and inherently stable technique for the reproduction of FBGs. The close proximity of the fibre behind the phase-mask in the near field of diffracting UV beams reduces the sensitivity to mechanical vibrations. The main drawback of the phase-mask technique is the limited tuneability of the inscribed Bragg wavelength since it is determined by the fixed periodicity of a phase-mask. According to experimental findings, the magnification of the phase-mask periodicity using an extra lens has only resulted in limited tuneability in the order of a few percent (Prohaska, Snitzer, Rishton, & Boegli, 1993). It is not desirable to place an optical fibre in contact with the fine grating corrugations, since it might cause damage to the phase-mask. Therefore, the improvement of the spatial coherence of the UV inscription beam not only enhances the quality and strength of the FBGs but also alleviates the need for the optical fibre to be in contact with the phase-mask (Ivanov, 2004; Singh, Jain, & Aggarwal, 2002).

The schematic representation of the grating inscription setup using the phase-mask technique with a UV laser source, employed in the current research study is demonstrated in Figure 2.9 below. The optical beam shutter shown in Figure 2.9 is helpful in controlling the laser irradiation on the fibre so that stable and undisturbed transmission spectra can be recorded by the optical spectrum analyser (OSA) throughout the experiment. The optical beam shutter is controlled by a LabVIEW program. The control panel of this program and a segment of its block diagram are included in the Appendix.

Figure 2.10 indicates the optical fibre placement behind the phase-mask during FBG inscription including the three axis positioning stage. One end of the optical fibre is generally connected to the amplified spontaneous emission (ASE) source via a circulator whereas the other end is connected to the OSA.

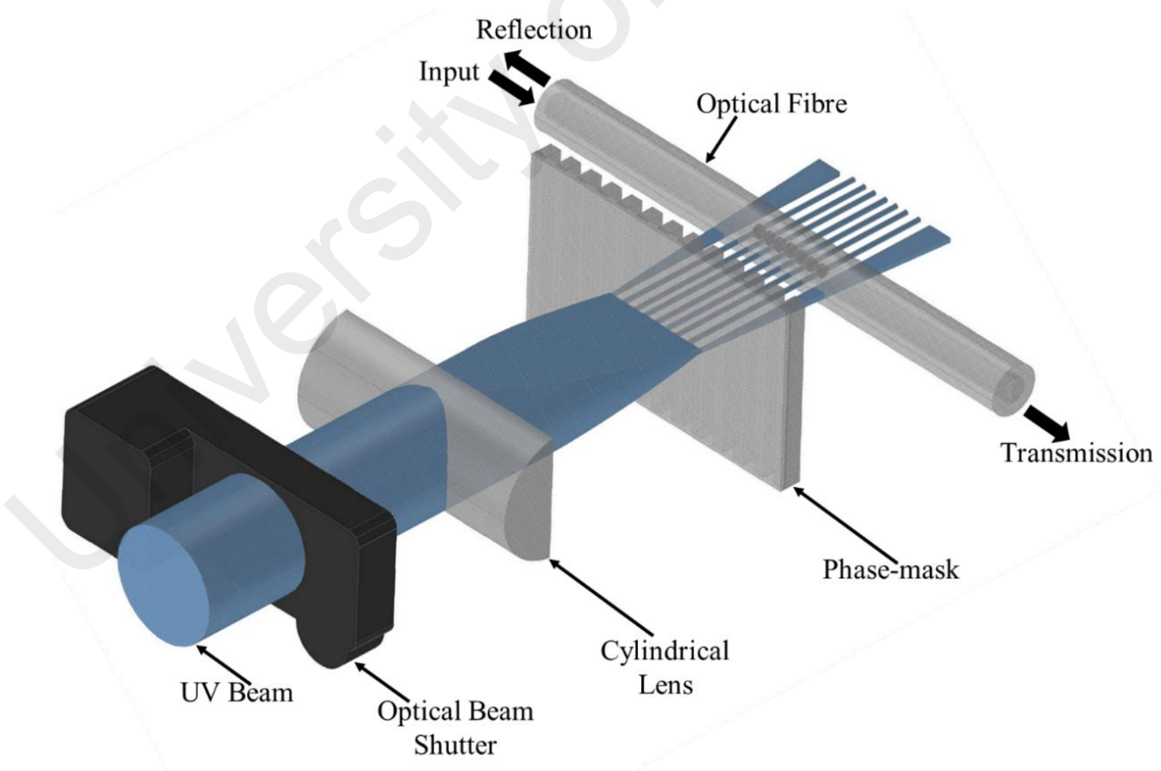

Figure 2.9: Schematic representation of the FBG inscription setup.

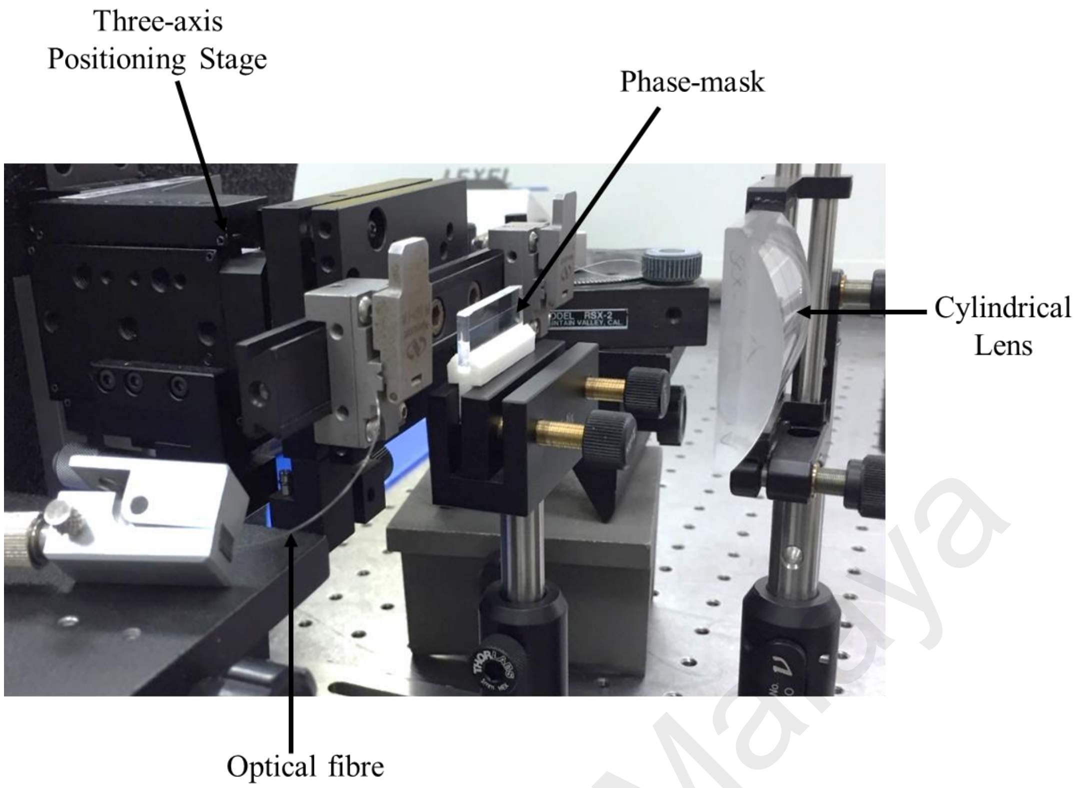

Figure 2.10: Phase-mask technique for grating inscription.

2.4.5.1 Sources for FBG inscription and their specifications

The sources utilised in the fabrication of various Bragg gratings and the thermal annealing procedures discussed in this research are namely, 193 nm ArF excimer laser, 248 nm KrF excimer laser and CO_2 laser. The specifications of these laser sources are shown in Table 2.1 and Table 2.2 below.

Table 2.1: Specifications of excimer laser sources

Excimer Laser CL-5100		
Parameter	ArF	KrF
Wavelength	193 nm	248 nm
Nominal Pulse Energy	20 mJ	40 mJ
Average Power	2 W	4 W
Max Repetition Rate	100 Hz	
Pulse Duration	8-10 ns	9-11 ns
Beam Size	5×12 mm	6×12 mm
Power	220 V/50 Hz, 10 A, not more than 1000 VA	

Table 2.2: Specifications of CO_2 laser source

CO_2 Laser	
Parameter	Specification
Wavelength	10600 nm
Average Power	>31.1 W
Power Stability	±5%
Rise Time	≤150 μs
Fall Time	≤150 μs

2.5 Summary

In this chapter, an insight to the theory of FBGs was provided using coupled-mode theory. A comprehensive review on the different types of Bragg gratings based on their coupling, growth characteristics and their importance was presented. A brief overview on different grating inscription techniques was provided, particularly highlighting the phase-mask technique. The sources and their specifications used for grating inscription and thermal annealing procedures in the current research study were outlined as well.

CHAPTER 3: PHOTOSENSITIVITY AND CHARACTERISATION OF GRATING STRENGTH

The capability to vary the refractive index with UV irradiation is referred to as photosensitivity of optical fibres. During grating inscription, the optical fibre is placed in the field of interference and this particular pattern of interference is imprinted in the fibre core through a UV light-induced refractive index change. The visibilities of the interference fringe and the Bragg grating have a strong influence towards the grating reflectivity and the grating strength. This chapter is a discussion of the fibre photosensitivity and characterisation of the grating strength in terms of grating and interference visibilities. Several mechanisms accountable for the change in refractive index including different methods to enhance fibre photosensitivity are discussed. A brief overview of the material considerations to enhance fibre photosensitivity is provided and a new photosensitive dopant is introduced. In addition, this chapter further elaborates on different characterisation techniques to precisely determine the grating and interference visibilities.

3.1 Photosensitivity Mechanisms

Photosensitivity of optical fibres was first discovered by Hill et al. in germanosilicate fibre (Hill et al., 1978; Othonos, 1997). Since then, different models have been suggested for these photo-induced refractive index changes. Colour centre model, compaction/densification model and stress relaxation model are a few of them. In the early stages, the photosensitivity of germanosilicate fibre has been associated with an absorption band peaking at a wavelength of ~240 nm which is ascribed to germanium-oxygen deficiency centres (GODC) (Meltz et al., 1989). Irradiation of the fibre core to a wavelength coincident with this band leads to bleaching while producing other absorption bands which results in a change in the refractive index. It has been described using the

Kramers-Kronig relationship by Hand and Russel (1990) and Dong, Archambault, Reekie, Russell, and Payne (1995) which is given by

$$\Delta n_{eff}(\lambda) = \frac{1}{2\pi^2} P \int_0^\infty \frac{\Delta\alpha_{eff}(\lambda)}{1-(\frac{\lambda}{\lambda'})^2} d\lambda \tag{3.1}$$

where λ, $\Delta\alpha_{eff}(\lambda)$ and $\Delta n_{eff}(\lambda)$ represent the wavelength, effective change in the absorption coefficient and the effective refractive index change respectively. P represents the principal segment of the integral and λ' denotes the wavelength for which the refractive index is calculated (Othonos & Kalli, 1999).

Two types of oxygen deficient defects in Ge have been identified to be responsible for the absorption at ~240 nm (Takahashi, Fujiwara, Kawachi, & Ikushima, 1997) namely, neutral oxygen monovacancy (NOMV) which is associated with Ge─Ge or Ge─Si bonds and neutral oxygen di-vacancy (NODV) such as Ge^{2+} that incorporates two oxygen atoms. During UV irradiation, NOMV experiences a photochemical conversion where the bond promptly breaks resulting in a GeE′ centre. Nevertheless, due to the existence of a lone pair of electrons of Ge at the uppermost level, NODV appears to exhibit a photochemically stable structure against 5 eV photons (240 nm) (Hosono et al., 1992). NOMVs are observed at low intensity exposures whereas NODVs are observed only at high intensities (Fujimaki et al., 1998; Nishii et al., 1995). Since Bragg gratings could also be inscribed in GODC free Ge-doped optical fibre with the aid of two photon absorption process (Albert et al., 1999), the photosensitivity of germanosilicate fibre is not only limited to the GODCs. Another model, referred to as the stress relaxation model relying on the relaxation of the thermoelastically-induced stress in the fibre core during UV exposure has been proposed by Wong, Poole, and Sceats (1992). The differentiation in the thermal expansion coefficients of the fibre core and cladding suggests that there is a presence of residual stress in the fibre core.

Even though the colour centre model has been supported by many experiments (Atkins & Mizrahi, 1992; Atkins, Mizrahi, & Erdogan, 1993; Simmons, Griscom, LaRochelle, Mizrahi, & Stegeman, 1991; Williams, Davey, Kashyap, Armitage, & Ainslie, 1992) it cannot completely explain the observations of all the experiments conducted (Niay et al., 1994; Xie et al., 1993) with different fibre types and various dopants. Another model which relies on glass densification induced by photoionisation (Bernadin & Lawandy, 1990) of the Ge defects has also been proposed with experimental assistance (Chiang, Sceats, & Wong, 1993). Densification in germanosilicate optical fibre and preforms induced by UV light has been demonstrated through the changes in Raman spectra (Dianov, Plotnichenko et al., 1997) and the fibre core tension (Fonjallaz, Cochet, Leuenberger, Limberger, & Salathé, 1995). The compaction in the core glass has been explained through the correlation of increment in the refractive index, to the increment in the tensile stress in the fibre core. However, up-to-date colour centre model can be considered the most widely used model to demonstrate the mechanism behind the FBG formation (Othonos, 1997).

3.2 Techniques for photosensitivity enhancement

This section demonstrates the main methods used to enhance the photosensitivity response of optical fibres. Over the past few years, a considerable effort has been put into enhancing the photosensitivity of silica optical fibres by hydrogen (H_2) loading, flame brushing, pre-sensitisation and by using different photosensitive dopants.

3.2.1 Hydrogenation

H_2 loading is a simple and the most widely used technique in achieving high UV photosensitivity levels in optical fibres and was first discovered by Lemaire, Atkins, Mizrahi, and Reed (1993). This highly effective approach has been used extensively prior to UV exposure where the optical fibres are immersed in H_2 gas at temperatures over a range of 25-80 °C and at a typical pressure of 150 atm. This produces a diffusion of the hydrogen molecules into the fibre core and once irradiated with UV laser, produces OH absorbing species due to the reaction of the hydrogen molecules with Ge-O-Si bonds in the glass structure. In H_2 loaded standard telecommunication fibres, refractive index changes reaching 10^{-3} have been reported (Lemaire et al., 1993). The enhancement in photosensitivity involves thermally induced reactions and photolytic mechanisms (Atkins, Lemaire, Erdogan, & Mizrahi, 1993) which result in Si-OH, bleachable GODCs and germanium related defects. The diffusion rate of the hydrogen molecules depends on the temperature and pressure of the H_2 gas. Typically, H_2 loading for one week at room temperature is required to attain the necessary photosensitivity level in the optical fibre. Nevertheless, the desired time can be reduced to a few days by loading at a higher pressure or temperature. When accessing photosensitivity, H_2 loading eliminates the requirement of using UV wavelengths which coincide with the defect absorption bands (Grubsky, Starodubov, & Feinberg, 1999a). Figure 3.1 below indicates the difference in index change in the presence and the absence of H_2 during grating inscription in germanosilicate fibres. Evidently, much higher index changes can be observed for H_2 loaded fibre compared to that of H_2 free fibre.

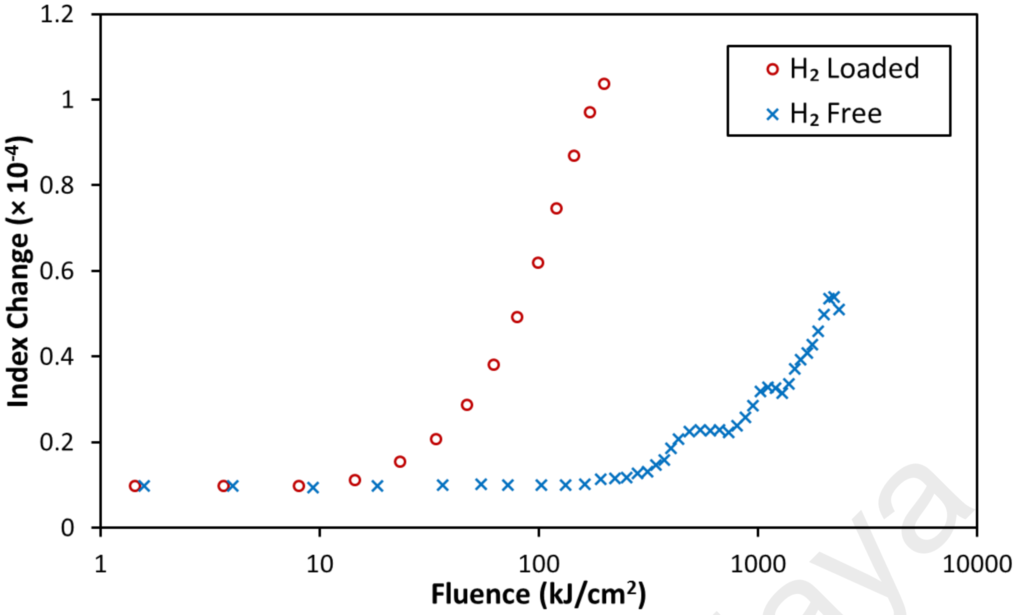

Figure 3.1: Index change of H_2 loaded and non-loaded germanosilicate fibre during grating inscription process.

3.2.2 Flame Brushing

Flame brushing is another effective technique used to increase photosensitivity of optical fibre where a flame fuelled with H_2 gas and a limited amount of oxygen (O_2) gas at a temperature of 1700 ˚C, is used to repetitively brush a specific region of the optical waveguide for photosensitisation (Bilodeau et al., 1993). The process requires a time duration of ~ 20 minutes. This method results in an increase in the UV absorption spectra including the 240 nm absorption band due to the in-diffusion of hydrogen into the fibre core and reacting with the germanosilicate glass structure resulting in GODC defects. The flame brushing method is capable of achieving a refractive index change higher than 10^{-3} (Bilodeau et al., 1993). In comparison to H_2 loading, enhanced photosensitivity in the fibre by the flame brushing technique is more permanent since the hydroxyl species are created in the fibre and does not suffer from degradation in photosensitivity due to out-diffusion of the residual H_2 as in the case of H_2 loading technique. However, the mechanical deterioration of the fibre glass due to prolonged processing can be considered as a drawback of this method.

3.2.3 Thermal Treatment using CO_2 Laser

CO_2 laser irradiation on germanosilicate fibre as a pre-treatment, before grating inscription has shown higher photosensitivity and a greater Δn_{mod} owing to the increase in the 240 nm absorption band as demonstrated by Brambilla, Pruneri, Reekie, and Payne (1999). A 248 nm KrF excimer laser has been used in this investigation. Therefore, the photosensitivity response of H_2 loaded Ge/B co-doped silica fibre, pre-treated using a CO_2 laser with a subsequent slow cooling process was investigated by inscribing 10 mm long gratings using 193 nm ArF excimer laser irradiation. The index change during the inscription process is shown in Figure 3.2. It is evident from Figure 3.2 that with increasing UV fluence the CO_2 laser treated fibre exhibits a higher index change being up to ~2.5×10^{-4} compared to that of the non-treated fibre.

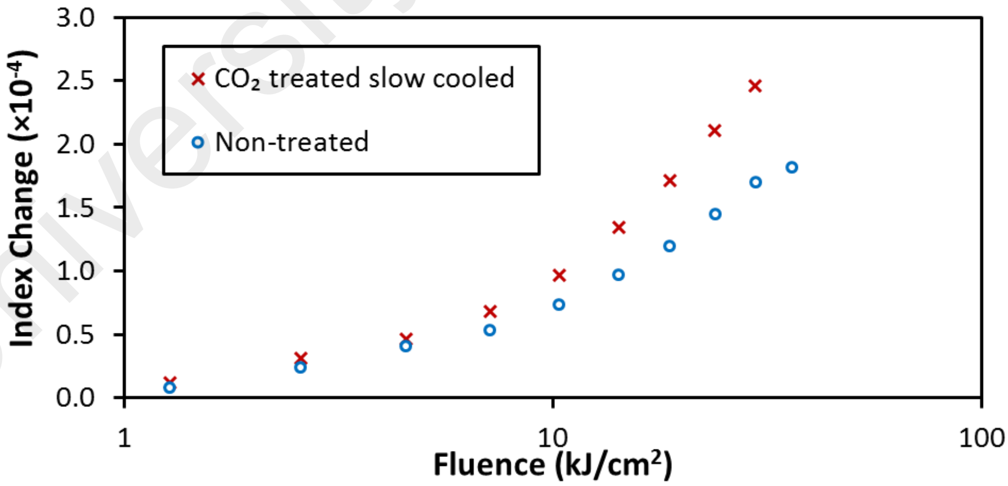

Figure 3.2: Growth of index change of CO_2 treated slow cooled fibre and non-treated fibre during grating inscription with exposure to 193 nm ArF excimer laser.

3.2.4 UV pre-exposure

Fringeless UV irradiation on H_2 loaded fibre has resulted in increased photosensitivity even when the residual H_2 has been removed (Åslund, Canning, & Yoffe, 1999; Kohnke, Nightingale, Wigley, & Pollock, 1999). As discussed in the previous sections, this might be due to the fact that UV exposure or heat generation leads to defects and the production of hydroxyl species in the fibre. The photosensitivity characteristics of H_2 free germanosilicate fibre with UV pre-exposure has also been investigated. Initially, each germanosilicate optical fibre (5.5wt% Ge concentration) was exposed to 248 nm UV irradiation for 50, 200 and 500 pulses. Subsequently, 15 mm long gratings were inscribed in them with the employment of 193 nm ArF excimer laser using the phase-mask lithography technique. The optical fibre was placed at the beam waist point where it received the optimum laser intensity. To validate that the UV pre-irradiated portion of the optical fibre was entirely exposed to the UV laser beam, the fibre ends were fastened at the fibre clamps which were installed on a three axis positioning stage. The transmission spectra were recorded and monitored using an optical spectrum analyser (OSA) controlled by a LabVIEW program via a GPIB interface for automatic data acquisition. Moreover, an optical beam shutter was used as described in Chapter 2 (Figure. 2.9) with a close time duration of 4.08 s. Furthermore, consecutive FBG inscription in untreated germanosilicate fibres was also carried out for comparison purposes. It is illustrated in Figure 3.3 that compared to the untreated optical fibre, the UV pre-exposed germanosilicate fibre provides a higher Bragg transmission depth (BTD) and a longer wavelength shift.

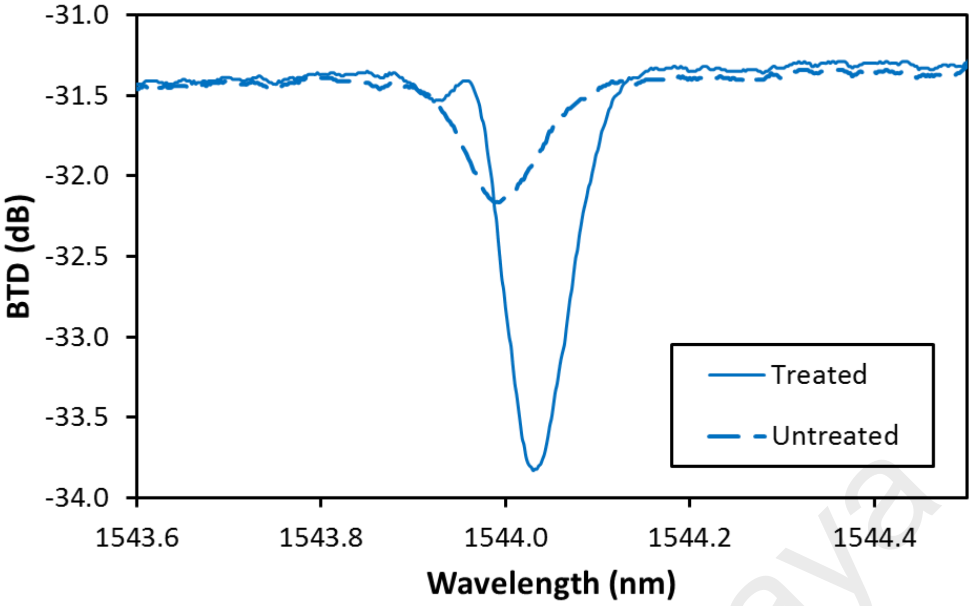

Figure 3.3: Transmission spectra of the FBGs inscribed in treated and untreated germanosilicate fibre using ArF excimer laser after a time duration of 3.5 min.

Figure 3.4, demonstrates the variation of index change based on the number of pulses to which the fibres have been pre-exposed.

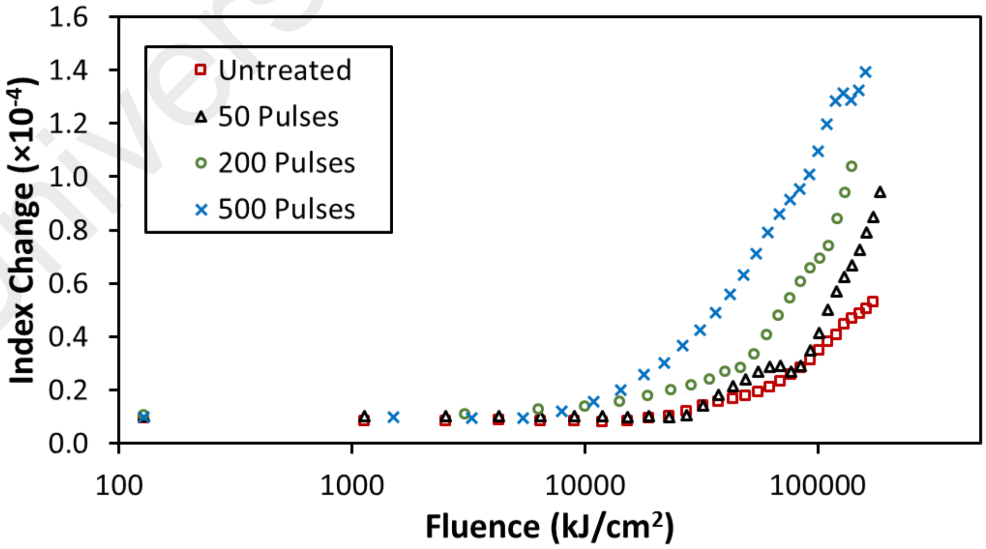

Figure 3.4: Index change during grating inscription using 193 nm irradiation in UV pre-exposed fibre with 50, 200, and 500 pulses and untreated germanosilicate optical fibre.

An increase in the index change for fibres with an increasing number of pulses during the pre-exposure is clearly observed whereas the untreated fibre indicates the least index change. The range of UV-fluence for each experiment differs based on the type of fibre and the type of laser used.

3.2.5 Choice of dopant

The following section gives a brief summary of various types of dopants reported in enhancing the photosensitivity of optical fibres. Each dopant possesses its own unique characteristics.

3.2.5.1 Germanium (Ge)

Since the first grating inscription, GeO_2 still appears to be the most widely used dopant in photosensitive optical fibre manufacturing. Photosensitivity and the GeO_2 concentration indicate a linear relationship. The photosensitivity characterisation of germanosilicate fibres usually refers to the 240 nm absorption band which is related to the germanium oxygen deficient centres (GODCs). Medvedkov, Vasiliev, Gnusin, and Dianov (2012) have demonstrated the degree of photosensitivity in heavily GeO_2 doped silica optical fibre which consists of a GeO_2 concentration of 75 mol%. Co-doping with B_2O_3 or SnO_2 has also managed to produce a notable enhancement in photosensitivity.

3.2.5.2 Boron (B)

Germanosilicate fibre co-doped with B_2O_3 exhibits higher photosensitivity compared to the fibre which solely consists a high germanium concentration (Williams, Ainslie, Armitage, Kashyap, & Campbell, 1993). In B_2O_3- SiO_2 glass, the presence of 240 nm absorption band is not visible but at ~ 190 nm the UV absorption band starts to increase (Dong, Pinkstone, Russell, & Payne, 1994). The enhancement mechanism of B_2O_3 co-doping can be ascribed to the increase in densification as a result of the stress effects (Camlibel, Pinnow, & Dabby, 1975). This softens the glass, thereby increasing the probability of structural rearrangement of the defects and the glass network. The low thermal stability of B_2O_3 co-doped fibre compared to fibre doped with GeO_2, can be cosidered as a drawback (Williams & Smith, 1995; Baker, Rourke, Baker, & Goodchild, 1997). Photosensisitvity enhancement in B_2O_3-GeO_2 co-doped fibre due to increased tension during fibre drawing has been investigated by Ky, Limberger, Salathé, Cochet, and Dong (1998). Long period gratings (LPGs) have been fabricated using the thermal release of drawing induced stress (C.S. Kim et al., 2000).

3.2.5.3 Aluminium (Al)

Introducing Al_2O_3 to GeO_2 results in a decrease in the 240 nm absorption band but produces an absorption band at ~205 nm (Dong et al., 1994). According to J.M. Kim, Oh, Park, Kim, and Jeong (2000) Al_2O_3 has been used as an index change modifying dopant with insignificant effect on photosensitivity while uniform photosensitivity is maintained between the core and the inner cladding using constant concentration of B_2O_3-GeO_2 where the refractive index of the cladding matches that of silica.

3.2.5.4 Tin (Sn)

Photosensitive fibre co-doped with SnO_2 and GeO_2 was first reported by Dong, Cruz, Reekie, Xu, and Payne (1995). Lower losses at the 1.5 µm telecommunication window and high thermal stability in comparison with the B_2O_3-GeO_2 co-doped fibre are among the advantages of SnO_2 co-doping. UV-induced index changes amounting to 1.4×10^{-3} has been achieved for these tin co-doped germanosilicate fibres. However, increased tension during fibre drawing decreases the photosensitivity of SnO_2-GeO_2 doped silica fibre and indicates the characteristics of a type IIa grating during grating inscription (Ky et al., 1998). Nevertheless, type I and type II gratings have been successfully inscribed in highly photosensitive SnO_2-P_2O_5-doped silica fibre (Dong, Cruz, Tucknott, Reekie, & Payne, 1995). According to Brambilla, Pruneri, and Reekie (2000), refractive index modulations of 2.8×10^{-4} have been observed in 0.15 mol% SnO_2-doped fibre with exposure to 248 nm laser irradiation. Volatile SnO_2 being burnt off during preform collapse and crystallisation at ~1 mol% SnO_2 levels, complicate the preform fabrication process of these fibres.

3.2.5.5 Nitrogen (N)

Highly photosensitive nitrogen doped germanosilicate fibre consisting of a 2.8×10^{-3} refractive index change at 244 nm wavelength in the absence of H_2 loading has been reported by Dianov, Golant, Mashinsky, et al. (1997). In the presence of H_2, the refractive index change has been recorded as 1×10^{-2}. However, a large amount of H_2 in N-doped fibre results in a negative effect as the N-H bond shows absorption at ~1506 nm, the third telecommunication window (Dianov, Golant, Khrapko, Kurkov, & Tomashuk, 1995; Grand et al., 1990). Grating inscription using 193 nm wavelength in hydrogen and Ge free N-doped fibre has also been reported (Dianov, Golant, Khrapko et al., 1997). These type IIa gratings have indicated a high thermal stability at temperature levels beyond 1000 ˚C. In addition, LPGs written in N-doped silica fibres using CO_2 laser or arc discharge have appeared to indicate ultra-thermostable capabilities withstanding temperatures over 1000 ˚C (Karpov, Grekov, Dianov, Golant, & Khrapko, 1998). The nitrogen thermodiffusion process in silica has been used to fabricate these LPGs.

3.2.5.6 Lead (Pb)

PbO-doped silica based photosensitivity has been reported in multicomponent glasses. Refractive index changes amounting to $\Delta n \sim 0.09$ in UV-induced surface relief gratings have been reported by Long and Brueck (1999a, 1999b).

3.2.5.7 Titanium (Ti)

TiO_2 is generally used to dope the outer-cladding of the fibre since it results in a higher mechanical strength. High refractive index changes have been discovered in gratings inscribed in optical fibres consisting of TiO_2-doped outer cladding during 244 nm CW laser irradiation (Wang et al., 1999). Furthermore, the hydrogenation time duration has been reduced to one day at room temperature for these fibres. The TiO_2 layer efficiently absorbs the 240 nm light which leads to a notable increase in the temperature of the fibre (200 °C at 40 mW, CW 244 nm) leading to enhanced photosensitivity.

3.2.5.8 Fluorine (F)

Deviating from Ge and P which are considered to be network formers, fluorine acts as a network modifier. Fluorine is among the two dopants that manage to decrease the refractive index of silica (Lancry & Poumellec, 2013). This has resulted in fluorine being extremely popular when doping with silica since it has the capability of controlling the refractive index profile of optical fibres. In the viscosity-matching technique, fluorine is used to decrease the excess imperfection loss. This technique involves other dopants such as GeO_2, P_2O_5 and fluorine in matching the viscosity of the core and cladding. In the field of photolithography, particularly as a material for photomasks relying on 157 nm technology, fluorine-doped silica is used for high and stable transmission over a wide spectral range (Liberman et al., 1999; Mizuguchi, Skuja, Hosono, & Ogawa, 1999a, 1999b). A small amount of fluorine up to a level of 1 mol% is sufficient to blue shift the absorption edge of pure silica (Saito & Ikushima, 2002). Furthermore, Si-F groups result in radiation toughness of silica samples. The decrease of defect precursors are assumed to be the reason behind the positive effect of Si-F groups (Kajihara et al., 2004). Defects such as non-bridging oxygen hole centres (NBOHC) and E′ centres are generated from strain bonds which absorb in the visible and UV spectral range.

3.2.5.9 Phosphorus (P)

Based on the Lancry and Poumellec (2013) research study, P_2O_5 results in a strong decrease in the glass viscosity. This leads to a comparatively low fibre drawing temperature during manufacture. Nevertheless, it also results in a rise in the thermal expansion coefficient creating a mismatch between the cladding and the silica tube. Hence phosphorus is seldom used singly as a dopant in silica even though many studies use phosphorus co-doped with either germanium or fluorine. Fluorine/phosphorus co-doped cladding contributes in making the viscosity of the cladding similar to that of the fibre core, thereby decreasing the excessive loss.

Doping with phosphorus results in a weak absorption band centred at ~210 nm. A noteworthy decrease in the 240 nm absorption band is observed when germanosilicate fibre is co-doped with phosphorus. After a long period of irradiation, photosensitivity in H_2 or deuterium loaded P-doped fibre has been noticed. Figure 3.5 below demonstrates the index change growth of a H_2 loaded P-doped fibre with 193 nm irradiation during the inscription of a 15 mm FBG. A refractive index change of 1.9×10^{-4} was achieved and the spectral properties of a grating with 99.5 % reflectance is shown in the inset.

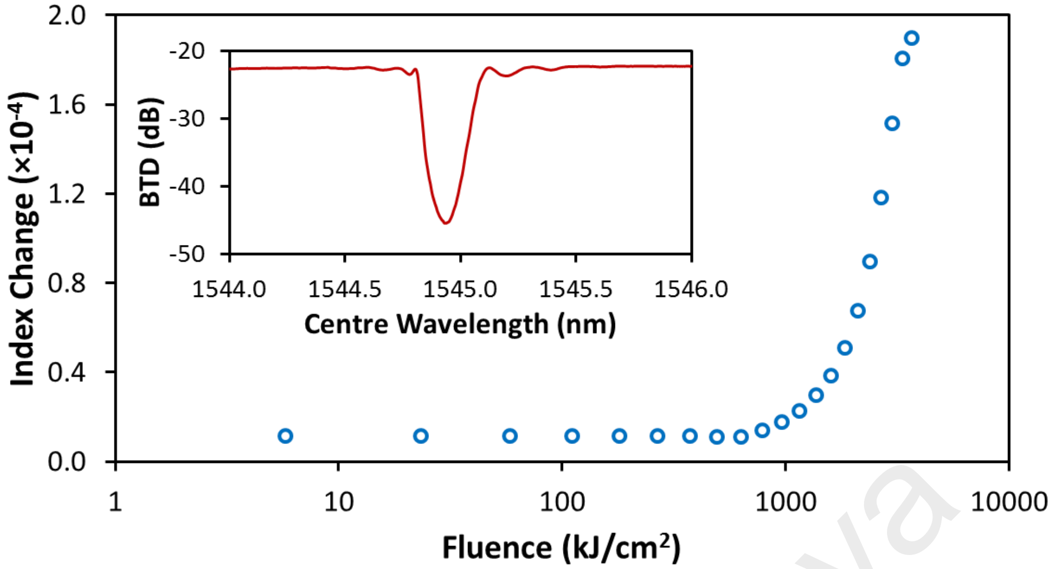

Figure 3.5: Growth of index change of H_2 loaded phosphorus doped fibre during grating inscription with exposure to 193 nm ArF excimer laser irradiation. Inset, transmission spectrum of a 15 mm long FBG inscribed in P-doped fibre.

3.3 Gallium as a photosensitive dopant

3.3.1 Fabrication of gallosilicate fibre

Modified chemical vapour deposition (MCVD) and standard solution doping technique (Townsend, Poole, & Payne, 1987) were used in the fabrication of Gallium (Ga) doped optical fibre preforms. The procedure commenced with the deposition of optical fibre preform soot where $SiCl_4$ vapour and oxygen gas were entrained into a rotating high quality substrate tube (Heraeus F300). The $SiCl_4$ vapour was converted to partially sintered white particles or soot with the involvement of an external flame source which moved along the 0.5 m long substrate tube. During this process the temperature was controlled within the range of 1700-1750 °C. The thermophoretic process governed the deposition of the soot whereby a porous layer of soot was created. When the required thickness of the soot preform was reached, it underwent the solution doping process. At this point, the soot preform was soaked in a 1.5 M of Gallium (III) nitrate hydrate solution (Sigma-Aldrich 99.9%) Ga $(NO_3)_3.xH_2O$ diluted with an ethanol/H_2O mixture. After soaking and drying the soot preform with N_2 gas, standard MCVD process was carried out where oxidation, sintering and collapsing took place. Using a fibre draw tower, the optical fibre preform was then drawn into optical fibre.

In order to determine the elemental composition of Ga content in the core region of the fibre preform, Energy Dispersive X-ray spectroscopy (EDX) measurement was carried out. The results obtained at forty different points, where a distance of ~ 36.2 µm exists between two index points including the micrograph of the Ga-doped optical fibre are illustrated in Figure 3.6.

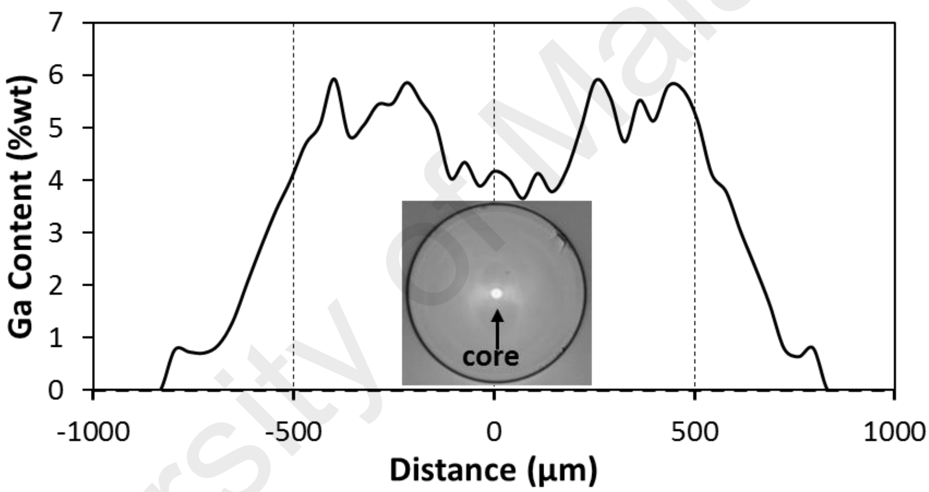

Figure 3.6: Ga content of the preform core at 40 different points with 36.2 µm distance between each point including the micrograph of the Ga-doped optical fibre where the arrow marks the position of the core. SiO_2-95 wt% Ga-5 wt%.

Figure 3.7 and 3.8 demonstrate the radial contour plots across the fibre cores from a grid 10 × 10 measurement. The Green contour represents the Ga concentration in wt%. The pattern shows that the Ga content starts to increase from 1 wt% up to 7.5 wt%. Since a comparison of gallosilicate fibre with germanosilicate fibre was intended to be carried out, an elemental analysis of the germanosilicate fibre was performed as well. The blue contour represents the Ge concentration in wt%. The pattern shows a more homogenous radial distribution of Ge.

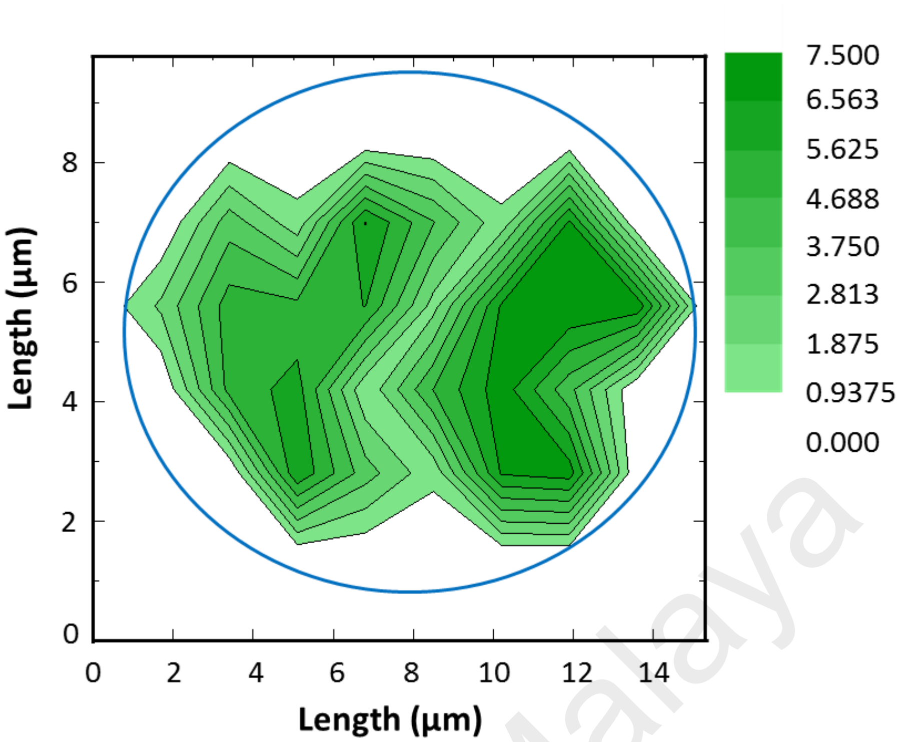

Figure 3.7: Radial contour plot of fibre elemental analysis and Ga distribution profile across the fibre core.

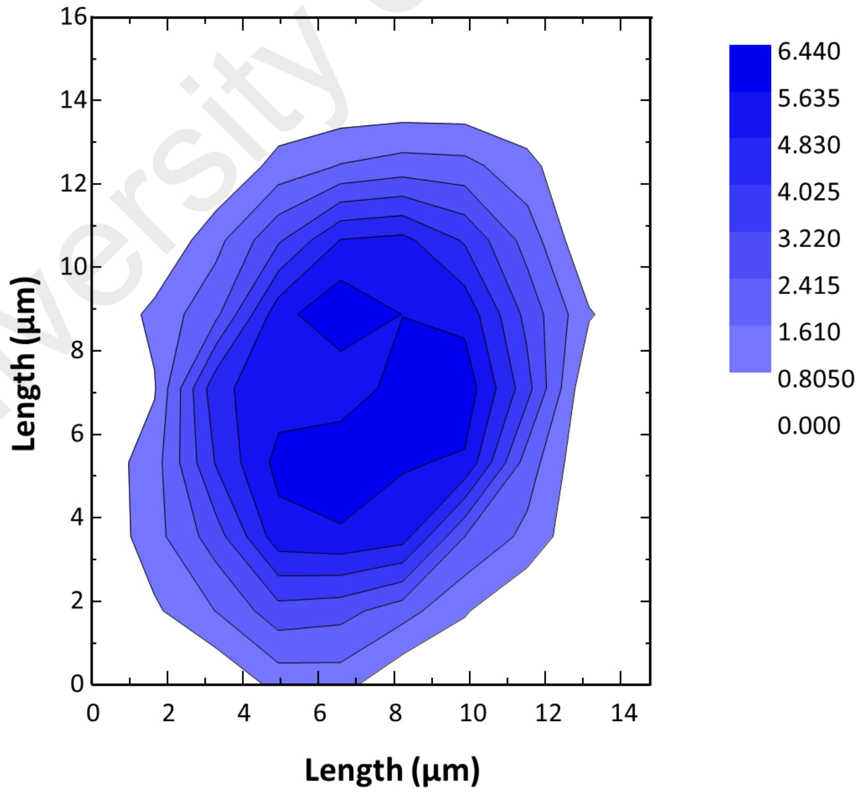

Figure 3.8: Radial contour plot of fibre elemental analysis and Ge distribution profile across the fibre core.

3.3.2 Grating inscription and index growth

Gratings with a grating length of 15 mm were inscribed in both commercially available germanosilicate single cladding optical fibre (5.5 wt% Ge concentration OFS Zero Water Peak Fibre) and Ga-doped single cladding optical fibre (5wt% Ga concentration). Phase-mask lithography together with a 193 nm ArF excimer was used for the inscription process. A pulse energy of 8 mJ (single pulse fluence of 640 mJ/cm^2) with a repetition rate of 4 Hz and 40 Hz was used during the fabrication procedure for H_2 loaded and H_2 free conditions respectively. The UV beam size was adjusted using a beam expander and the grating length was controlled at 15 mm by limiting the beam width with the aid of an adjustable vertical slit. The core, cladding diameters and the numerical apertures (NA) of Ga and Ge-doped optical fibres are listed in Table 3.1 below.

Table 3.1: Specification of Ga and Ge-doped optical fibres

Parameter	Ga-doped fibre	Ge-doped fibre
Core diameter	11.8 µm	8.2 µm
Cladding diameter	125 µm	125 µm
NA	0.15	0.13

An optical spectrum analyser (OSA) controlled by a LabVIEW program via a GPIB interface was used to monitor and record the transmission spectra. The laser irradiation on the fibre was controlled by an optical beam shutter with a close time duration of 4.08 s, which was useful in obtaining stable transmission spectra. Subsequently, the experiment was repeated using a 248 nm KrF excimer laser for comparison purposes.

Analysis of the recorded data was carried out to determine the refractive index changes of the fibres using the following relationship

$$\Delta n_{\text{mod}} = \frac{\lambda_C(F)\tanh^{-1}(\sqrt{R})}{\eta\pi L} \tag{3.2}$$

where Δn_{mod} denotes the index modulation, $\lambda_c(F)$ the centre wavelength as a function of F the fluence, R the grating reflectivity, η the mode overlap parameter and L the grating length (Ky et al., 1998). The mode overlap parameter can be expressed as

$$\eta = \frac{\pi^2 d^2 k^2}{\lambda^2 + \pi^2 d^2 k^2} \tag{3.3}$$

where d, k and λ indicate the fibre core diameter, the NA of the fibre and centre wavelength respectively. At both H_2 loaded and H_2 free conditions, the index changes were calculated with exposure to the two types of excimer lasers. Figure 3.9(a) demonstrates the refractive index changes in Ga-doped and Ge-doped optical fibres with exposure to ArF excimer laser. The influence of hydrogenation of the fibres was discovered by conducting a comparative study between a batch of H_2 loaded Ge and Ga-doped optical fibres with another batch of H_2 free fibres. For the H_2 free condition, Ga-doped optical fibres showed consistently higher refractive index changes compared to that of Ge-doped fibre and in the H_2 loaded scenario, Ga-doped fibre also indicated higher index changes in comparison to Ge-doped optical fibre at low fluence levels. The induced refractive index of Ga-doped optical fibre amounted to 6.72×10^{-5} in the absence of H_2 loading and 1.11×10^{-4} in the presence of H_2 loading.

A 3.7 times higher refractive index change is observed for H_2 loaded Ga-doped fibres at a moderate fluence level of 23 kJ/cm^2, compared to H_2 loaded Ge-doped optical fibres. According to Figure 3.9(b), in the ensuing inscription process with KrF excimer laser (single pulse fluence of 250 mJ/cm^2), a much higher refractive index change is observed for H_2 loaded Ge-doped optical fibres compared to H_2 loaded Ga-doped optical fibre. Therefore, it is understood that Ge-doped fibres remain the best preference for FBG fabrication using 248 nm KrF excimer laser compared to Ga-doped optical fibres. Such phenomenon can be explained with reference to the absorbance characteristics of the specific fibres.

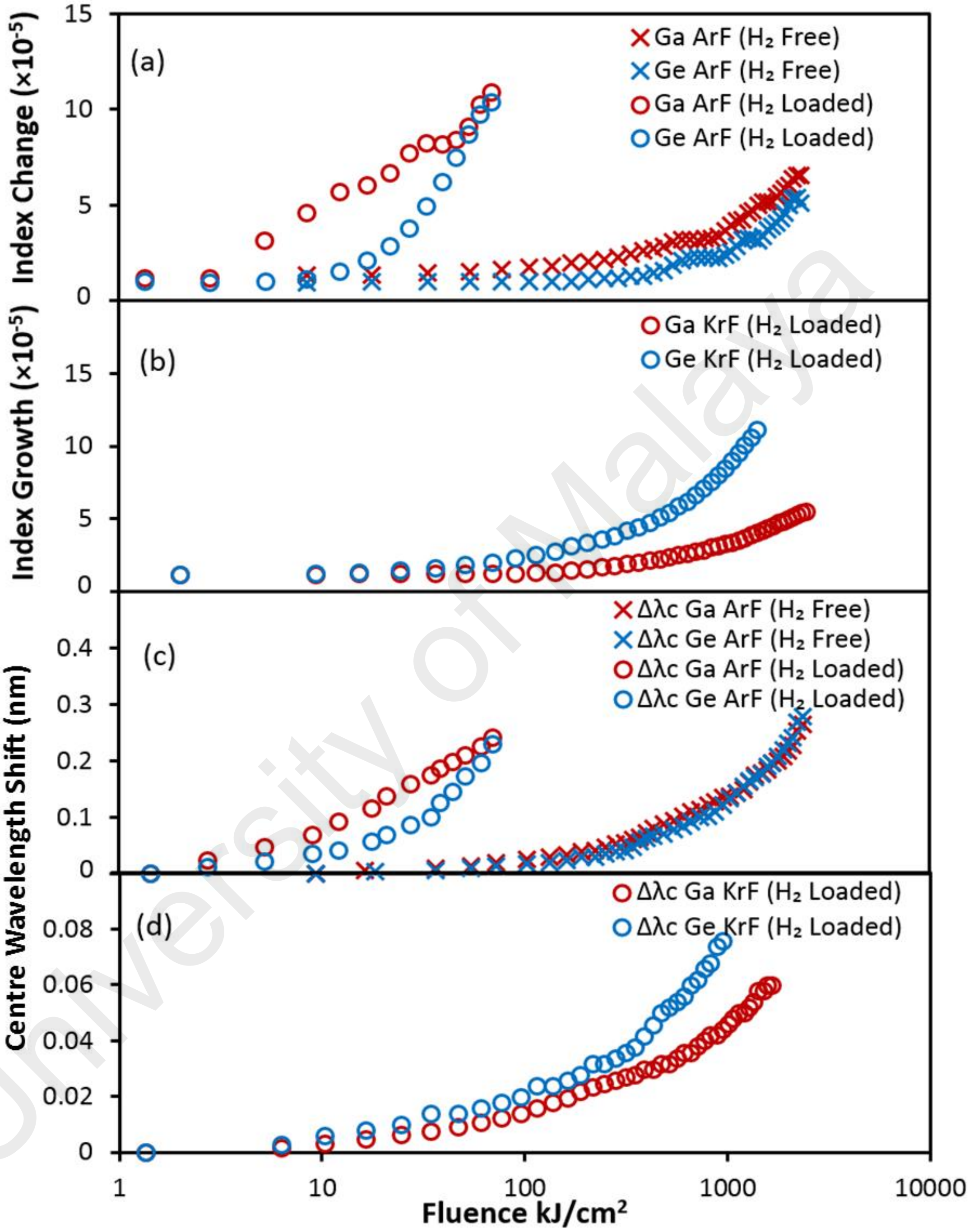

Figure 3.9: Optical properties of Ga-doped and germanosilicate optical fibres. (a) Index change at H_2 free and H_2 loaded conditions with ArF Excimer laser irradiation. (b) Index growth at H_2 loaded condition with KrF Excimer laser irradiation. (c) Centre wavelength shift at H_2 free and H_2 loaded conditions with ArF excimer laser irradiation. (d) Centre wavelength shift at H_2 loaded condition with KrF excimer laser irradiation.

The variation in the centre wavelength experienced by Ga and Ge-doped fibres, with increasing UV fluence at H_2 loaded and non-loaded conditions when subjected to ArF laser irradiation is illustrated in Figure 3.9(c). It is observed that at H_2 loaded and non-loaded conditions, both Ga and Ge-doped optical fibres exhibit a similar trend of progression. The same study was performed on Ga and Ge-doped optical fibres with KrF laser irradiation (see Figure 3.9(d)).

3.3.3 Structural analysis

3.3.3.1 UV spectroscopy

UV absorption measurements were carried out using a Perkin-Elmer Lambda 750UV-vis spectrometer on Ga and Ge-doped optical fibre preform slices before and after UV irradiation in order to clarify the differentiation in the response of the two types of fibres with exposure to ArF and KrF excimer lasers. Both sides of the fibre preform slices were UV irradiated with a 193 nm ArF excimer laser, for 2000 pulses with a pulse energy of 20 mJ at a 40 Hz repetition rate. Each side of the fibre preform slices were polished to optical quality prior to the measurement, to improve the light propagation.

From Figure 3.10, it is revealed that a considerable growth of UV absorption for both Ga and Ge-doped optical fibre preforms before UV irradiation occur below 330 nm with a strong tail existing in the longer wavelength region. In the case of the Ga-doped optical fibre preform, where Ga is doped into the SiO_2 glass as an index riser a UV absorption peak of 7.6 dB/mm is produced which is evidently much higher than the 5 dB/mm absorption peak at the 192-194 nm region in germanosilicate optical fibre preform before UV irradiation. Moreover, in the region of ~ 275 nm, another minor absorption peak is observed for both Ga and Ge-doped optical fibre preforms which results in a much higher absorption post UV irradiation.

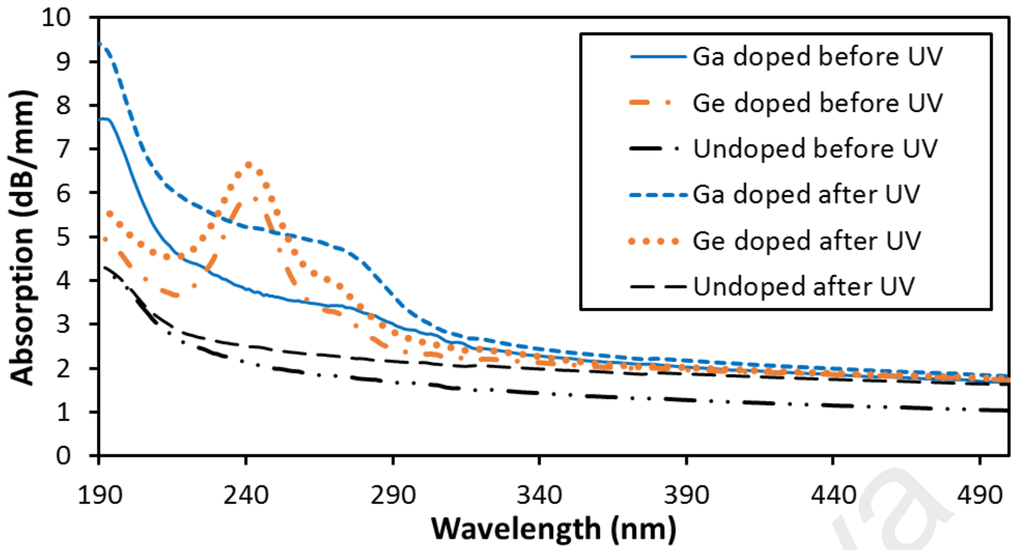

Figure 3.10: Growth of absorption in Ga and Ge-doped core with respect to undoped glass (cladding).

It is further inferred from Figure 3.10, that an increase in the absorption is observed for both Ga and Ge-doped optical fibre preforms after UV irradiation. In the Ge-doped fibre preform, the formation of GeE′ centres is considered to be the reason behind the absorption band peaking at ~193 nm (Hosono, Mizuguchi, Kawazoe, & Nishii, 1996). In addition, the Ge-doped optical fibre preform exhibits another absorption peak centred at 240-242 nm region which is due to the Ge related oxygen deficient centre (GODC). The presence of these absorption bands explains the findings in Figure 3.9(a) and Figure 3.9(b) where ArF excimer laser yielded higher refractive index changes for Ga-doped optical fibre compared to that of Ge-doped fibre whereas the exact opposite is observed during grating inscription using KrF excimer laser. Thus, Ga-doped optical fibres therefore appear to be a better choice for grating inscription using 193 nm ArF excimer laser.

3.3.3.2 Photoluminescence spectroscopy

The photoluminescence properties of a slice of Ga-doped preform sample of 2.4 mm thickness were investigated. When exposed to ArF laser irradiation, a broad blue-green emission band in the 450 nm-600 nm wavelength region was observed for the Ga-doped preform sample as shown in Figure 3.11. The blue emission can be ascribed to the electron-hole recombination, where the electron from oxygen vacancy or Gallium centre combines with a hole in a Gallium ion vacancy. However, direct interpretations cannot be drawn on the existence of the green luminescence (Harwig & Kellendonk, 1978; N. H. Kim, Kim, & Lee, 2004). The photoluminescence characteristics of Ga-doped silica have been analysed by Barsanti, Cannas, and Bicchi (2007).

In a similar manner, the photoluminescence characteristics of Ge-doped fibre preform used in the current experiment was also analysed. A violet-blue emission peak at 400 nm was discovered as indicated in Figure 3.11. This intense luminescence band peaking at 400 nm is considered as the fingerprint of Ge related defects and is attributed to the germanium luminescence centre which is coordinated in a two-fold manner (Allard, Albert, Brebner, & Atkins, 1997; Skuja, Trukhin, & Plaudis, 1984).

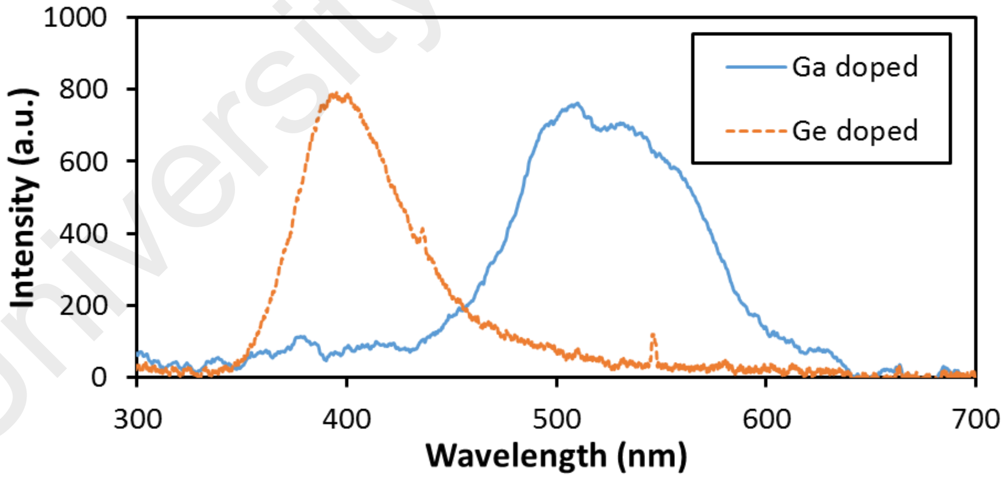

Figure 3.11: Photoluminescence spectra of Ga-doped and Ge-doped optical fibre preforms excited by 193 nm laser.

3.4 Grating Characterisation

3.4.1 Interference and grating visibilities

Grating formation in an optical fibre is attained by positioning the fibre in the field of interference where the interference pattern is imprinted in the fibre by virtue of a UV-induced index change. The interference fringe visibility is expressed by

$$v_i = \frac{I_{\max} - I_{\min}}{I_{\max} + I_{\min}} \tag{3.4}$$

where $I_{\max}$ and $I_{\min}$ refer to the intensity levels occurring at the constructive (bright fringes) and destructive positions (dark fringes) of the interference (Huebner et al., 1997). Maximum interference visibility (v_i = 1) is achieved through ensuring equal intensity between the two beams, which leads to a complete destructive superposition ($I_{\min}$ = 0). In comparison to the expression of v_i, the grating visibility v_g is denoted as

$$v_g = \frac{\Delta n_{\max} - \Delta n_{\min}}{\Delta n_{\max} + \Delta n_{\min}} \tag{3.5}$$

where $\Delta n_{\max}$ and $\Delta n_{\min}$ are the maximum and minimum local refractive index changes in the grating. The grating visibility is assumed to be 1 in some literatures for simplicity of analysis (Erdogan, 1997; Ky et al., 2003). In real scenarios ($v_i < 1$ and $v_g < 1$), higher UV fluence is necessary in the development of an FBG which consists of an equivalent grating strength. The grating strength ($\delta n/n$) of a Bragg grating can be explained with reference to its refractive index perturbation (δn) and the modal index (n) (Hill & Meltz, 1997). This results in a much higher average refractive index change and a shift in Bragg wavelength. Such a phenomenon can be explained using the linear relation in Eq. (2.21) introduced in Chapter 2, where σ is responsible for Bragg wavelength shift and κ is accountable for the growth of grating reflectivity (Erdogan, 1997).

An accurate control of the etched depth *d*, in the design of ±1st order diffraction phase-mask is essential in order to obtain the least intensity of the zeroth order. This ensures optimal and uniform fringe visibility across the interference field distribution. The optimum etched depth *d* is given by

$$d(n_{uv}-1)=\frac{\lambda_{uv}}{2} \tag{3.6}$$

where n_{uv} is the refractive index of the phase-mask and λ_{uv} is the wavelength of the UV source (Kashyap, 1999, p. 60).

Due to the high production efficiency and reliability, the technique of excimer laser irradiation along with the phase-mask is the favoured choice for the fabrication of gratings in fibres (Herbst & Govorkov, 2003). The significance of enhancing the interference visibility has been realised by Dyer, Farley, and Giedl (1995). During grating inscription, spatial and temporal coherences of the excimer laser are some of the key factors to be considered (Othonos & Lee, 1995). In the execution, to obtain the maximum interference visibility, the optical fibres were placed closely or sometimes in contact with the phase-mask. Nevertheless, such restrictions can be diminished through the use of a laser with smaller line width and beam divergence.

It has been realised that apart from the irradiation wavelengths (Chen, Herman, Taylor, & Hnatovsky, 2003; Zhang, Herman, Lauer, Chen, & Wei 2001) and various types of dopants (Brambilla et al., 2000; Ghosh et al., 2011; Shen, Xia, Sun, & Grattan, 2004), the photosensitivity of an optical fibre can be influenced by the single-pulse-fluence (Zhang et al., 2001) as well. Low single-pulse-fluence is capable of resulting in a higher index change in an optical fibre compared to high single-pulse-fluence, regardless of the fact that the fibres are irradiated with an equivalent cumulated fluence. The phenomenological model has been proposed for the investigation of UV-induced index change when analysing the grating formation (Chen et al., 2003; Zhang et al., 2001).

Clearly, interference visibility is a prime factor which influences the grating visibility and grating strength of an FBG. However, the limited amount reported in the literature on their association with and significance on the performance of the gratings, make it an aspect to be further explored as demonstrated in Section 3.4.2.

3.4.2 Characterisation of phase-mask interference visibility and the evolution of grating visibility during grating inscription

During the inscription process, a KrF excimer laser was employed and for the convenience of investigation, a uniform grating structure was chosen. Initially, the laser beam was expanded horizontally from ∼0.6 to ∼4.5 cm with the aid of a Keplarian expander assembled from two cylindrical lenses. A tuneable vertical slit was incorporated to restrict both tails of the Gaussian beam to create a small (0.5 - 2.5 cm) flat top beam. The vertical beam divergence was reduced through gradual alteration of the position of one of the lenses, in the effort to optimise the interference visibility. In order to achieve optimum interference visibility, the fibre was placed as close as possible to the phase-mask. When the thicknesses of the coating and cladding were taken into account, the closest separation between the phase-mask and the fibre core centre was recorded as ~ 123 μm. The FBG transmission spectra were recorded and monitored with the involvement of an Optical Spectrum Analyser (OSA, Ando AQ6331) controlled by a LabVIEW program via a GPIB interface during the FBG inscription process. λ_C and R were acquired from the recorded transmission spectra, and used to determine Δn_{ave} and Δn_{mod} based on Eq. (3.7) and (3.2).

$$\Delta n_{ave} = \frac{\lambda_C(F)n_{eff}}{(\lambda_D - 1)\eta} \tag{3.7}$$

Figure 3.12(a) demonstrates the growths of Δn_{ave} and Δn_{mod} for a grating inscribed in FUD-2300 (Nufern) photosensitive fibre as a function of F, the fluence. It is noticed that both Δn_{ave} and Δn_{mod} originate from the same value during the growth of index change at the early stage of grating inscription. Subsequently, Δn_{ave} outgrows Δn_{mod} as the grating inscription process continues. Figure 3.12(b) shows the results of Δn_{max} and Δn_{min} obtained using Eq. (3.8) and (3.9) below.

$$\Delta n_{\max} = \Delta n_{ave} + \Delta n_{\mathrm{mod}} \tag{3.8}$$

$$\Delta n_{\min} = \Delta n_{ave} - \Delta n_{\mathrm{mod}} \tag{3.9}$$

For ease of demonstration, let [F, Δn_{max}] and [F, Δn_{min}] designate the coordinates of the two sets of data in the graph. The data sets of [F, Δn_{max}] and [F, Δn_{min}] can be accurately fitted with curves of Δn [$(1 + v_i)F$] and Δn [$(1 - v_i)F$] by altering the value of v_i, represented by the red and blue dotted curves in Figure 3.12(b). Both these functions are derived from the same equation $\Delta n[F]$ indicated by the grey dotted curve in the same figure. The best fit value for v_i was 0.89. The measurement of v_i can be carried out using another approach where the array F of Δn_{max} and Δn_{min} is multiplied by a factor of $(1 + v_i)$ and $(1 - v_i)$ respectively to remove these factors in Δn_{max} and Δn_{min}.

Therefore, both curves are translated to the new coordinates, [$(1 + v_i)F$, Δn_{max}] and [$(1 - v_i)F$, Δn_{min}] where they overlap with each other near the curve of $\Delta n[F]$. This technique is referred to as the curve-matching technique (see Figure 3.12(c)). The information of grating visibility v_g can be deduced by referring to the data of Δn_{ave} and Δn_{mod} presented in Figure 3.12(a). It is assumed that v_g commences with a similar value to v_i at the start of the grating fabrication process. The selection of λ_D for Eq. (3.7) helps in obtaining this parameter. The grating visibility initiates with ~0.89 and gradually decays with increasing cumulated fluence as shown in Figure. 3.12(d).

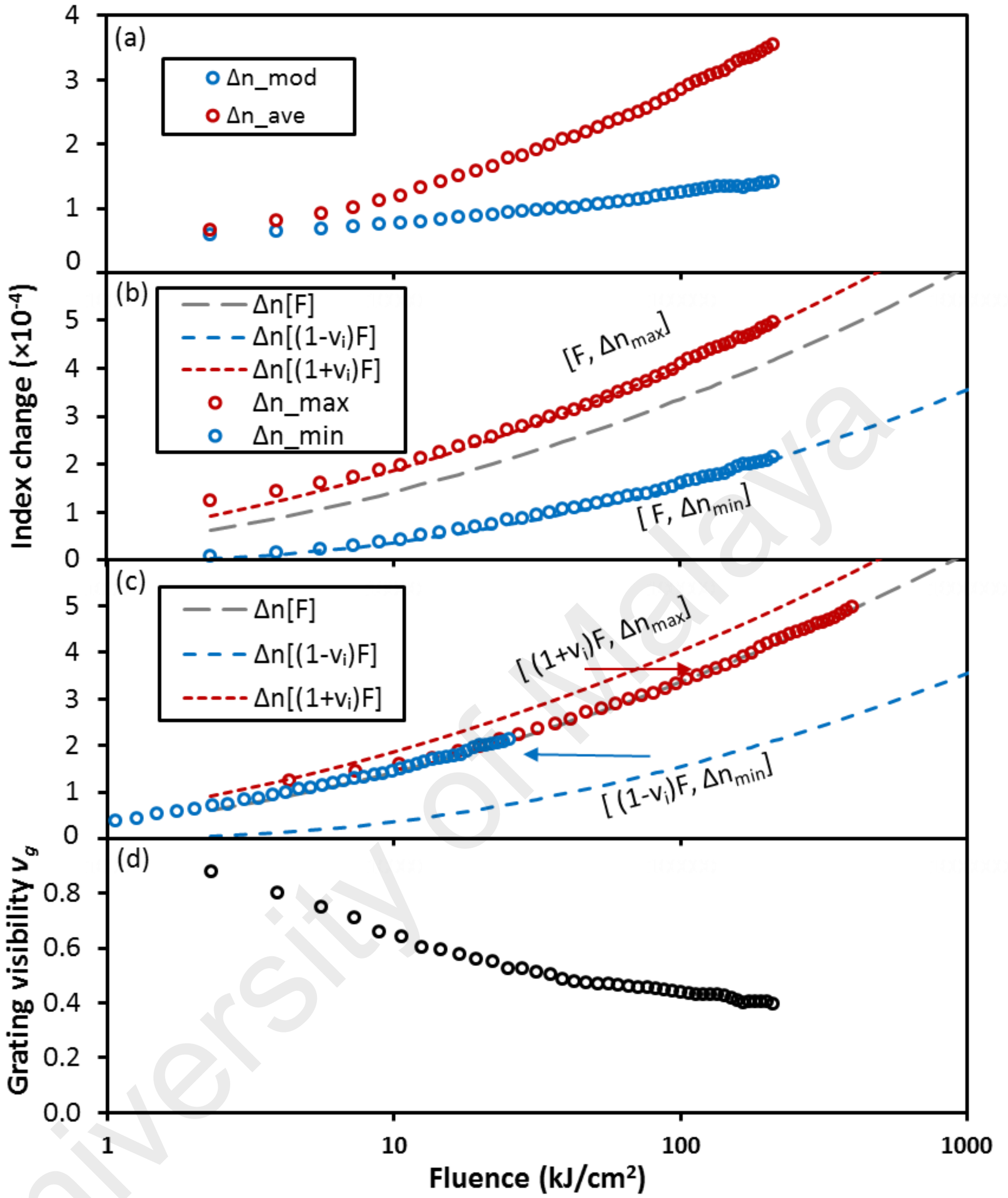

Figure 3.12: Dynamics of (a) Δn_{ave} and Δn_{mod}, (b) Δn_{max} and Δn_{min} as a function of cumulated fluence F. The dotted curves depict the phenomenological functions $\Delta n\,[(1 + v_i)F]$ (blue) , $\Delta n[(1 - v_i)F]$ (red) and $\Delta n[F]$ (grey). (c) The data points of Δn_{max} and Δn_{min} are shifted to the new coordinates of $[(1 + v_i)F, \Delta n_{max}]$ and $[(1 - v_i)F, \Delta n_{min}]$ and they overlap with the curve of $\Delta n[F]$. (d) Variation of v_g during grating inscription process (Lim et al., 2015).

At F=192 kJ/cm^2, it reaches a value of ~0.36. This particular degradation does not reflect any decay in terms of grating strength during the inscription procedure. For an efficient inscription process, achieving a high grating visibility with longer tolerance during the fabrication procedure is beneficial. Apart from the estimation of the interference visibility, the curve-matching technique discussed in this chapter can also be incorporated in assessing the quality and effectiveness of the fabrication system.

Figure 3.13 demonstrates the measured interference visibility with varying fibre-phase-mask distance. It is observed that at further distances, the interference visibility diminishes possibly due to the restricted coherence length.

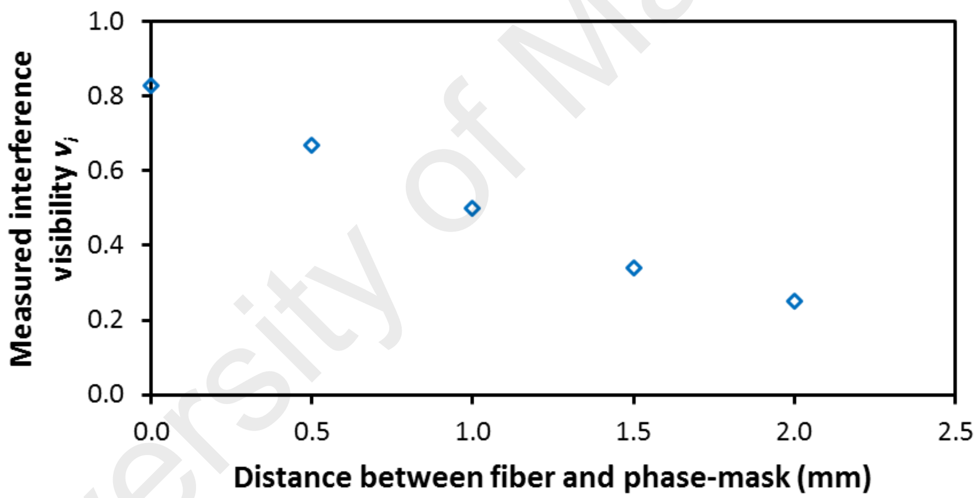

Figure 3.13: Variation of measured interference visibility at different fibre-phase-mask distances (Lim et al., 2015).

Figure 3.14(a) and 3.14(b) indicate the growth of Δn_{max} and Δn_{min} when subjected to different single-pulse-fluence F, values of 13 J/cm², 39 J/cm² and 52 J/cm² but with equivalent interference visibility (v_i = ~0.85). Based on the comparison, it is observed that a higher index growth rate (per unit fluence) is produced by a lower single-pulse-fluence. Moreover, a similar value for Δn_{max} and Δn_{min} is reached at a less total amount of fluence referred to as cumulated fluence. In addition, the decreased index growth caused by the high single-pulse-fluence can be due to the laser damage and the occurrence of opacity inside the fibre as a result of the high laser pulse energy (Chen et al., 2003).

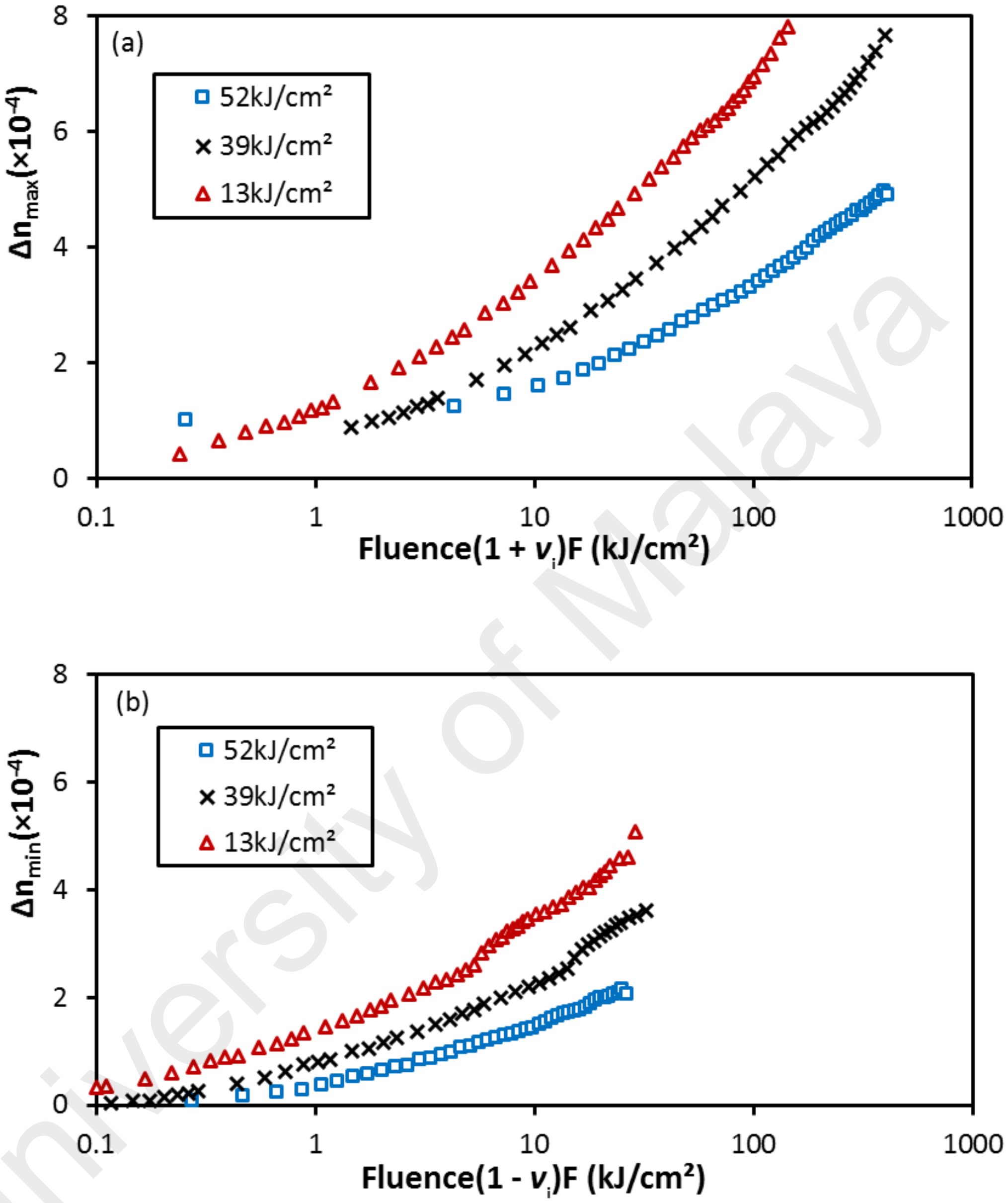

Figure 3.14: Growth of Δn_{max} and Δn_{min} based on different single-pulse-fluences F = 13 J/cm² (Δ), 39 J/cm² (×) and 52 J/cm² (□). v_i= ~0.85 (Lim et al., 2015).

The characteristics during the grating inscription process are shown in Figure 3.15 with an extended UV fluence level up to 1.88 MJ/cm². Based on Figure 3.15(a), it is observed that Δn_{mod} attains its maximum at position A.

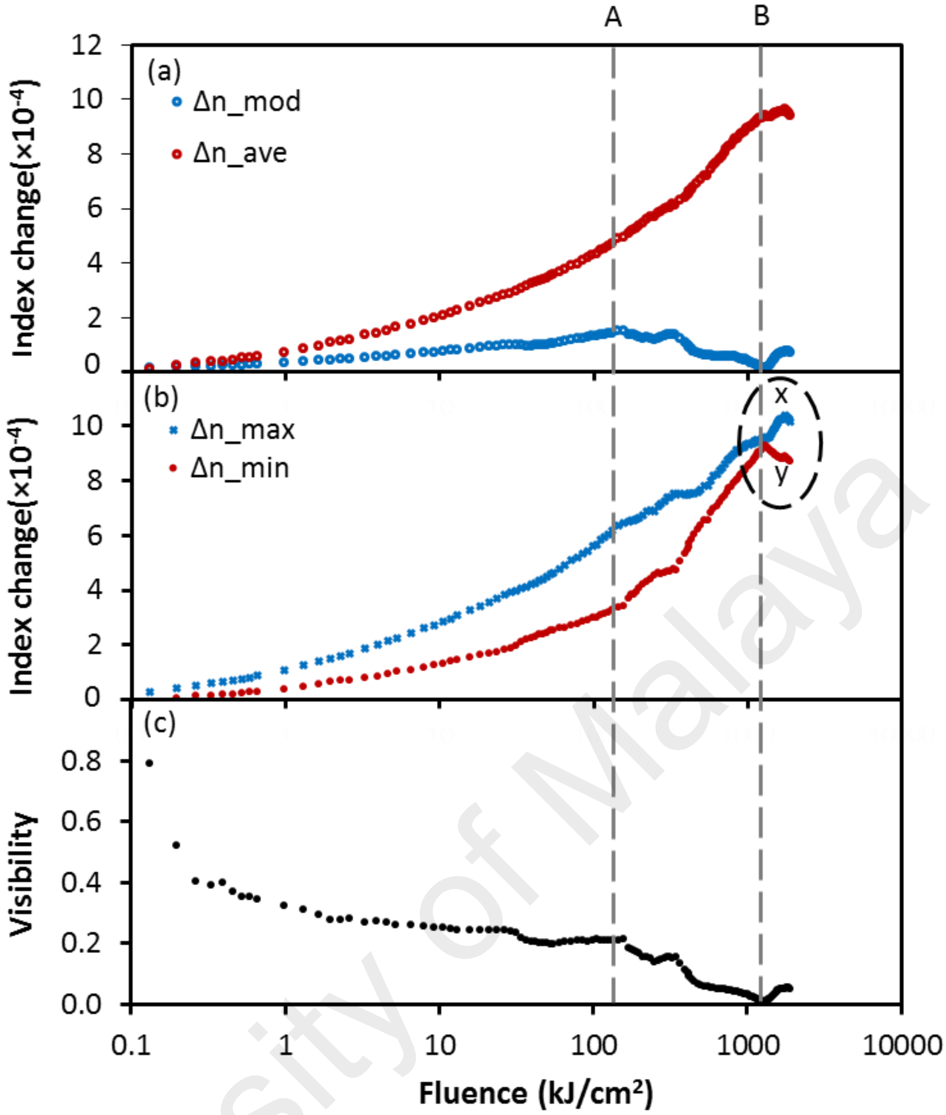

Figure 3.15: Evolution of grating inscription with extended cumulated fluence. (a) Δn_{ave} and Δn_{mod}, (b) Δn_{max} and Δn_{min} and (c) grating visibility as a function of cumulated fluence F (Lim et al., 2015).

At this point, an accelerated variation in the growth direction of Δn_{max} occurs whereas a continuous increase in the growth rate of Δn_{min} is noticed (see Figure 3.15(b)). At B, both Δn_{max} and Δn_{min} intersect with each other and at which point Δn_{mod} reaches its minimum value before it increases again. From the findings of Figure 3.14, it is understood that different growth rates and responses may be produced by the index changes of Δn_{max} and Δn_{min} which occur in bright and dark fringes. At ~1.28 MJ/cm^2, Δn_{ave} turns to be stagnant, at which point Δn_{mod} has reached minimum. Since Δn_{mod} is an absolute value, this leads to a miscalculation of Δn_{max} and Δn_{min} after position B. Subsequently, Δn_{max} continues to increase, as indicated by X and Δn_{min} begins to plummet as indicated by Y.

3.4.3 Measurement of grating visibility via bent-spectral analysis

The experiment discussed in this section consists of two stages. Firstly, the FBGs were fabricated using the excimer-phase-mask technique. During fabrication, the size of the UV beam was set to 2 cm with the aid of a beam expander and the grating length was adjusted with an adjustable vertical slit. A UV pulse energy in the range of 10-20 mJ and a repetition rate of 2 Hz were used in this experiment. During grating formation, a similar procedure was followed as discussed in the previous section to record the transmission spectra. Grating and interference visibilities after FBG inscription were determined by analysing the data obtained during the grating growth process. These results were useful in the estimation of the grating visibility value which will subsequently be compared with that after the bending process.

Secondly, the FBG was recoated using a UV curable acrylate to increase the flexibility of the fibre so that the fibre can be bent to achieve small bending radii limiting the breakage of the fibre. The fibre was bent into a knot without the use of any additional tool, which was a complete circle consisting of a 360º bending angle as demonstrated in Figure 3.16. This technique was helpful in keeping the fibre stable for a long period of time throughout the experiment (Lim et al., 2013). Furthermore, it also allowed a longer fibre length to be accommodated in the knot when compared with the calipers technique (Marcuse, 1976) which allows a bend length of only πR. Therefore, the experimental setup was not disturbed in any circumstance when the reading at each decreasing bending radius was recorded. Gradually, the bending radius was decreased until the fibre reached its saturation level (the critical bend radius) and the corresponding transmission spectra were recorded. The recorded data was used to calculate the grating visibility of the bent FBG.

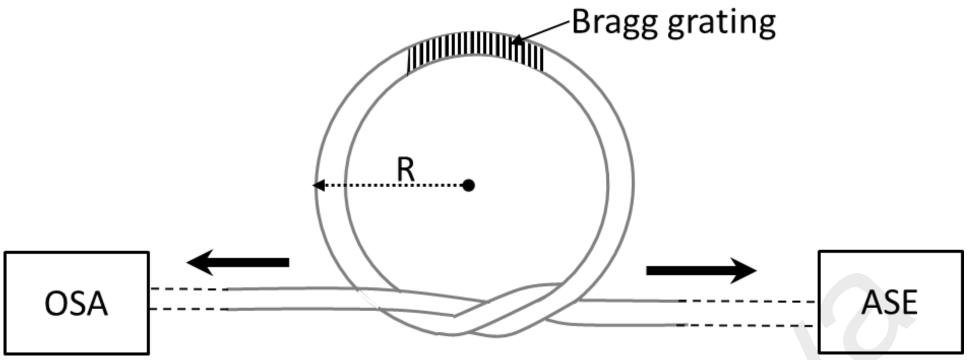

Figure 3.16: Schematic experimental setup for the proposed FBG bending technique. OSA: Optical Spectrum Analyser, ASE: Amplified Spontaneous Emission Source.

3.4.3.1 Mathematical model for the bent-spectral analysis technique

Coupled-mode equations (Erdogan, 1997) can be used to explain the wave characteristics of a bent FBG. The coupling coefficients and attenuation constant are affected by the bending process. Therefore, the modified coupled-mode equations can be expressed as (Lim et al., 2013)

$$\frac{dA(z)}{dz} = (-\alpha + j\hat{\sigma})A(z) + j\kappa B(z) \tag{3.10}$$

$$\frac{dB(z)}{dz} = (\alpha - j\hat{\sigma})B(z) - j\kappa^{*} A(z) \tag{3.11}$$

where $A(z)$ and $B(z)$ denote the forward and backward propagating wave amplitudes and α the new field amplitude attenuation constant. The coefficients of the coupled-mode equations are described as

$$\hat{\sigma} \equiv \delta + \sigma \tag{3.12}$$

$$\delta \equiv 2\pi n_{eff}(1/\lambda - 1/\lambda_B) \tag{3.13}$$

$$\sigma = \frac{2\pi\varepsilon\overline{\delta n}}{\lambda} \tag{3.14}$$

$$\kappa = \kappa^* = \pi\upsilon\varepsilon\overline{\delta n}/\lambda \tag{3.15}$$

where σ represents the "dc" coupling coefficient, κ the "ac" coupling coefficient, n_{eff} the effective refractive index of the fibre, λ_B the design Bragg wavelength, $\overline{\delta n}$ the index modulation amplitude and υ the visibility of the index modulation. ε, the relative coupling factor which is a function of the bending radius R, takes a value between 0 and 1. When the fibre is straight, R is assumed to be infinitely large. When the index modulation amplitude, coupling coefficients and attenuation along the fibre are assumed to be constant, solutions for coupled-mode equations can be achieved depending on the boundary conditions, $B(L_g) = 0$ and $A(0) = 1$. Hence, the amplitude reflection function and the transmission function are derived as

$$\rho = B(0)/A(0) = \frac{j\kappa\sinh(\gamma L_g)}{\gamma\cosh(\gamma L_g) - \phi\sinh(\gamma L_g)} \tag{3.16}$$

$$\tau = A(L)/A(0) = \frac{\gamma}{\gamma\cosh(\gamma L_g) - \phi\sinh(\gamma L_g)} \tag{3.17}$$

where

$$\gamma \equiv \sqrt{\phi^2 + \kappa^2} \text{ and } \phi \equiv -\alpha_{BC} + j\hat{\sigma} \tag{3.18}$$

and L_g denotes the length of the FBG. In the case of an unbent and a lossless grating ($\alpha_{BC} = 0$ and $\varepsilon = 1$), the reflectance and transmittance functions turn out to be similar to the ones discussed by Erdogan, 1997. At the centre wavelength of the FBG spectrum,

$$\hat{\sigma} = 0 \tag{3.19}$$

and

$$\lambda_{centre} = (1 + \varepsilon\overline{\delta n} / n_{eff})\lambda_B \tag{3.20}$$

$$\lambda_{centre}(R = \infty) = (1 + \overline{\delta n} / n_{eff})\lambda_B \tag{3.21}$$

The minimum transmission at this point can be calculated with reference to Eq. (3.17) which results in

$$\tau(\lambda_{centre}) = \frac{\gamma}{\gamma\cosh(\gamma L_g) + \alpha_{BC}\sinh(\gamma L_g)} \tag{3.22}$$

The background transmission at wavelengths which are away from the λ_{centre} is expressed as

$$\tau_{background} = \exp(-\alpha_{BC} L_g) \tag{3.23}$$

and the Bragg transmission depth (BTD) is given by

$$\begin{aligned} BTD &= 20\log_{10}(\tau_{background} / \tau(\lambda_{centre})) \\ &= 20\log_{10}\left[\exp(-\alpha_{BC} L_g)\left\{\cosh(\gamma L_g) + \frac{\alpha_{BC}\sinh(\gamma L_g)}{\gamma}\right\}\right] \end{aligned} \tag{3.24}$$

The BTD is equivalent to the original reflectivity of the grating in dB in the presence of bending loss ($\alpha_{BC} = 0$) and when the coupling coefficient ε = 1, in the case of a straight grating. This means that the BTD can be referred to as the grating strength which degenerates when the bending radius is decreased.

3.4.3.2 Grating inscription and visibility analysis

This section describes the effect of the grating and interference visibilities which are considered as important parameters when analysing the properties of a bent FBG. In an ideal scenario, both interference and grating visibilities are unity, but it is practically challenging due to several factors such as: unsuppressed zeroth order, low spatial and spectral coherences. The ultimate intention of this approach is to estimate the grating visibilities of the fibre after the grating inscription and bending processes.

The FBGs used in this experiment were fabricated in low bending loss photosensitive fibres (Nufern FUD-2300) with the employment of a KrF excimer laser and phase-mask method as shown in Figure 2.9. The UV beam was divided into two components which eventually recombined creating an interference pattern. Enhanced spatial coherence length of the excimer laser provided an interference field with good contrast behind the mask. The gratings were formed in the fibre by exposing it to the overlapping zone of the two beams. The parameter v_i was predicted in such a way, that it was almost equal to the initial grating visibility value v_g of the fibre which was similar to the ideal grating visibility value. In order to obtain accurate values for v_g and v_i, low single-pulse energy was used particularly at the beginning of the FBG inscription process, so that the BTD induced by the first pulse fluence was small and that the design wavelength of the FBG could be accurately estimated.

FUD-2300 fibre Bragg gratings consisting of different reflectivity values were fabricated to investigate the influence on the grating visibilities. Figure 3.17 illustrates the transmission spectra of a grating inscribed in FUD-2300 fibre. It is observed that each of the subsequent transmission spectra red shifts implying that the centre wavelength and the BTD of the grating gradually increase with increasing fluence. The grating whose transmission spectrum is shown in Figure 3.17 indicates a BTD of 23.9 dB. Figure 3.18

indicates the linkage of the centre wavelength and the BTD against increasing fluence of a grating inscribed in FUD-2300 fibre. Both centre wavelength and BTD show similar trends of progression. The gradual increase of the two parameters, BTD and centre wavelength is due to the increment of the "ac" and "dc" coupling of the fibre. With reference to Eq. (3.20), it can be explained that λ_{centre} can be influenced by bending due to its relationship with the relative coupling coefficient of the fibre.

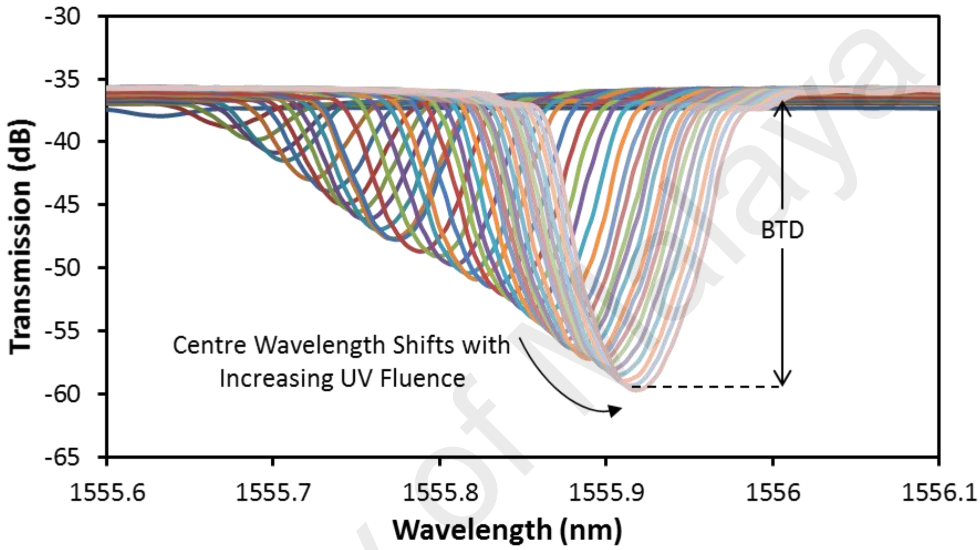

Figure 3.17: Transmission spectra of a 2 cm long grating written in FUD-2300 fibre.

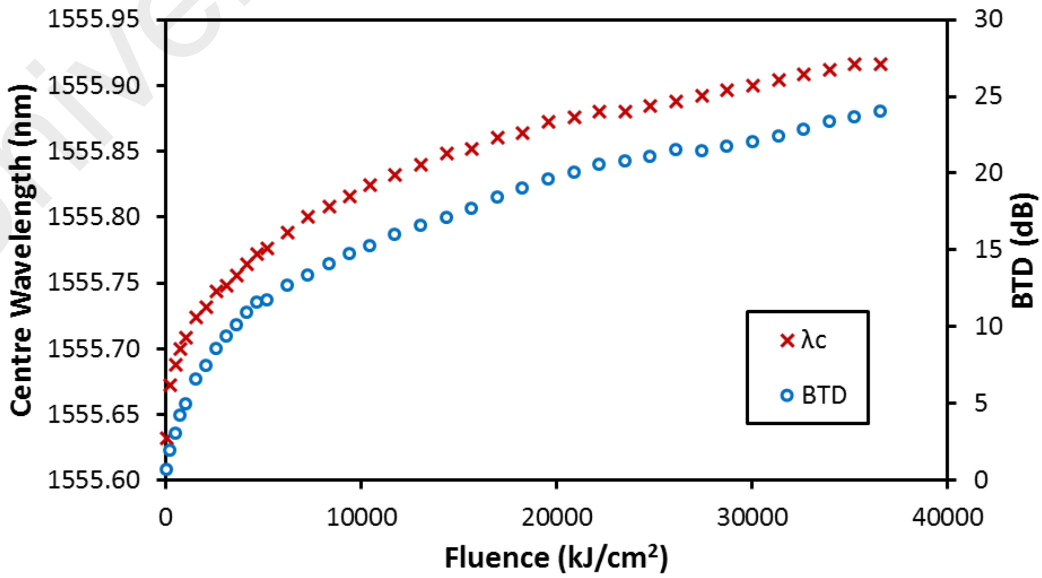

Figure 3.18: Overlaid graph of centre wavelength shift and variation of BTD with increasing UV fluence.

Figure 3.19(a) shows two functions Δn_{ave} and Δn_{mod} which are represented in terms of UV fluence. These two functions initiate from the same value at the commencement of the grating inscription process and eventually Δn_{ave} deviates from Δn_{mod} as the UV fluence increases. Figure 3.19(b) indicates the functions of Δn_{max} and Δn_{min}. Similar to the procedure proposed in section 3.4.2, the array F of these two functions was subsequently multiplied by the factors $(1 + v_i)$ and $(1 - v_i)$ respectively (Figure 3.19(c)) where v_i lies within the range of 0 and 1. The best fit value for v_i was obtained as 0.86.

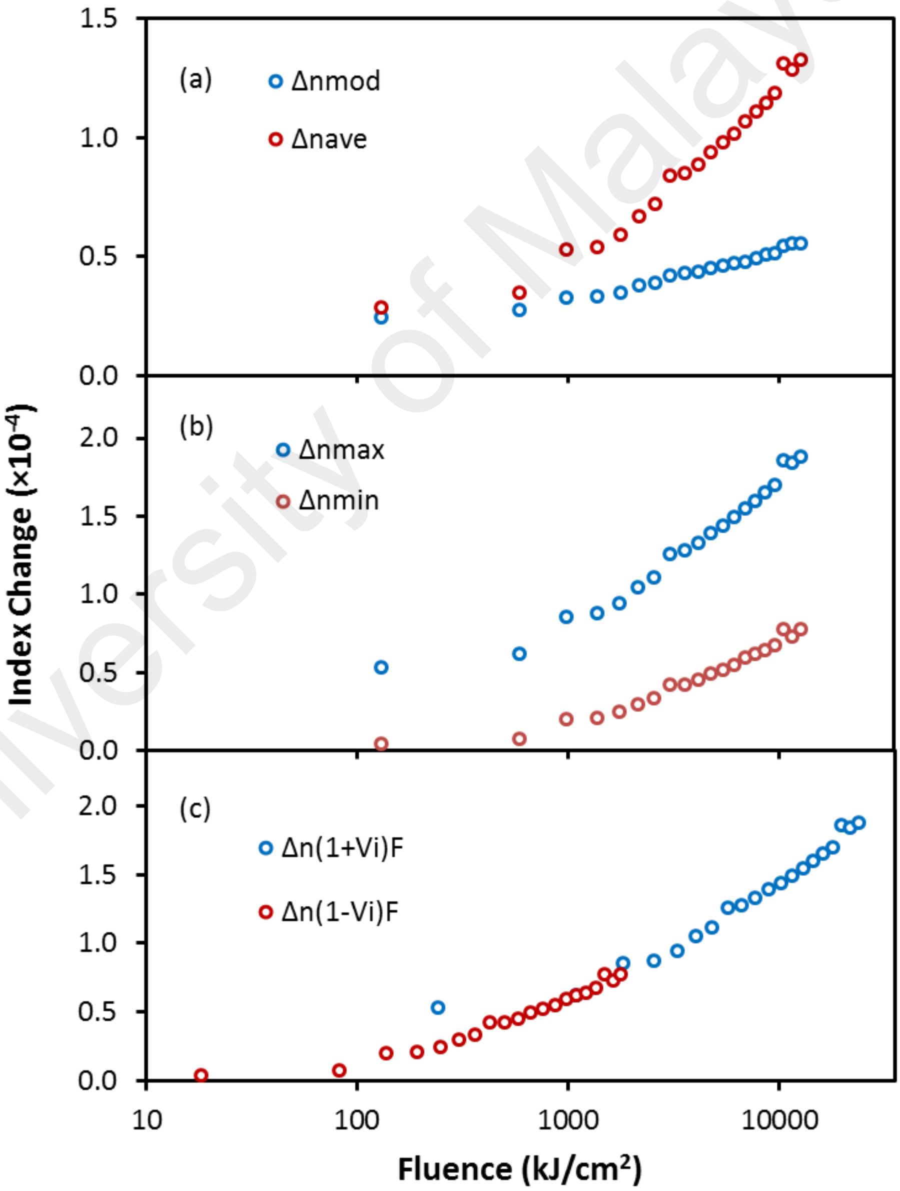

Figure 3.19: (a) Growth of Δn_{ave} and Δn_{mod}, (b) Δn_{max} and Δn_{min} represented as a function of cumulated fluence F. (c) The points of Δn_{max} and Δn_{min} are moved to the new points $\Delta n[(1+v_i)F]$ and $\Delta n[(1-v_i)F]$.

The grating visibility of the FBG gradually drops as shown in Figure 3.20 with increasing UV fluence. It initiates at 0.86 and decays to a value of 0.37 at the end of the fabrication process. The index modulation, Δn_{mod} (Figure 3.19(a)) is directly associated with the grating strength.

During the grating inscription process, the Bragg wavelength red-shifts as a result of the increase in Δn_{ave} and the BTD also increases due to the increase in Δn_{mod}. At the start of the grating fabrication procedure, Δn_{ave} increases and gradually slows down compared to that of Δn_{mod}. With reference to Eq. 3.5, this leads to a decrease in the grating visibility value with increasing UV fluence. The gradual decrease of the grating visibility is closely associated with Δn (Ramecourt, Niay, Bernage, Riant, & Douay, 1999).

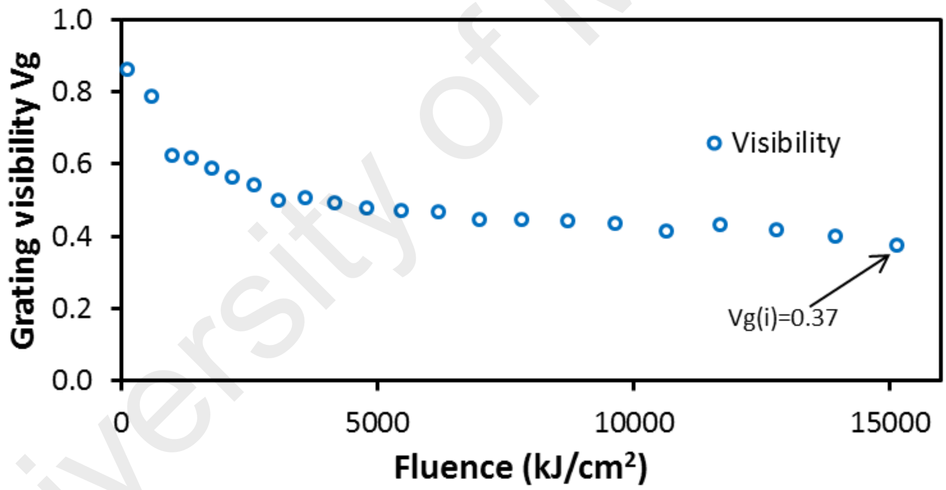

Figure 3.20: Variation of the grating visibility during FBG inscription process.

3.4.3.3 Determination of grating visibility via bending

After the inscription process, the bending investigation was carried out to analyse the spectral response of the FBG. Figure 3.21 presents the transmission spectra of the FBG at different bending radii in the range of 0.55 – 1.5 cm.

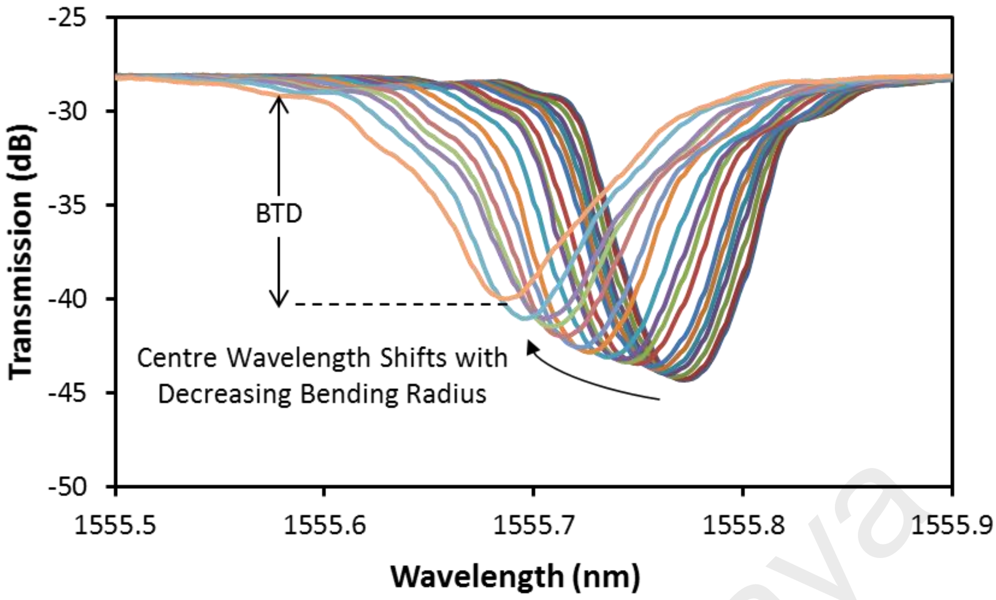

Figure 3.21: Transmission spectra of an FBG inscribed in FUD-2300 at decreasing bending radii.

The centre wavelength and the BTD of the spectra gradually decrease which is the exact reverse behaviour of Figure 3.17. Even though the shift in the centre wavelength is approximately 0.1 nm in FUD-2300 FBG, a significant change is visible in the BTD. The reason behind this decrease is the increased bending loss which takes place with decreasing bending radius. It is observed in several studies that higher bend losses in different fibres result in larger changes in BTD (Thompson, Cadusch, Robertson, Stoddart, & Wade, 2012; Wade, Robertson, Thompson, & Stoddart, 2011).

The equation below can be derived from Eqs. (3.20) and (3.21) as

$$1-\eta=\frac{(1-\varepsilon)\overline{\delta n}}{n_{eff}} \tag{3.25}$$

when $n_{eff} >> \overline{\delta n}$.

Furthermore,

$$\eta=(\lambda_{centre}(R))/(\lambda_{centre}(R=\infty)) \tag{3.26}$$

The values of LHS of Eq. (3.25) were calculated using the data of centre wavelengths while the RHS of Eq. (3.25) were calculated using the BTD data. In order to acquire the best fitting graph of these two functions, the visibility value was adjusted until the curves of the functions overlapped with each other and the optimum cross correlation coefficient was achieved. The cross correlation coefficient can be computed with

$$\rho = \frac{\frac{1}{K+1}\Sigma(x-\bar{x})(y-\bar{y})}{\sqrt{\frac{1}{K+1}\Sigma(x-\bar{x})^2 \frac{1}{K+1}(y-\bar{y})^2}} \tag{3.27}$$

where x and y represent the data of LHS and RHS of Eq. (3.25). $\bar{x}$ and $\bar{y}$ denote the respective mean values and the summations $\sum$ are taken over a segment of length K+1 (Aarts, Irwan, & Janssen, 2002). Afterwards, the grating visibilities before the bending process, $v_{g(i)}$ and after the bending process, $v_{g(b)}$ were compared and analysed. It is observed that the final value of $v_{g(i)}$ is as same as the value of $v_{g(b)}$ which is obtained after bending. The misalignment of LHS and RHS only occurs after exceeding the critical bend radius of FUD-2300 which is 0.63 cm. NA, core and cladding radii are important parameters in this experiment. It is also realised that a smaller bending radius prior to fibre breakage results in high optical losses due to the leakage of wave power from the core to the cladding.

Figure 3.22 shows the results obtained based on Eq. (3.25). The two graphs are matched by varying the grating visibility of the fibre. The graphs in Figure 3.22 were obtained when $v_{g(b)}$ = 0.37 which is almost equivalent to the final value of the grating visibility, $v_{g(i)}$ obtained during the FBG inscription process demonstrated in Figure 3.20. This finding shows that the grating visibility of a specific FBG can be determined from the variation in the transmission spectrum with decreasing bending radius.

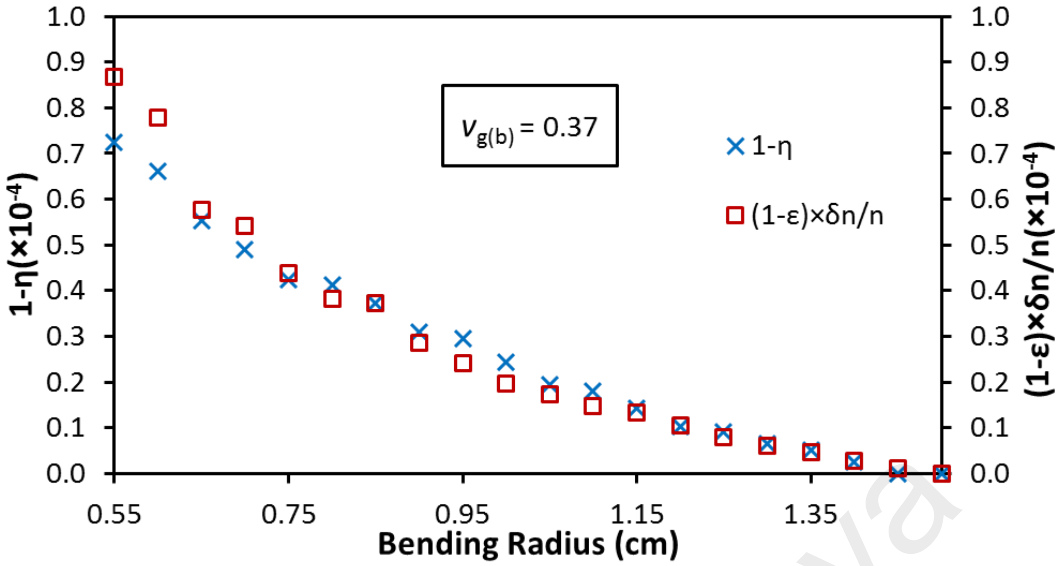

Figure 3.22: The values of LHS and RHS calculated using data of centre wavelength shift and BTD against the variation of bending radius based on Eq. (3.25).

This concept was further tested for FUD-2300 fibres at different ranges of grating visibilities by repeating the same procedure described above. Figure 3.23 (a), (b) and (c) show the overlaid graphs for the data calculated from LHS and RHS of Eq. (3.25). The best fitting graphs were obtained by setting the values of $v_{g(b)}$ as 0.19, 0.29 and 0.4 respectively. The fibres were bent starting from a bending radius of 1.55 cm until it reached 0.55 cm. It is observed that the disagreement between LHS and RHS only occurs when the bending radius reaches 0.63 which is the critical bending radius of FUD-2300 fibre. The accuracy of the overlapping of these two functions was assessed based on the calculation of the cross correlation coefficient. The best grating visibility value was attained when the optimum cross correlation coefficient was achieved.

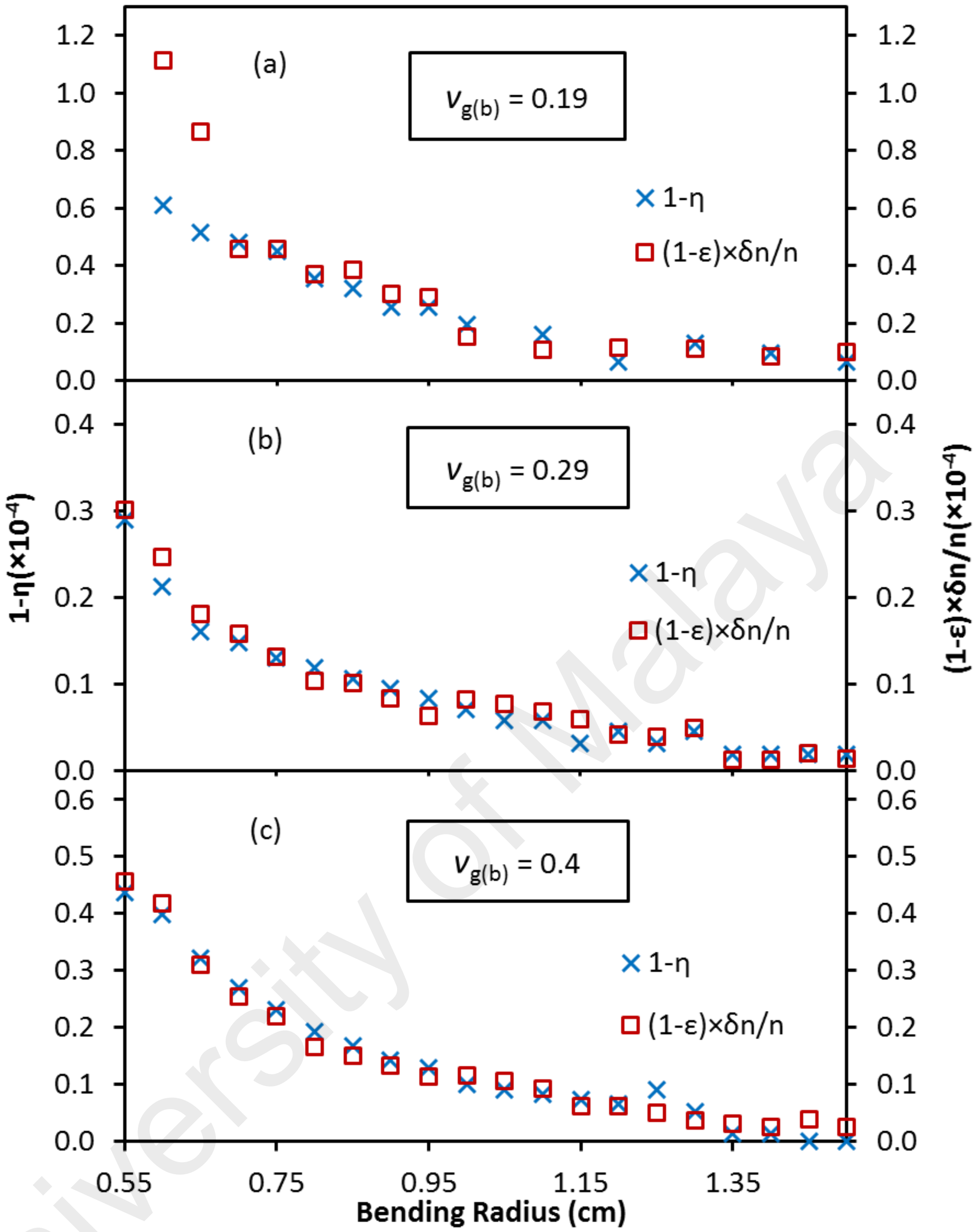

Figure 3.23: (a), (b) and (c). The values of LHS and RHS calculated using data of centre wavelength shift and BTD against the variation of bending radius based on Eq. (3.25).

Table 3.2 summarises the grating visibilities determined from the transmission spectra obtained during FBG inscription, $v_{g(i)}$ the measured result based on bent-spectral analysis, $v_{g(b)}$ and the corresponding optimum cross-correlation coefficients.

Table 3.2: The values of grating visibility obtained after FBG inscription and bending comprising the respective cross correlation coefficients

$v_{g(i)}$	$v_{g(b)}$	Cross correlation coefficient ρ
0.18	0.19	0.91
0.30	0.29	0.96
0.37	0.37	0.99
0.39	0.40	0.94

Evidently, the measurement based on bent-spectral analysis is in good agreement with the data acquired from the earlier inscription process. Four different grating visibilities (acquired from inscription process) ranging between 0.18 – 0.39 were investigated and a small error of ~0.01 was observed in the measurement with cross correlation coefficients greater than 0.9. In order to achieve a high value for $v_{g(i)}$, grating inscription with lower cumulative fluence should be carried out. Nevertheless, it may result in a lower Δn and BTD. This increases the difficulty in achieving accurate results due to low values in Δn_{ave} and Δn_{mod}. The variations in the spectral characteristics with decreasing bending radius are smaller if compared with the experimental uncertainty. This results in larger error in the measurement. Therefore, this study concentrates on a specific range of the grating visibility (0.1 – 0.4). The increased probability of fibre breakage due to smaller bending radii during the bending process can also be considered as a major challenge in the measurement. Additionally, accurate measurements rely on several other factors such as the uniformity of the fibre, the bend radius when the fibre is bent into a knot of 360°, bending angle and stress incurred along the fibre or twisting of the fibre.

It is beneficial to achieve the grating visibility which reflects the performance of the grating inscription system. Moreover, these measurement results provide information that can be incorporated in the performance optimisation of the grating inscription system. It is particularly useful for the FBG manufacturers in achieving efficient production of quality FBGs and preventing excessive UV irradiation which would potentially weaken the fibre glass strength and lead to glass brittleness.

3.5 Summary

In this chapter, a short description of the existing photosensitivity mechanisms and the various techniques for photosensitivity enhancement were presented. A brief study of different photosensitive dopants has been carried out. The role of Gallium as a photosensitive dopant, detailed information about fabrication of gallosilicate fibre, its grating inscription characteristics under different conditions and structural behaviour were investigated.

A mathematical model to characterise the growth in the refractive index change during grating inscription process was proposed. The curve matching and bent spectral analysis techniques were introduced as two characterisation techniques. The data of local refractive index change, Δn_{max} and Δn_{min} were generated by determining both Δn_{ave} and Δn_{mod} from the recorded transmission spectra. A single characteristic function Δn (F) was used to characterise the curves of Δn_{ave} and Δn_{mod}. Interference visibility was also measured using the curve-matching technique. The spectral properties of FBGs under applied UV fluence and bending conditions were analysed. The coupled-mode equations were modified since the coupling coefficients and the attenuation constant were affected by the bending process. Using the bent-spectral analysis technique, measurement of grating visibility after the inscription process and with decreasing bending radii were determined by representing the two individual functions on an overlaid graph. Finally, the repeatability of this measurement technique was tested at different ranges of grating visibility.

CHAPTER 4: THERMAL STABILITY OF FIBRE BRAGG GRATINGS

Fibre Bragg gratings (FBGs) are fabricated through a process of permanent refractive index change in the fibre core. However, the refractive index modulation of these structures begins to decay with increasing temperature and eventually it is completely erased when a specific temperature limit is exceeded. When FBGs are isothermally annealed for a sufficient time duration at a certain temperature and subsequently annealed at temperatures lower than this set temperature, it does not result in further degradation of the grating due to grating stabilisation (Meltz & Morey, 1991). An overview of the decay models, techniques to enhance thermal stability and gratings with high temperature resistivity are discussed. The regeneration characteristics of gallosilicate fibre are also highlighted in this chapter.

4.1 Decay Models

Thermal stability of Bragg gratings depend on numerous factors namely, the type of fibre (Williams & Smith, 1995), the inscription wavelength (Starodubov, Grubsky, Feinberg, Kobrin, & Juma, 1997) and hydrogenation (Grubsky, Starodubov, & Feinberg, 1999b; Kannan & Lemaire, 1996). Erdogan et al. (1994) proposed two models to describe the thermal decay characteristics of FBGs inscribed in erbium-doped silica optical fibres. They are widely known as the accelerated ageing model and the power law model. These models assume that the UV-induced defects can be thermally reversed since they possess a diverse range of activation energies which are the reason behind the change in refractive index. A schematic diagram of the model is shown in Figure 4.1.

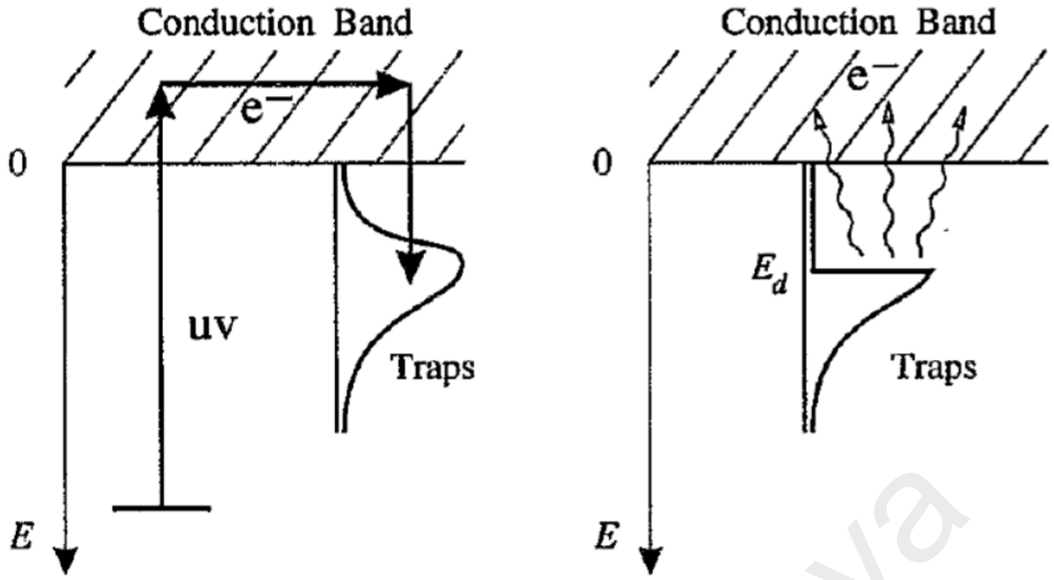

Figure 4.1: Schematic model for proposed decay of refractive index through thermal excitation of trapped electrons (Erdogan et al., 1994).

The power law approach is based on an energy dispersion of trapping sites with reference to a bell shaped curve. The decay measurements are fitted into the equation stated below.

$$\eta = \frac{1}{1 + A(\frac{t}{t_1})\alpha} \tag{4.1}$$

where η denotes the normalised index change, t is the time, A and α are the fitting parameters and t_1=1 min is included to maintain consistent dimensions. Determination of A and α helps in the calculation of thermal decay at any given time or temperature. However, determining fitting parameters to various types of fibre using this model complicates the process (Erdogan et al., 1994; Kannan, Guo, & Lemaire, 1997). Figure 4.2 indicates the validity of the experimental observations with reference to Eq. (4.1).

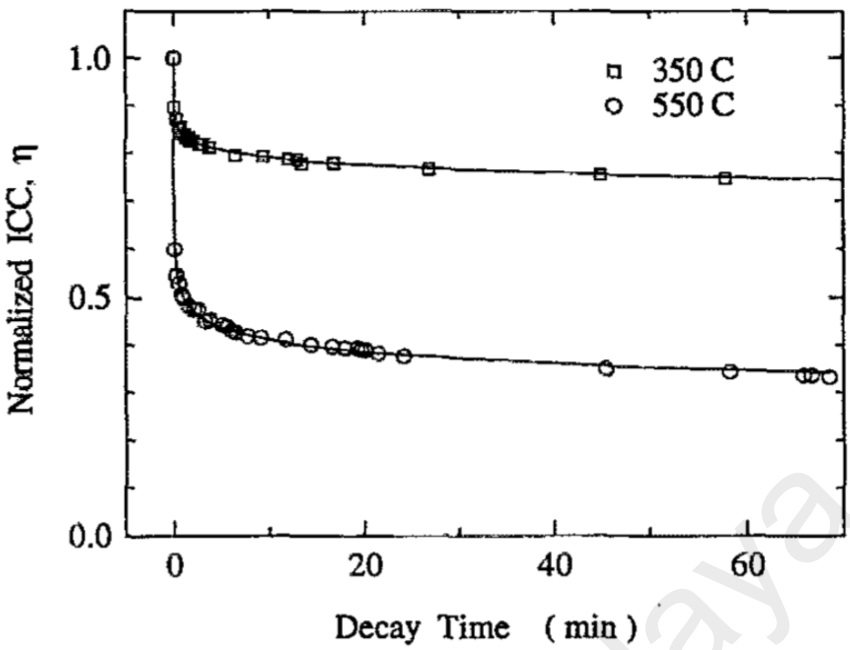

Figure 4.2: Measured integrated coupling constant (*ICC*) values normalised with respect to the initial values for two gratings annealed until 350 and 550 ˚C as a function of decay times. Solid lines represent the fits to Eq. 4.1 (Erdogan et al., 1994).

According to Erdogan et al. (1994), the exponent α can be expressed as $\alpha = \frac{T}{T_0}$ where T_0 = 5250 K and A is expressed as

$$A = A_0 \exp(\alpha T) \tag{4.2}$$

where $A_0 = (1.86 \pm 0.22) \times 10^{-3}$, $\alpha = (7.64 \pm 0.19) \times 10^{-3}$ K^{-1} and T is the temperature in Kelvin. Figure 4.3 demonstrates the dependence of A, the power law factor with temperature.

The characterisation of the decay in the refractive index in the accelerated energy model relies on an ageing parameter which is known as the demarcation energy (E_d) and is given by

$$E_d = k_B T \ln(\nu t) \tag{4.3}$$

where k_B, T, t and v denote the Boltzman's constant, temperature, time and the fitting parameter respectively. v is obtained empirically using a sequence of decay measurements.

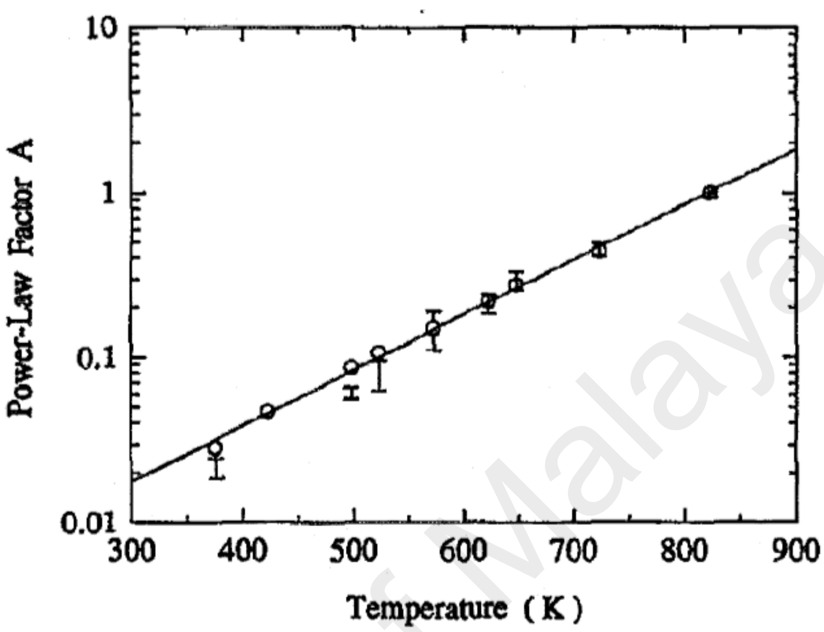

Figure 4.3: The power law factor *A* obtained from curve fits to Eq. (4.1) with *α* allowed to vary freely (error bars), and *α* fixed by *α* =T/5250 K (open circles) (Erdogan et al., 1994).

The experimentally obtained data is used to determine the η values and are shown in Figure 4.4 as a function of the demarcation energy E_d. The different types of icons represent different experiments conducted at various temperature levels. The plot of refractive index modulation change in the demarcation energy domain produces the ageing curve and η can be written as

$$\eta = \frac{1}{1 + \exp(\frac{E_d - \Delta E}{k_B T_0})} \tag{4.4}$$

Differentiation of the ageing curve provides information about the energy dispersion of the defects which causes the variation in the refractive index (Erdogan et al., 1994; Kannan et al., 1997; Rathje, Kristensen, & Pedersen, 2000).

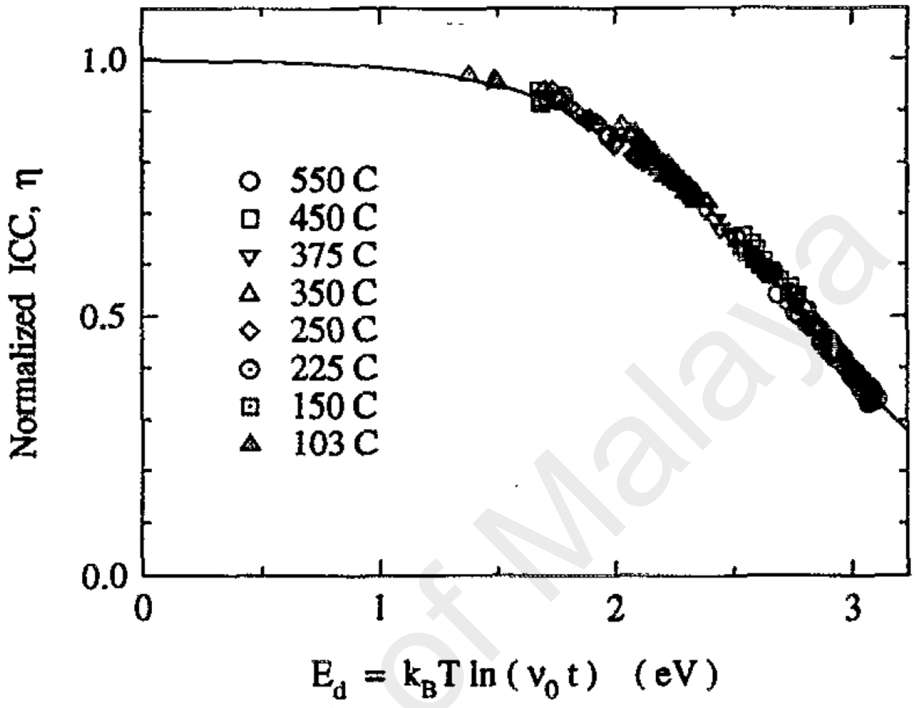

Figure 4.4: Normalised *ICC* in the demarcation energy, E_d domain. The solid line is obtained using the fitting to Eq. (4.4) (Erdogan et al., 1994).

A broader energy distribution leading to a lower thermal stability can be found in gratings inscribed in hydrogen (H_2) loaded fibre compared to the non-loaded fibre.

Dong, Liu, and Reekie (1996) proposed a three energy level system (TEL) which states that a negative index change follows the initial positive index change. This growth rate of index change is proportional to the beam intensity and is also a saturated index change which is independent from the inscription beam intensity. According to this study, a complex decay process has been observed and the thermal stability for Bragg gratings with both positive and negative index changes have been measured to predict the grating lifetime.

Figure 4.5 indicates the schematic diagram of the three energy level system. Depletion of Level 1 populates Level 2 and is followed with a quick relaxation into Level 2a to provide a positive index change. A similar process where Level 3a is populated from Level 2a via Level 3 results in a negative index change. The energy barrier for the relaxation of Level 3a population is at a higher level compared to that of Level 2a which leads to a much more stable negative index change. In this scenario, where population of both Levels 2a and 3a occurs, the rate of change of positive index change starts to decrease at the beginning and subsequently the negative index changes, giving rise to a complex thermal decay mechanism. This is due to the fact that the total index change represents the summation of both the effects. During annealing, growth of the grating is observed if the negative index change is dominant. Further details about this complex decay mechanism can be found in Dong and Liu (1997).

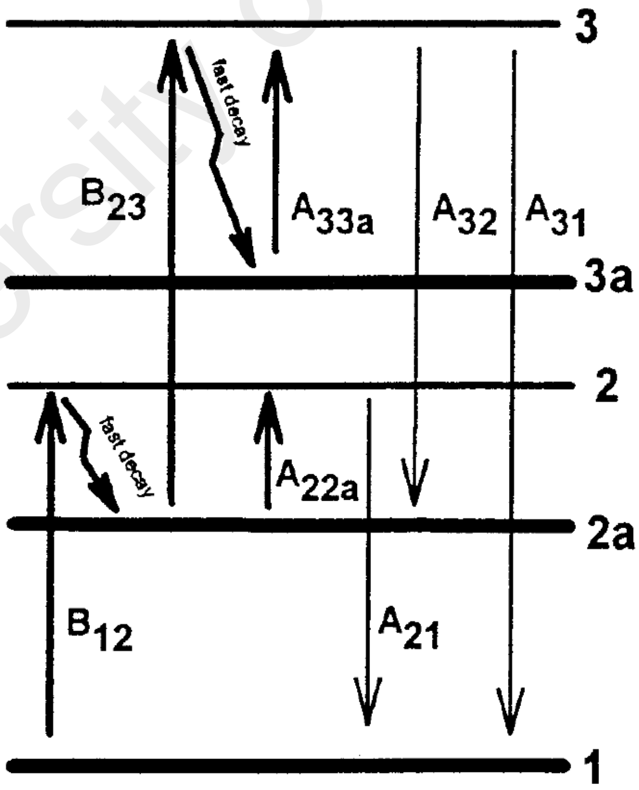

Figure 4.5: Schematic diagram of the TEL system (Dong & Liu, 1997).

4.1.1 Types of accelerated ageing experiments

Accelerated ageing tests can be performed in three different ways. They are namely, true isochronal annealing, step isochronal annealing and isothermal annealing (Lancry, Poumellec, Costes, & Magné, 2014). True isochronal annealing is carried out by annealing the exact same gratings with a rising temperature for a set time duration. In this method, at each annealing temperature, a new grating is used. The step isochronal annealing method differs from the true isochronal method in the sense that for each independent annealing step, the same grating is incorporated. This also makes it possible for a reliable approximation to be made about the true isochronal annealing method (Razafimahatratra, Niay, Douay, Poumellec, & Riant, 2000). This is the most commonly used technique since it consumes a lesser amount of time. The isothermal annealing technique comprises holding the temperatures at set values above room temperature for identical gratings where the transmission spectra of the gratings are recorded periodically (Erdogan et al., 1994).

4.1.2 Determination of thermal decay during accelerated ageing experiments

The thermal degradation of a grating can be modelled in terms of its normalised integrated coupling coefficient (*NICC*) since the *ICC* is directly proportional to the peak reflectivity. At any given time, the peak reflectivity of a grating can be represented as

$$R = 1 - T_{\min} \tag{4.5}$$

where $T_{\min}$ is the minimum transmission of the grating which occurs at the Bragg wavelength (λ_B). The *ICC* is given by

$$ICC = \tanh^{-1}(\sqrt{1 - T_{\min}} \tag{4.6}$$

Hence, the *NICC* values (η) can be depicted as

$$NICC = \frac{\tanh^{-1}(\sqrt{R_{t,T}})}{\tanh^{-1}(\sqrt{R_{0,T_0}})} \tag{4.7}$$

where $R_{t,T}$ is the peak reflectivity after an annealing time t at an annealing temperature T and R_{0,T_0} refers to the initial reflectivity at room temperature.

4.2 Shift of Bragg Wavelength

With reference to Eq. (3.2), L is the grating length. The reflectivity of the grating is given by Eq. (4.5). Since L is assumed to be a constant value, the amplitude of Δn_{mod} is proportional to the grating reflectivity and therefore starts decreasing when the FBG thermally decays. Moreover, when Δn_{mod} reduces due to thermal decay, the Bragg wavelength gets blue-shifted. The Bragg wavelength red-shifts with increasing temperature as a result of the thermal optic effect on Δn_{mod} and the thermal expansion effect which alters the grating period. The red-shift of the Bragg wavelength with increasing temperature during heating can be observed in Figure 4.6.

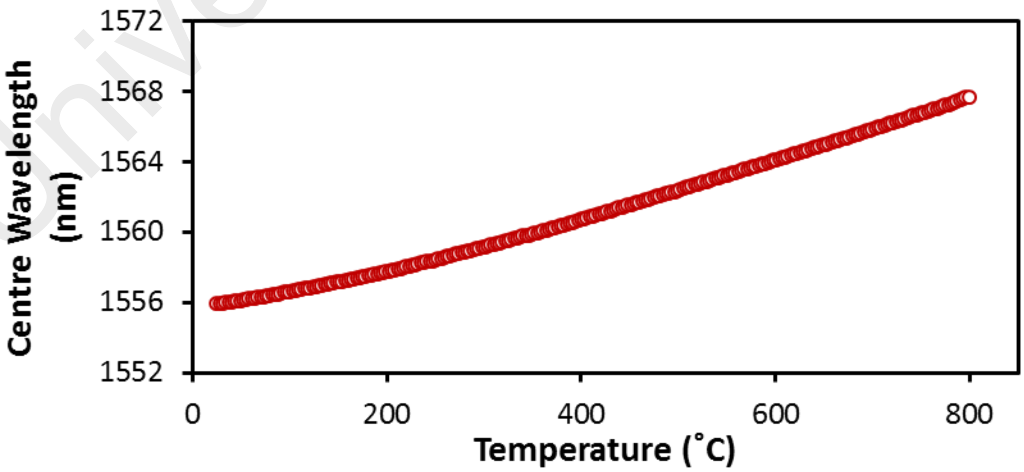

Figure 4.6: The shift of Bragg wavelength during heating of a 15 mm long grating inscribed in SM 1500.

Figure 4.7 indicates segments of the reflection spectra obtained during the thermal annealing procedure of a 15 mm long grating written in SM 1500 fibre and the red-shift of the Bragg wavelength is clearly visible with increasing temperature. The operating principal of an FBG based temperature sensor relies on the shifting of the Bragg wavelength and also possesses several advantages compared to other temperature sensors.

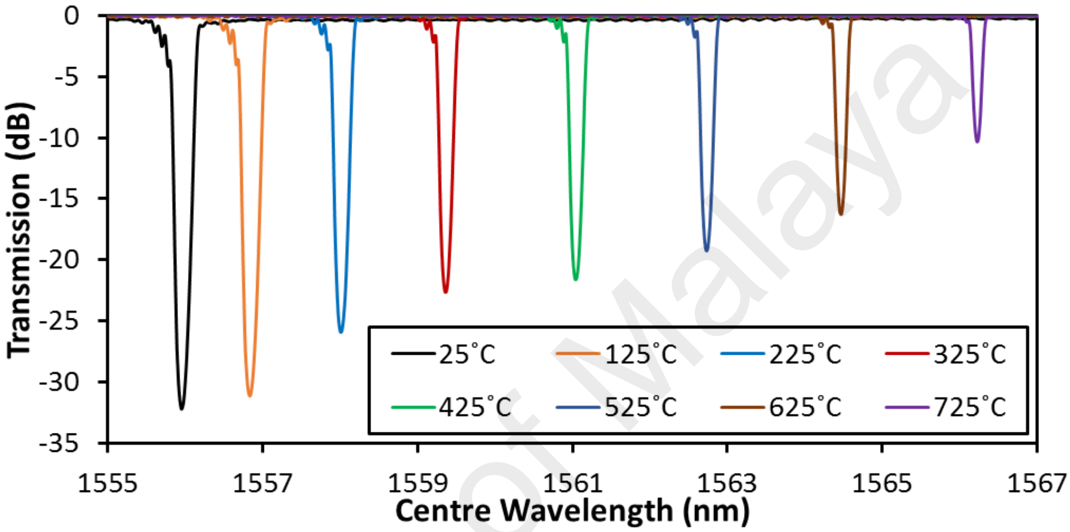

Figure 4.7: Transmission spectra indicating the red shift of the Bragg wavelength inscribed in SM 1500 fibre during thermal annealing process.

4.3 Methods to Increase Thermal Stability

4.3.1 Pre or post exposure

A model, with the assumption of the existence of an energy barrier, responsible for structural changes and defect formation has been proposed by Salik, Starodubov, Grubsky, and Feinberg (1999). Distribution of the energy barriers allows some of the glass structures to be easily transformed but complicates the transformation for those with higher energy barriers. The model implies a relationship between the photosensitivity of the defects and the thermal stability of the grating, suggesting that the least stability can be expected from the gratings which are easily inscribed. Uniform pre or post UV exposure of the fibre effectively eliminates the unstable component of the index modulation. The model further explains the enhanced thermal stability of the gratings when inscribed using a phase-mask since the 0^{th} order fringe from the phase-mask creates a uniform exposure on the fibre which stabilises the Bragg grating. An equivalent behaviour has also been noticed in H_2 loaded fibre that has been pre-exposed (Åslund & Canning, 2000).

4.3.2 Thermal annealing using CO_2 Laser

The fabrication procedure was commenced with the CO_2 laser treatment on Ge/B co-doped photosensitive fibre (Fibrecore PS 1250/1500) over a fibre length of 15 mm. The fan-cooled CO_2 laser (SYNRAD 48-2 SAM) was placed on a stainless steel optical table and operated in an air-conditioned laboratory. It consists of a maximum output power of 35 W ± 2% (max). A 15 mm long vertical beam was produced by initially expanding the laser beam with the aid of two convex lenses and subsequently compressing with a cylindrical lens of 50.8 mm focal length. The schematic diagram of the CO_2 laser annealing setup is illustrated in Figure 4.8 below.

Figure 4.9 shows the actual CO_2 laser annealing setup including the sapphire furnace and the three-axis positioning stage which was used to achieve precise alignment of the optical fibre position.

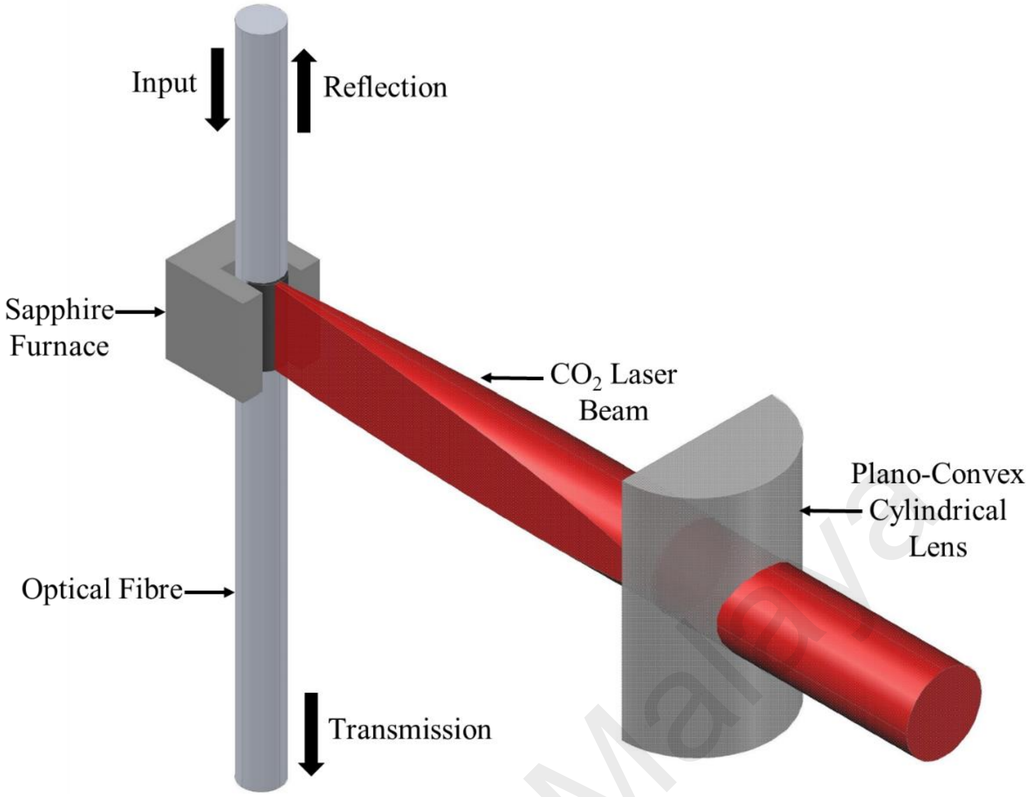

Figure 4.8: Schematic diagram of the CO_2 laser annealing setup.

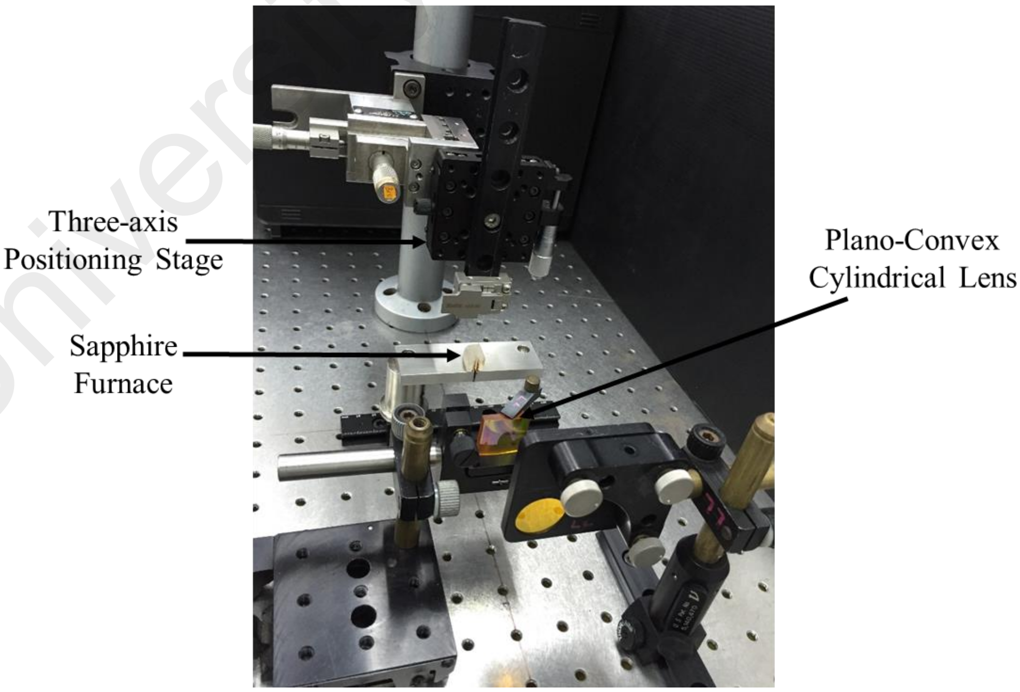

Figure 4.9: CO_2 laser annealing setup.

During the CO_2 laser pre-treatment, the laser power irradiation on the fibre was raised from 0 W to 14.4 W (80% of the maximum laser power) at a rate of 0.18 W/s with a hold time of 5 min after the ramping procedure. A slow cooling process was followed after the annealing process of the PS fibre using the CO_2 laser where the laser power was reduced at a rate of 0.09 W every 10s. Subsequently, the CO_2 laser treated fibre along with non-treated fibre were loaded in a pressurised H_2 gas chamber at 1800 psi for 10 days. Afterwards, the FBG inscription procedure was carried out in both types of fibres and 10 mm Bragg gratings were inscribed using 193 nm ArF excimer laser until similar reflectivity levels were achieved for each fibre. The reflectivity of both gratings amounted to ~ 40 dB. Monitoring of the transmission spectra of the two types of fibres was achieved using an Optical Spectrum Analyser (OSA). Prior to the annealing process, both the treated and non-treated PS fibre were kept inside an oven at 80 ˚C for 8 hours to achieve out-diffusion of the residual H_2 from the fibre core.

The annealing process was carried out on both CO_2 laser treated and non-treated PS fibre under similar temperature conditions to achieve accurate measurements. The fibres were placed inside a tube furnace (see Figure 4.10) where the temperature increment was controlled using the inbuilt program in the furnace. During the annealing procedure, the temperature was initially increased from room temperature (25 ˚C) to 100 ˚C at a ramping time of 5 min. Subsequently, the temperatures were incremented to 200 ˚C and 300 ˚C and dwelled at each temperature for 3 hours. During the treatment, the transmission spectra were observed and recorded within a time interval of one minute for each fibre in a similar manner as discussed in Chapter 3. The experiment was repeated at 100 ˚C, 150 ˚C and 250 ˚C in order to analyse the accelerated ageing curves of the treated fibre and to verify the validity of this study.

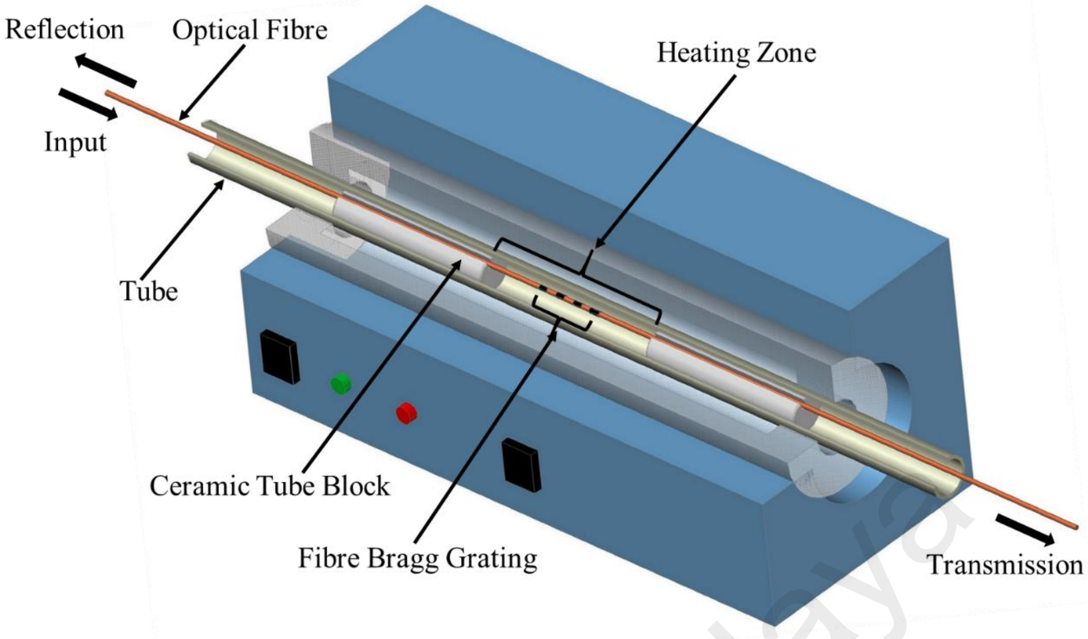

Figure 4.10: Schematic representation of the thermal annealing procedure conducted in the tube furnace.

It is observed from Figure 4.11 that with increasing annealing temperature, the Bragg transmission depth (BTD) gradually decreases. At 100 °C and 200 °C, BTD for both CO_2 treated and non-treated fibres indicate a similar kind of progression whereas this behaviour subsequently differs when the fibres reach 300 °C. After isothermal annealing at 300 °C for 3 hours, a 25 dB BTD can be observed for CO_2 treated fibre compared to the increased decay in the grating strength of non-treated fibre. Davis, Gaylord, Glytsis, and Mettler (1999) has demonstrated that CO_2 laser induced long-period fibre gratings are highly stable even when subjected to high temperatures for longer time intervals. Since the BTD of CO_2 laser treated fibre indicates a stabilised grating strength, it would be very useful in the production of temperature sensors for long term usage where the decay of grating strength is considerably low. Furthermore, Figure 4.11 demonstrates the red shift in the centre wavelength for both types of fibre with increased annealing temperatures. From the beginning to the end of the annealing process a centre wavelength difference of ~1 nm is observed between the CO_2 laser treated and non-treated fibres. The gratings inscribed in treated fibre indicates a longer wavelength compared to that of gratings in non-treated fibre.

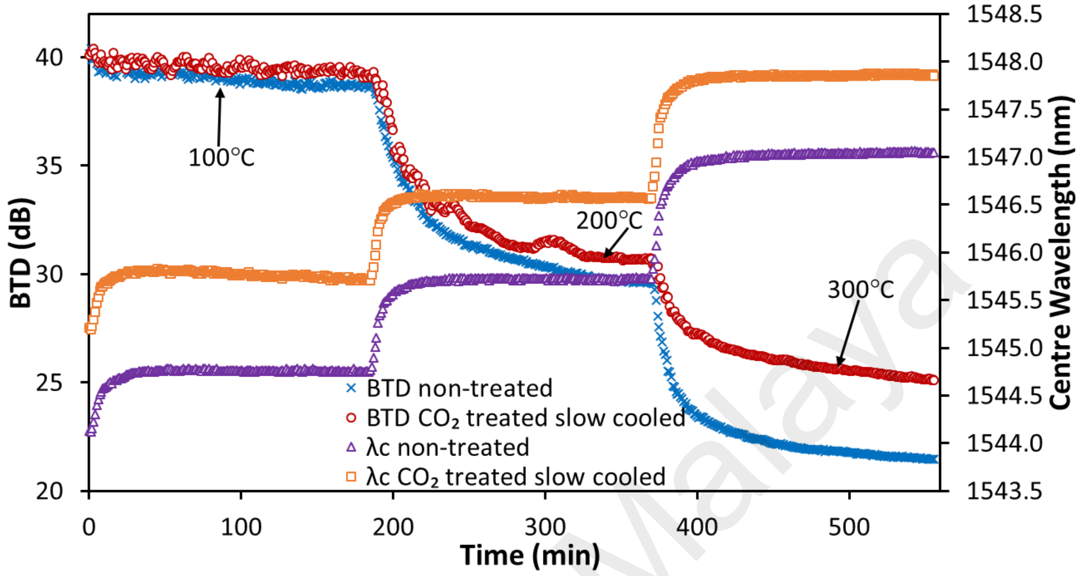

Figure 4.11: The evolution of the Bragg transmission depth and centre wavelength of treated and non-treated fibre at 100 °C, 200 °C and 300 °C.

The reason for this red shift in centre wavelength of the CO_2 treated slow cooled fibre is the sufficient time available for the fibre glass to undergo structural relaxation at low viscous state when slow cooling occurs during CO_2 laser annealing. As a result of this glass structural relaxation, the T_g of the fibre core glass decreases. This leads to the reduction in thermal stress between the fibre core and cladding and the red-shift in Bragg wavelength (Lai, Lim, et al., 2015).

Figure 4.12 indicates the normalised decays of ac index modulation ratio $\eta=\Delta n(t)/\Delta n_0$, of CO_2 laser treated slow cooled fibre at three different annealing temperatures with a dwelling time of 1 hour. The highest stability is observed at 100 °C followed by 150 °C and 250 °C where the latter is the least stable. A monotonical decrease of η leading to an overall decay of 1 %, 8 % and 10 % in the FBGs at these three different temperatures is observed.

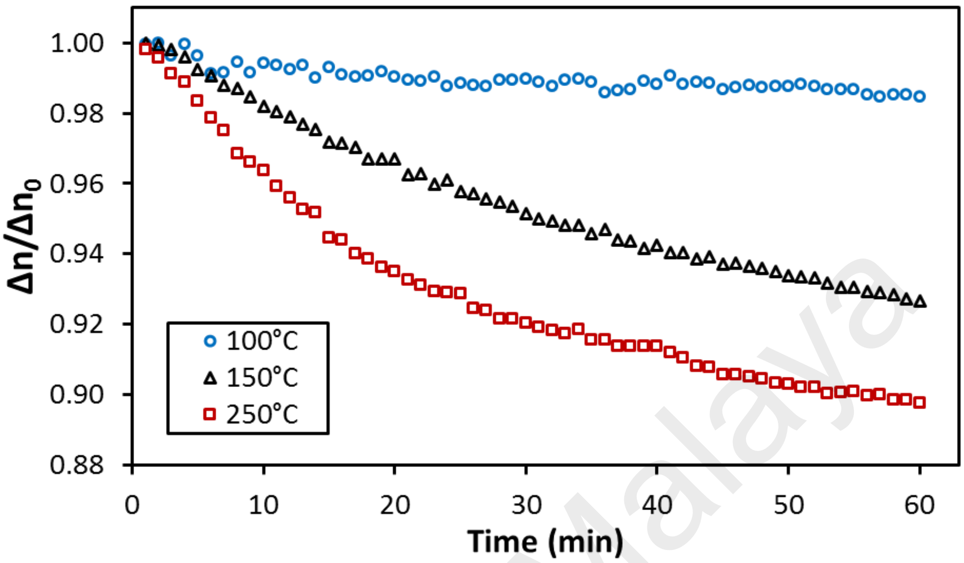

Figure 4.12: Accelerated ageing curves for gratings in CO_2 treated slow cooled PS fibre at 100 °C, 150 °C and 250 °C.

4.3.3 Gratings with intrinsically high thermal stability

As discussed in chapter 2, type II gratings fabricated through high power single-pulse exposure possess high temperature resistant characteristics. In the case of type IIa gratings, the resultant grating consists of two superimposed gratings. The first grating, which is related to type I grating formation, exhibits a lower thermal stability compared to the second grating which has a negative refractive index change. According to Dong and Liu (1997), the thermal stability relies on the fact at which point grating inscription is halted since it is possible for the two gratings to counteract in refractive index modulation. In addition, gratings inscribed in SnO_2-doped and N-doped optical fibres have resulted in increased thermal stability compared to Ge or Ge/B co-doped fibres (Brambilla & Pruneri, 2001; Dong, Cruz, Reekie, et al., 1995).

4.3.4 Molecular water induced gratings

The main concept of molecular water induced FBGs relies on the Δn_{mod} of the fibre using molecular water (Zhang & Kahrizi, 2007). The disintegration of molecular water is unfeasible over temperatures ranging from freezing point (0 ˚C) to melting temperature of silica (Tomozawa, Kim, & Lou, 2001) owing to the strong bonds that exist in molecular water. Therefore, the molecular water induced FBG possesses the capability of withstanding much higher temperatures compared to the erasing temperature of the general H_2 loaded FBGs. In addition, at 1000 ˚C molecular water has a relatively low diffusivity of $D_{H_2O}=2\times10^{-7}$ cm^2/s in the silica fibre (Davis & Tomozawa, 1995). Hence, the diffusion of molecular water from segments of high concentration to that of low concentration will be extremely slow at high temperature.

It has also been discovered that the reflectivity and thermal sustainability of molecular water induced FBGs rely on the Si-OH concentration in the core of the fibre (Zhang & Kahrizi, 2007). The maximum operating temperature for these molecular water induced high reflectivity FBGs has been recorded above 1100 ˚C. This has resulted in the production of high reflectivity gratings with high temperature stability.

4.4 High temperature resistant gratings

FBGs with operating temperature limits beyond the standard telecommunication conditions are vital in the production of fibre based temperature sensors. Emerging as a strong opponent for conventional electrical and electronic sensors, FBGs possess a vast number of advantages. For instance, their immunity to electro-magnetic interference, low fabrication cost, high sensitivity and multiplexing capabilities (Kersey et al., 1997). Hence FBG based temperature sensors have proved successful in certain sectors such as oil and gas industry and microwave related applications where there is explosion hazard or electromagnetic interference.

The type of the grating and the process of refractive index modification in a particular grating are crucial factors when accommodating them as temperature sensors in high temperature applications. The thermal properties of the commonly used type I FBGs inscribed using UV irradiation have been comprehensively investigated in some research studies (Chen & Herman, 2003; Erdogan et. al., 1994). Erdogan et. al. (1994) has proposed a quantitative model for analysing the reduction of the UV-induced index change with respect to the temperature to predict the lifetime of these FBGs. However, apart from the thermally induced decay in the reflectivity of the conventional FBGs, a complete erasure of the original seed grating (SG) has also been observed when exposed to high temperature environments (400-500°C). These limitations restrict the deployment of FBGs in many high temperature applications. In an effort to address this shortcoming, various FBG based sensors have been fabricated using different approaches, such as the process of hypersensitisation of the fibre (Åslund & Canning, 2000) and formation of type II and type IIA gratings with exposure to femtosecond lasers (Archambault et al., 1993a; Groothoff & Canning, 2004). In recent research studies, new types of thermally resistant gratings with superior high temperature sustainability commonly known as chemical composition gratings (CCG) and regenerated fibre Bragg gratings (RFBG) (Bandyopadhyay, Canning, Biswas, Stevenson, & Dasgupta, 2011; Lindner et al., 2009;) have been reported.

4.4.1 Chemical composition gratings (CCG)

Bragg gratings stable at high temperatures can be achieved by changing the fluorine concentration of the fibre core periodically (Fokine, Sahlgren, & Stubbe, 1996). This change in fluorine concentration results in a refractive index change. The thermal stability of such a structure relies on the diffusing characteristics of fluorine. The alteration of the fluorine concentration in the fibre core is carried out with reference to the chemical equation below.

$$\equiv Si - OH + F - Si \equiv \xrightarrow{heat} Si - O - Si \equiv + HF \tag{4.8}$$

Kirchof, Unger, Pissler, and Knappe (1995) has proposed this equation to explain the decrease in the hydroxyl concentration in fluorine-doped silica. The reduction in hydroxyl concentration is ascribed to the formation and diffusion of hydrogen fluoride. It is predicted to be highly mobile compared to bound fluorine. Hydroxyl groups can be introduced to the fibre core thermally or by exposing hydrogen loaded fibre to UV irradiation. Fringed UV exposure leads to the formation of hydroxyl groups locally and consists of the periodicity of the interference pattern which results in sub-micron structures. Therefore, FBGs which consist of refractive index modulations due to a variation in the chemical composition are known as chemical composition gratings. According to Fokine (2002), thermal annealing of this particular type of gratings at high temperature levels of 1000 and 1200 ˚C have shown significant enhancement in the thermal stability compared to other different types of FBGs. However, a successive investigation based on high temperature thermal annealing of type I gratings has demonstrated that the existence of fluorine is not required to regenerate the index modulation (Trpkovski, Kitcher, Baxter, Collins, & Wade, 2005). The CCGs have been found in Er-doped fibre co-doped with Ge, Sn and Al as well. Moreover, the usual concept of grating regeneration has been noticed in simple H_2 loaded germanosilicate fibre (Zhang & Kahrizi, 2007).

4.4.2 Regenerated fibre Bragg gratings (RFBG)

The fabrication process involves an isothermal annealing process of the SG until the erasure of the grating properties which is followed by a grating regeneration. This new grating promises to provide more thermally stable operating conditions at elevated temperatures and is generally known as regenerated fibre Bragg grating or type R grating (RFBG). Usually, the annealing procedure is carried out using a furnace with an initial slow ramping of the temperature until the regeneration temperature is exceeded followed by a subsequent stabilisation of the temperature which might extend from minutes to hours in order to achieve a complete regeneration.

Figure 4.13 indicates the regeneration characteristics obtained from the reflection spectra of a 15 mm long grating written in SM 1500 fibre. At 750 ˚C, a rapid thermal decay in the grating is observed leading to a complete disappearance of the grating at 850 ˚C which is subsequently followed with the formation of a new grating. The grating regeneration process occurs until ~920 ˚C and starts to degrade again with increasing temperature. Figure 4.14 shows the reflection spectra of the seed and regenerated gratings at room temperature (25 ˚C) and at ~920 ˚C.

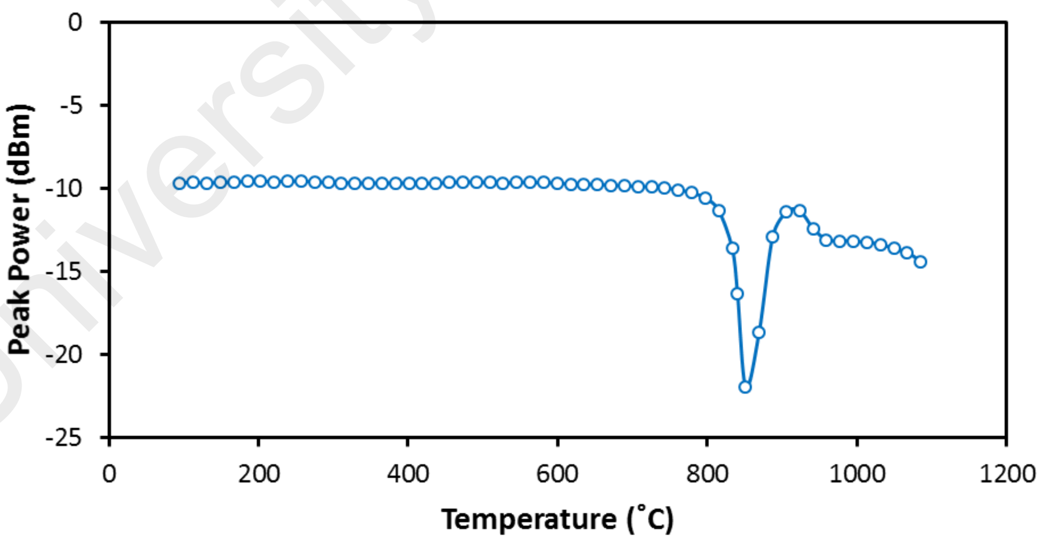

Figure 4.13: Evolution of the grating reflectivity of a 15 mm grating inscribed in SM 1500 fibre during thermal annealing.

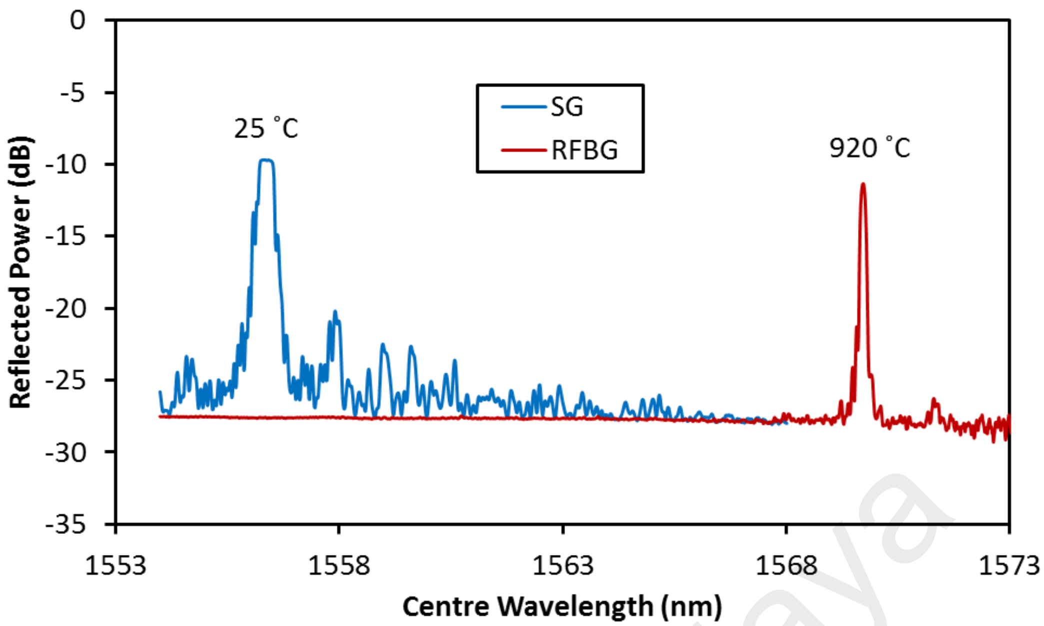

Figure 4.14: The reflection spectra of the seed and regenerated gratings (SM 1500).

The interest in RFBGs has resulted in the development of a new fabrication technique, deviating from the existing method of thermal annealing procedure using a furnace. Recently, it has been demonstrated with the incorporation of a CO_2 laser which is known as the direct CO_2 laser annealing technique. This technique appears to offer many benefits in terms of producing low-loss regenerated gratings, flexibility in beam manipulation in terms of small heating area and active control of temperature and heat (Lai, Gunawardena, Lim, Yang, & Ahmad, 2015). Furthermore, this study has managed to provide useful evidence demonstrating the presence of stress relaxation in the core of the fibre when regeneration occurs.

Bueno, Kinet, Mégret, and Caucheteur (2013) has discussed other aspects of thermal regeneration such as fast regeneration. This has been achieved by directly introducing the gratings to a pre-treated oven which has a temperature much lower than the regeneration temperature. H_2 loaded fibres with a high Ge concentration have appeared to provide better results. After a comparative study, a RFBG with a reflectivity of 13.7 dB has been created within a time span of only 31 s in Ge/B co-doped H_2 loaded photosensitive fibre exhibiting a time improvement factor of 110. Bandyopadhyay et al. (2008) has discovered ultra-high temperature regenerated gratings in 193 nm written H_2 loaded Ge/B co-doped optical fibre. The gratings which are subjected to tension with a load of 85 g have been annealed using an ultra-high temperature micro heater. The observation of Bragg wavelength shift is assumed to be the response as a result of the tension which is applied on the fibre. This is because the high temperature is near to the core-glass softening temperature as well as the stress relief that occurs between core and cladding owing to the variation in expansion coefficient.

Regeneration in Helium loaded Bragg gratings inscribed in germanosilicate fibre has been reported by Cook, Shao, and Canning (2012). These gratings are able to withstand temperatures exceeding 900 ˚C for more than 4 hours. The high temperature stability of the He loaded gratings makes them strong competitors to H_2 loaded gratings. The study using this inert gas further justifies the model which describes that the regeneration process is dominated by mechanical relaxation. According to this model, glass is transformed to a more stable position via a different rate of relaxation. This is plausible through high temperature and internal stress modification of the optical fibre.

In addition, non-hydrogen loaded regeneration (Lindner et al., 2009) opposed to the hydrogen loaded (Bandyopadhyay et al., 2011) regeneration has also been investigated in various research studies. Besides, regeneration characteristics of multiplexed RFBGs suitable for high temperature measurements (Laffont, Cotillard, & Ferdinand, 2013) and the presence of strain on the regeneration behaviour (Wang, Shao, Canning, & Cook, 2013) have also been investigated. However, many of these studies often concentrate on RFBGs produced using Ge-doped optical fibres, whereas only a few research studies have reported the existence of RFBGs in non-Ge-doped optical fibre (Yang et al., 2014).

Hence, these RFBGs are attracting the attention of the scientific community and are increasing the need for further exploration.

4.5 Thermally activated gallosilicate fibre Bragg gratings

After the inscription procedure (as discussed in Chapter 3.3), Ga-doped fibre was annealed in an oven at 80 °C for 8 hours in order to diffuse out the residue H_2 in the fibre. Subsequently, the thermal annealing process was carried out where the Ga-doped fibre was placed inside a tube furnace (refer to Figure 4.10) and the SG was adjusted in such a way that it was at the centre of the furnace. This allowed the temperature to be retained uniformly along the entire length of the SG. The increment in the temperature during the annealing process was achieved using an inbuilt program in the furnace, where the temperature was increased uniformly at a rate of ~4.16 °C/min until the grating was completely erased which was observed at 720 °C. Subsequently, the annealing temperature was held constant at this temperature for ~ 2 h and 45 min where a new grating appeared and was ultimately stabilised. The reflection spectra were monitored and recorded every minute using the procedure discussed in Chapter 3. The grating was subsequently cooled to room temperature and left for 24 hours prior to the thermal calibration process. The calibration process of the regenerated gallosilicate grating was carried out by placing the grating inside the tube furnace and recording the reflection spectra using an automated system in order to calculate the wavelength shift in accordance with the variation in temperature from 25 °C to 750 °C during heating and vice versa during cooling. This procedure was repeated for two more cycles in order to acquire accurate and reliable data on the temperature sensitivity of the RFBG. Furthermore, the centre wavelength stability of the RFBG was monitored over a time period of 8 hours where the temperature was dwelled at 720 °C throughout the investigation.

Figure 4.15(a) illustrates the progression of the grating reflectivity. As the temperature increases, the reflectivity of the SG gradually decays until its complete erasure and subsequently, the emergence of a regenerated grating is observed at 720 °C. The degradation in the reflectivity can be attributed to the fact that the increment in temperature leads to a reduction in the UV-induced refractive index modulation. The reflectivity spectrum indicates a rapid degradation in the grating reflectivity of the SG starting from 90 min which corresponds to a temperature of 400 °C. Furthermore, the shift in the centre wavelength can be associated with the variation in the temperature. A maximum centre wavelength shift of ~9 nm is observed from 25 °C until the point where complete regeneration occurs. The treatment takes a duration of 2 h and 45 min for the complete erasure of the reflectivity. The formation of RFBG and its stabilisation process under isothermal annealing at 720 °C, involves an additional duration of 2 h and 45 min.

Figure 4.15(b) shows the evolution of the 3-dB bandwidth throughout the annealing procedure. At the beginning, a gradual reduction of the bandwidth is observed until a stagnant point is reached when it gets close to the regeneration temperature. The highlighted region in Figure 4.15(a) indicates the region where regeneration occurs, thereby making it difficult to perform an accurate measurement of the 3-dB bandwidth since the reflected peak power decays down to the noise level. However, the measurement can again be achieved when the grating emerges from the noise level.

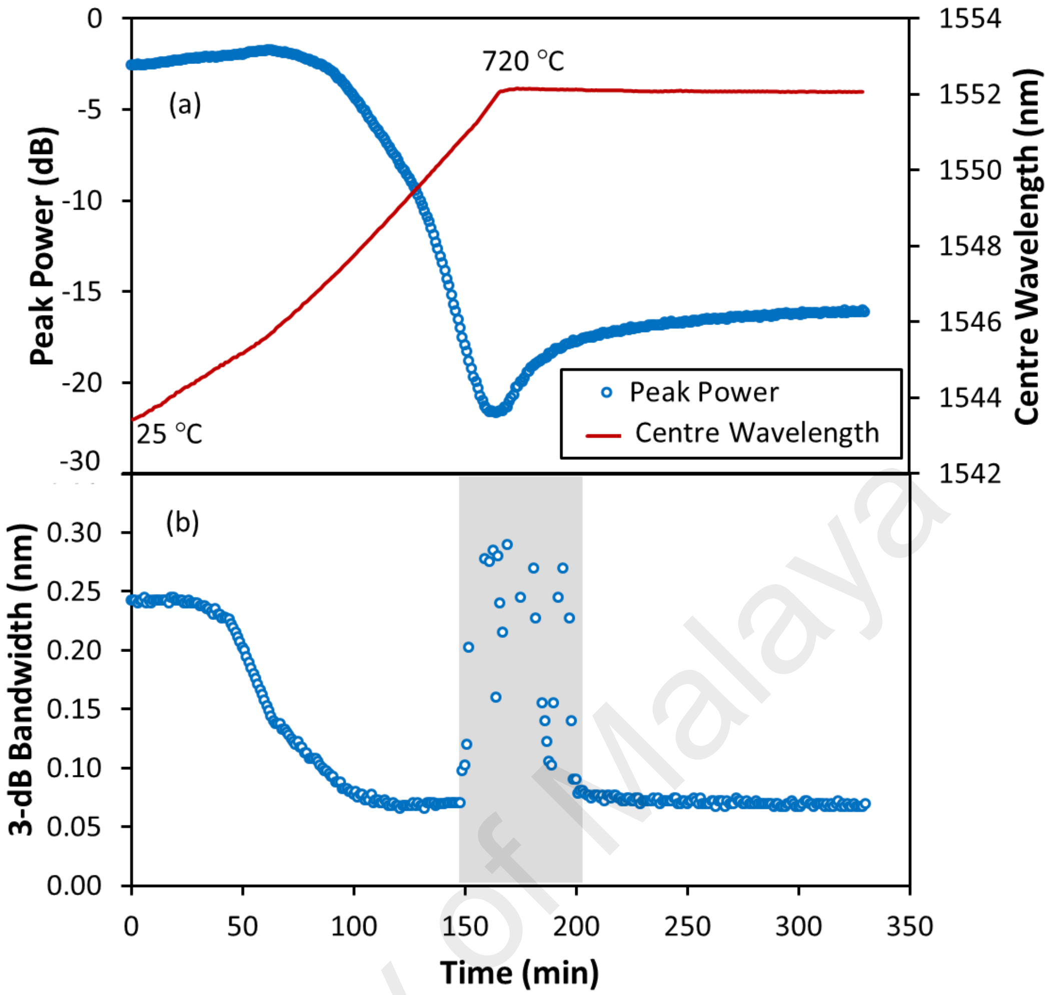

Figure 4.15: Progression of (a) grating reflectivity and shift of centre wavelength during thermal regeneration at the temperature range from 25 °C to 720 °C (b) 3-dB bandwidth.

Figure 4.16 shows the behaviour of the reflection spectra as they occurred throughout the regeneration process. During the process of ramping up from room temperature to 720 °C, the reflected power gradually decreases indicating a thermal decay of the SG. A narrower bandwidth along with a decrease in the reflected power of the SG is also noticed during the course of the annealing procedure. When the temperature is held at 720 °C, the reflected power rises from the noise level indicating the typical behaviour of a regenerated grating.

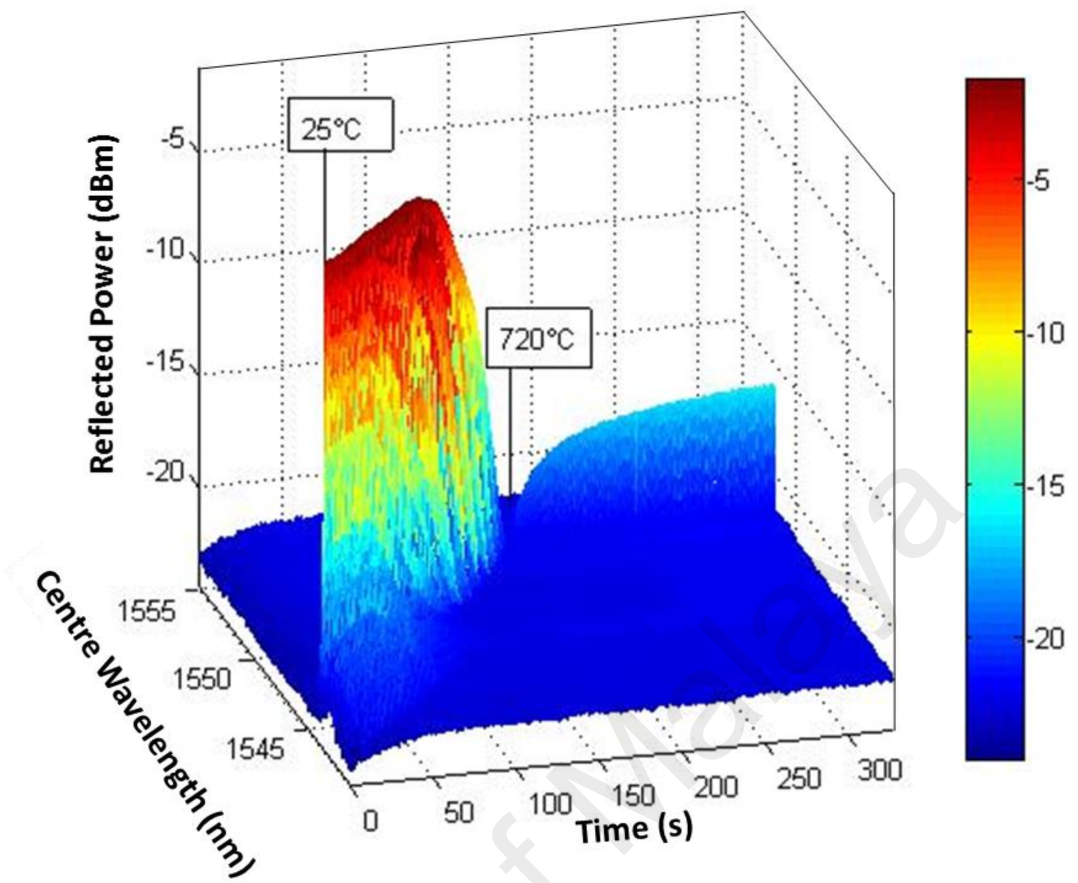

Figure 4.16: Reflection spectra of formation and growth of gallosilicate RFBG.

Figure 4.17(a) demonstrates the characteristics of the reflection spectra obtained at four different annealing temperatures whereas Figure 4.17(b) indicates the SG obtained after the FBG inscription process and the RFBG obtained at room temperature after the regeneration process. A significant decrease in the bandwidth, side lobes and the reflection peak power is observed for the RFBG when compared with SG indicating a lower contrast in the refractive index and grating strength. This reduction in the refractive index can be attributed to the erasure of UV-induced index modulation, resulting in a modification in the glass structure and eventually forming a new grating that has excellent temperature sustainability and resistance. This in turn can be attributed to stress relaxation or periodic change in the dopant concentration during the thermal annealing process (Fokine, 2004).

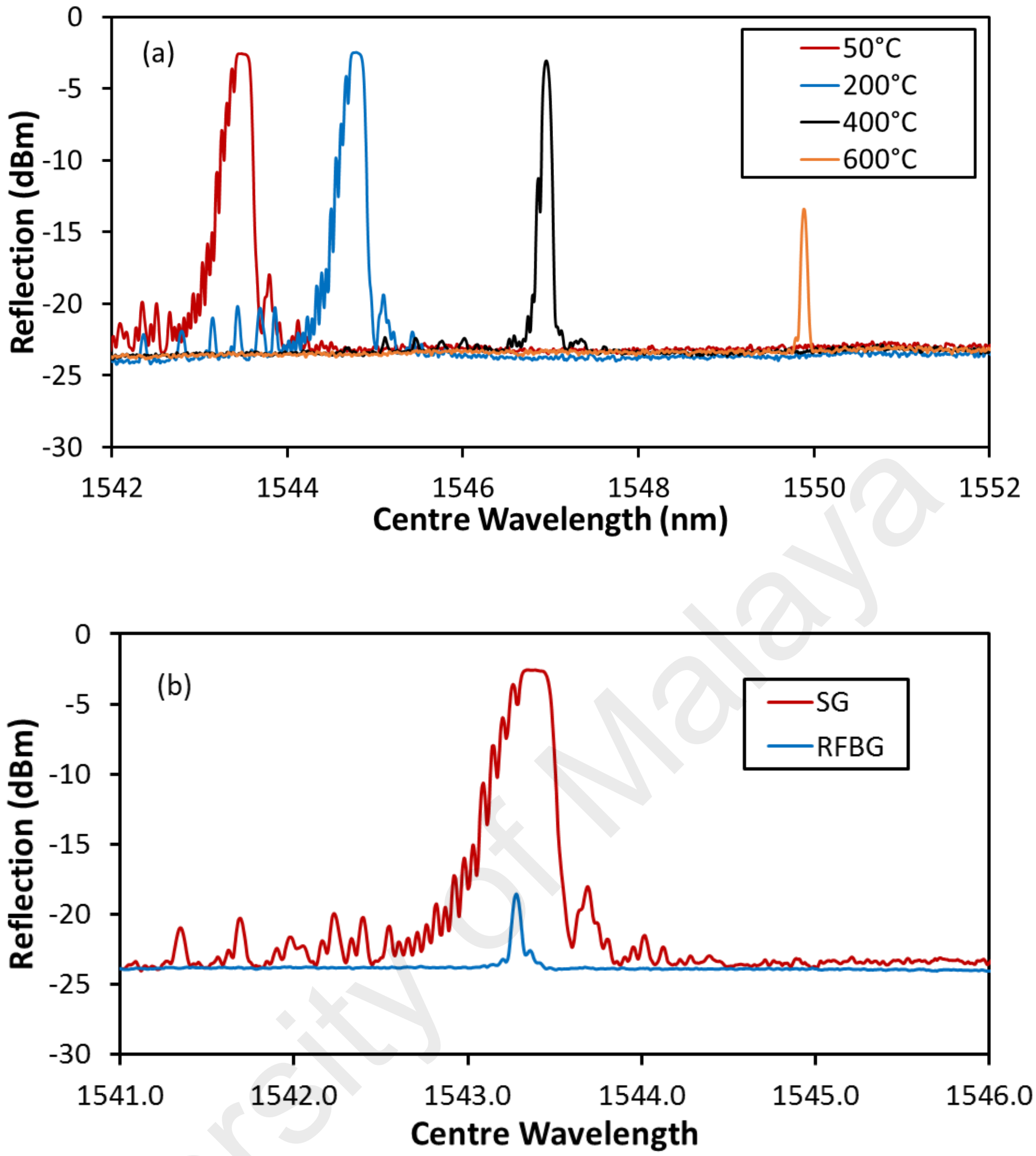

Figure 4.17: (a) Reflection spectra of the grating during the thermal annealing process at 50 °C, 200 °C, 400 °C and 600 °C (b) Reflection spectra of the seed and regenerated gratings at 25 °C.

The relaxation of UV-induced stress owing to thermal annealing in Ge-doped fibre through thermal annealing was first reported by Dürr et al. (2005). During the regeneration process, the UV-induced stress in the grating is reduced by thermal annealing to a minimum level at regeneration temperature. This is followed by the structural rearrangement of the molecules in the glass matrix where a new grating structure is slowly formed. Further research is being carried out to deduce the chemical procedures associated with Ga in the production of these RFBGs which would be beneficial in optimising the spectral properties and characteristics of these RFBGs.

From Figure 4.18, it can be seen that the gallosilicate regenerated grating exhibits a temperature sensitivity of 15.2 pm/°C and 15.0 pm/°C within the temperature range of 250 °C to 750 °C during the heating and cooling events, respectively. A ~ 9.4 nm wavelength shift can be observed over the full range up to 750 °C, the maximum calibration temperature. The slight difference in the temperature sensitivity during the heating and cooling procedures may be due to the temperature gradient between the RFBG and the thermocouple.

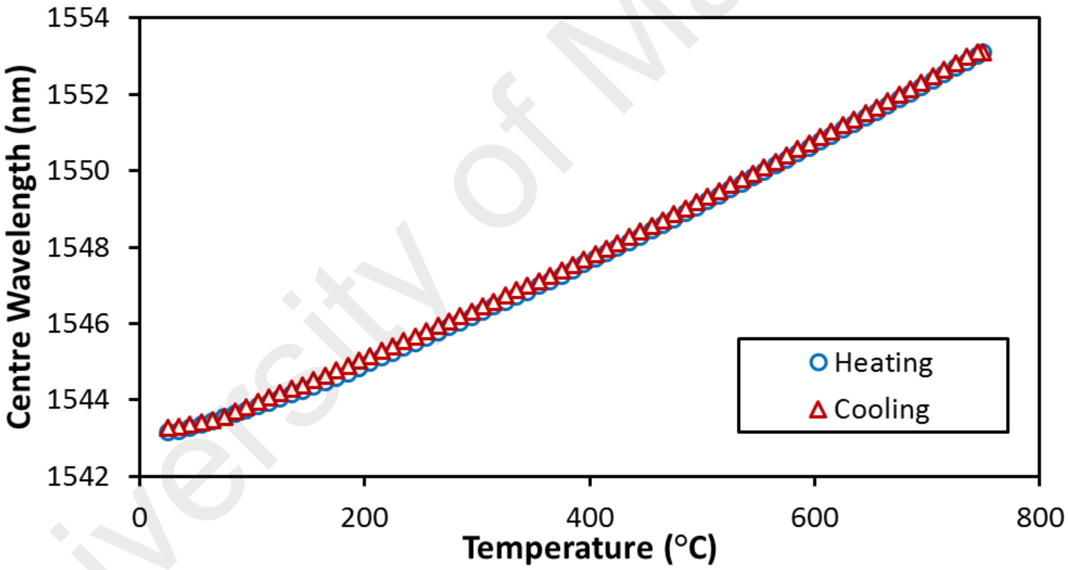

Figure 4.18: First cycle of temperature calibration of the regenerated gallosilicate grating in the range of 25-750 °C using a furnace with an increase rate of 2 °C/min.

The linear determination coefficient values (R^2) of 0.9991 and 0.9989 obtained during the two processes over the temperature range of 250 °C to 750 °C indicate a highly linear relationship during temperature calibration. However, a more non-linear behaviour is observed over the temperature range of 25 °C to ~250 °C. This non-linear pattern can be attributed to the non-linearity in the thermo-optic response of silica glass (Leviton & Frey, 2006). The almost similar sensitivity during heating and cooling without the presence of any hysteresis demonstrates a stable behaviour of the optical grating which ultimately leads towards a good sensing performance.

The centre wavelength shift of the RFBG is an important parameter when deducing the temperature variation and is crucial for sensors based on gratings. Figure 4.19(a) and (b) show the shift in the central wavelength against the temperature for three heating/cooling cycles including the initial cycle at a linear temperature variation rate of 2 ˚C/min. It is clearly noticed that the centre wavelength shift in each cycle overlaps with each other indicating a similar temperature sensitivity and excellent repeatability.

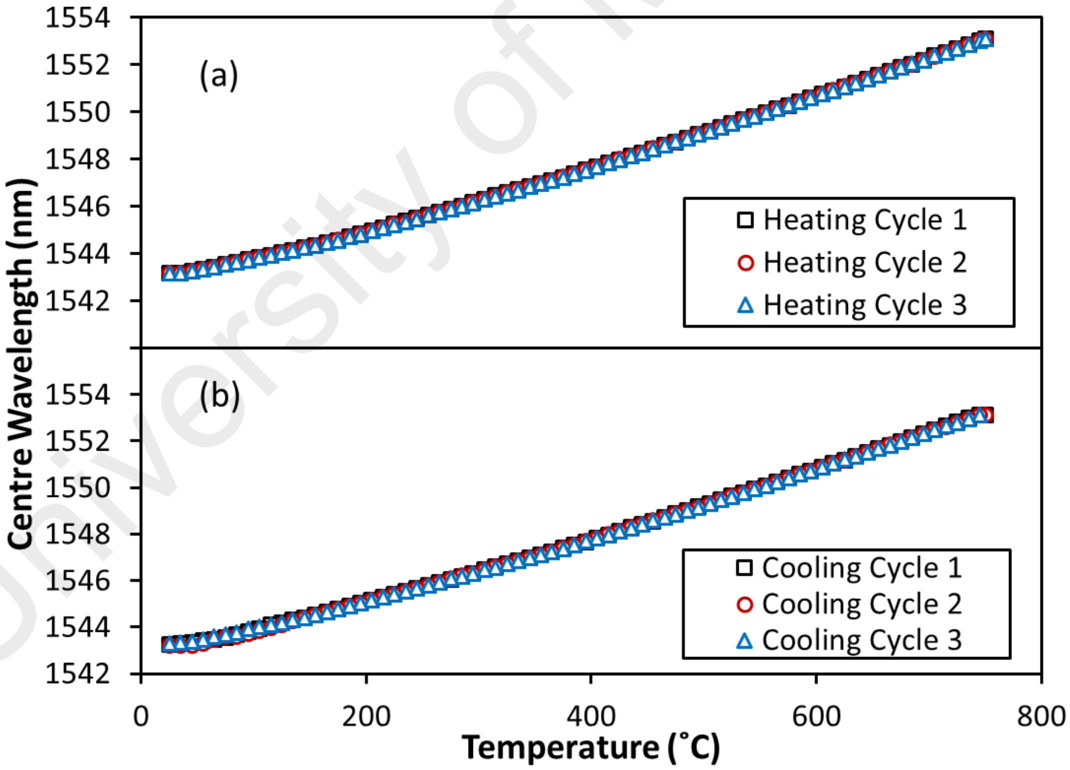

Figure 4.19: Centre wavelength shift of the RFBG with variation in temperature during (a) heating process and (b) cooling process.

Figure 4.20 indicates the shift in the centre wavelength monitored and recorded over a time period of 8 hours where each spectrum was swept at the resolution of 1 pm with the aid of an OSA. A wavelength variation of only 4.4 pm is calculated at 720 ˚C using standard deviation during this investigation.

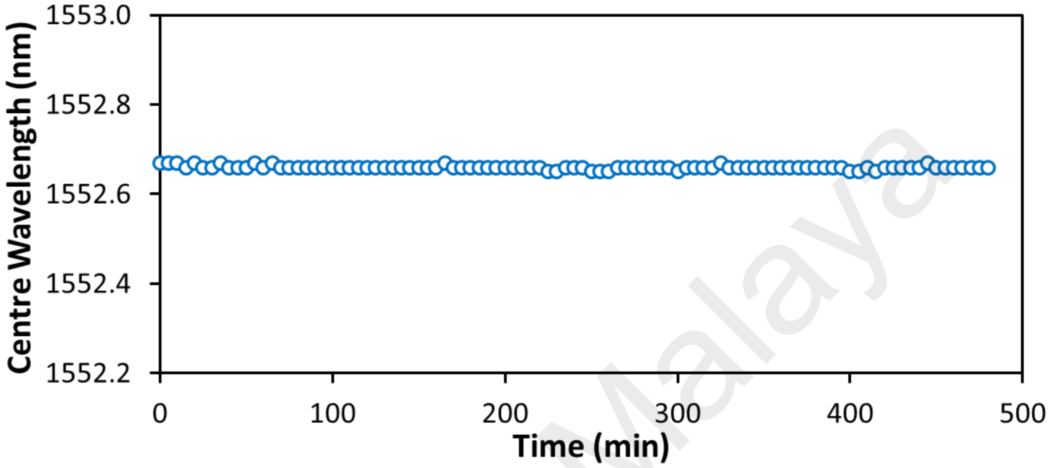

Figure 4.20: Wavelength stability performance over a time period of 8 hours at 720 ˚C.

The development of optical fibres with new glass compositions such as gallosilicate which consists of a single dopant with high photosensitivity characteristics as demonstrated in Chapter 3, together with its high temperature sustainability is essential for high temperature measurement applications and therefore provides the opportunity to be used as alternatives to the existing RFBG and can also be used as a substitute for rare earth doping. Apart from passive sensing applications, gallosilicate regenerated gratings can be considered as possible candidates for applications in high power-laser and active fibre sensing related research studies where conventional gratings are not suitable. This lays the platform for a new pathway of research in the field of active fibre sensing.

4.6 Summary

This chapter has focused on an investigation of the thermal stability of FBGs. Discussions of various decay models were included to provide comprehensive information to the reader. Additionally, the characteristic behaviour of FBGs during thermal annealing and different methods to enhance the thermal stability of a particular grating were discussed. CO_2 laser annealing was introduced as a technique to enhance thermal stability of an FBG. Numerous Bragg gratings capable of withstanding high temperatures were introduced and discussed. A thorough investigation on the regeneration properties of gallosilicate fibre was also carried out. Repetitive experiments to investigate the heating and cooling characteristics of gallosilicate fibre during the calibration of temperature sensitivity were performed and their outcomes analysed.

CHAPTER 5: THERMALLY ENDURING GRATINGS BASED ON THERMALLY INDUCED REVERSIBLE EFFECT

The main focus of this chapter is to emphasise the significantly high thermally induced reversible effect present in a grating as short as 10 mm inscribed in hydrogen (H_2) loaded Ge/B co-doped photosensitive fibre with 193 nm laser irradiation. A comprehensive investigation is carried out on this effect by performing both continuous and stepwise annealing procedures to demonstrate the grating decay behaviour in the demarcation energy domain, E_d and predict the operating lifetime of the grating. Further inspections are conducted on other types of fibre at various annealing rates to investigate the presence of the thermally induced reversible effect and to characterise the grating decay in the demarcation energy domain.

5.1 Thermally induced reversible effect

Many applications require the use of a grating with longer lifetime and good thermal stability for efficient functioning. In telecommunication standards, the grating based devices are required to have an operational lifetime of 25 years and function over a temperature range from -25 to +80 °C. It has been discovered by Erdogan et al. (1994) and Poumellec (1998) that pre-annealing an FBG wipes out a segment of the index change which has an irreversible decay ranging in the operating life span of the grating retaining simply the stabilised segment of the index change. Nevertheless, it is realised that temperature variation in a pre-annealed grating causes the Bragg wavelength to be shifted (Douay et al., 1993). This might be due to the fact that $\Delta\lambda_B$ is strongly influenced by the thermal expansion coefficients (Yoffe, Krug, Ouellette, & Thorncraft, 1995).

Reversible and irreversible changes in the reflectivity of a grating with increasing temperature have been observed by Razafimahatratra et al. (2000) in Ge, B and Sn co-doped silica fibre. Temperature induced isochronal and isothermal decays in Bragg gratings inscribed using CW exposure have been investigated. In the process, it has been noticed that the isochronal step decays aid in predicting the isothermal decays through consideration of reversible alterations in the reflectivity of a grating which occurs as a result of varying temperature. This is because the temperature variations occur in a stepwise process so that more control can be gained over the experiment. The accelerated ageing model discussed in Chapter 4 has been useful in sampling the initial dispersal of trapped site energies during isochronal annealing. Based on this observation, it is demonstrated that the initial dispersal for both weak and strong gratings are similar.

Hidayat et al. (2001) has reported the existence of reversible changes in highly Ge-doped fibres. However, this effect is not visible in H_2 loaded fibres. These changes have been induced by varying the temperature of the grating over the range of 77 K < T < 573 K and several factors responsible for the reversible changes have been investigated. The increased fraction of the guided optical power which travels through the fibre core due to heating of the fibre with reference to the dependence of overlap integral with temperature is considered as a possible explanation for the thermally induced reversible effect in the grating reflectivity (Hidayat et al., 2001). According to Hidayat et al. (2001) difference between core and cladding in dn/dT due to the chemical composition, the reliance of residual stress on temperature or due to UV-induced changes can be listed as the probable reasons for the reversible changes.

Gnusin, Vasil'ev, Medvedkov, and Dianov (2010), has reported the presence of reversible changes in grating reflectivity induced by strain and temperature in various types of FBGs. Based on the study, the reversible changes of type I, type IIa and H_2 loaded type I gratings have been investigated at elevated temperatures. An increase in the grating reflectivity by 3.1 % and 3.0 % has been observed for gratings with type I and type IIa characteristics respectively whereas the reflectivity of H_2 loaded type I grating remained unchanged. According to the study of Gnusin et al. (2010), when $\Delta n_{ind}(D)$ which is known as the photo-induced index change is a non-linear function of UV fluence, $\Delta n_{ind}(z)$ also referred to as the axial index profile is denoted as

$$\Delta n_{ind}(z) = \overline{\Delta n} + \sum_{m=1}^{\infty} A_m \cos\left(\frac{2\pi m}{\Lambda} z\right) \tag{5.1}$$

where $\overline{\Delta n}$ and m represent the average photo-induced index change and the diffraction order respectively. The axial UV intensity profile is assumed to be

$$I(z) = \frac{I_{\max}}{2}\left[1 + \cos\left(\frac{2\pi}{\Lambda} z\right)\right] \tag{5.2}$$

where $I_{\max}$ denotes the UV intensity at the crests of the interference fringe. The first diffraction order $m = 1$ in Eq. (5.1) is related to Δn_{mod} through $|A_1| = \Delta n_{\mathrm{mod}}$ where $A_1 > 0$ for type I and type I(H_2) FBGs and $A_1 < 0$ for type IIa. For varying temperature and strain conditions, the grating length varies even though the number of grating lines, N, remains the same. Hence, a non-dimensional alternating coupling parameter is proposed to study the temperature and strain effects on grating reflectivity of various FBGs. It is expressed as

$$\Omega = \frac{\pi \eta A_1}{2 n_{eff}} \tag{5.3}$$

It has a magnitude which is equivalent to the coupling coefficient per grating line and its relationship with the grating reflectivity is given by

$$R_{BR} = \tanh^2(|\Omega| N) \tag{5.4}$$

The importance of the coupling parameter has been highlighted and its relative changes as a function of temperature variation have been demonstrated. The effect of UV fluence and the concentration of Ge present in the core of the fibre on the reversible changes of the coupling parameter, Ω has been thoroughly analysed and it has been found that in relation to the UV fluence, reversible changes in the grating reflectivity are significant even at UV fluences as low as 1 kJ/cm^2. Furthermore, the initial increase in dΩ/dT for type I and IIa FBGs is correlated with the germanium concentration in the core of the fibre. Moreover, the results obtained to date suggest that the photo-induced transformations of defect centres which occur in the germanosilica glass network are responsible for the reversible changes at low fluence levels.

The thermo-optical coefficient undergoes spatial modulation during exposure of a germano-silicate glass to a UV fringe pattern. It is believed that this phenomenon has a considerable effect in the study of temperature induced reversible changes in refractive index modulation. The defects produced during the UV exposure, excluding Ge(1) and Ge(2) (Tsai, Williams, & Friebele, 1998) are generally presumed to be confined. This results in a spatial modulation of the UV-induced absorption spectrum along the fibre core (Leconte et al., 1997). An increase in the glass temperature leads to a reversible change of the absorption bands associated with defects, leading to a reversible alteration in the Δn_{mod}. Therefore, much effort has been directed towards testing these theories including the evolution of reversible changes of the index modulation with varying temperature and correlation with UV absorption and structural changes.

5.2 Origins of temperature reliance of grating reflectivity

5.2.1 Reliance of residual stress on temperature

Residual elastic stress and strain including frozen-in inelastic strains are present in many optical fibres. The thermal history, frozen-in viscoelasticity and UV-induced densification of a particular fibre is responsible for the frozen-in strains in the fibre (Fiori & Devine, 1986; Yablon, 2004; Yablon et al., 2003). Out of these factors, UV-induced densification is deemed as one of the main components of the index change in optical fibres (Fonjallaz et al., 1995; Limberger, Fonjallaz, Salathé, & Cochet, 1996; Raine, Feced, Kanellopoulos, & Handerek, 1999). UV densification results in a reversible effect during thermal annealing at high temperature regimes of 1000 ˚C (Fiori & Devine, 1986). Relaxation of the residual stress induced during fibre drawing can be attained through irradiation using a CO_2 laser.

At an annealing temperature exceeding the strain point of glass, thermal stress is present in the glass where the glass viscosity takes a value of $\eta=10^{14.5}$ poises. Permanent strain cannot be introduced to glass at values below this specific point. Atomic diffusion in the treated glass occurs at a greater rate beyond the glass transition temperature, resulting in the removal of residual stress within a time duration of 15 min. Complete removal of thermal stress can be achieved under uniform and controlled heating conditions which is subsequently trailed by a slow cooling procedure (Callister & Rethwisch, 2008; Ojovan, 2008).

5.2.2 Effect of structural changes

Some thermal properties of glass are modified by UV-induced structural alterations by varying its density which results in a temperature induced variation in Δn_{mod}. According to Limberger et al. (1996), the strong increase in the fibre core tension of a single-mode fibre during grating inscription is associated with the structural modification which results in compaction of the glass matrix. The study of Bazylenko, Moss, and Canning (1998) has demonstrated that plasma-enhanced chemical vapour deposition glass with continued UV exposure, tends to initially densify and then dilate. A straightforward relationship between growth of type IIA gratings and increasing compressive stress, orthogonal to the waveguide core with UV irradiation has been described by Canning and Åslund (1999). According to this study, the correlation is linked to structural changes through elastic dilations of the glass in the peak irradiation regions.

5.2.2.1 The relationship between structural changes and thermal expansion coefficient

Based on the research work of Chiang et al. (1993), the exposure of the fibre core to UV irradiation decreases the thermal expansion coefficient of the fibre by an amount of 15-30 % for a fibre doped with 15 mol% of GeO_2, due to strong UV-induced structural changes. When an optical fibre is exposed to a UV fringe pattern, a modulation of the expansion coefficient occurs due to its decrease at the bright fringes, along the fibre axis *Oz*. The increase in the fibre temperature results in a modulation of the stress being induced along *Oz*. This occurs at the region where bright and dark fringes indicate compression and dilation. UV-induced change in the thermal expansion coefficient affects the temperature sensitivity of the FBG. This causes the Bragg wavelength to be shifted by 16 and 5 pm for strong and weak gratings, respectively (Hidayat et al., 2001).

5.3 Characterisation of grating decay in the demarcation energy domain

Ge/B co-doped photosensitive fibres namely, PS 1250/1500 were loaded with H_2 at 2000 psi pressure for 12 days. Table 5.1 below indicates the specifications of this particular type of fibre.

Table 5.1: Specifications of Ge/B co-doped photosensitive fibre

Type of fibre	PS 1250/1500
Fibre diameter	125.1 μm
NA	0.13
Supplier	Fibrecore Ltd., UK

Afterwards, 10 mm long gratings were inscribed in them using ArF excimer laser-phase-mask technique. Recording and monitoring of the transmission spectra were carried out in a similar manner as discussed in Chapter 3. A pulse energy of 7 mJ and a repetition rate of 2 Hz consisting of a single pulse fluence of 560 mJ/cm^2 were used to fabricate FBGs with a peak reflectivity of ~99.98 %. Subsequently, the gratings were inserted to an oven and annealed at 80 ˚C for 24 hours and kept at room temperature for 10 days in order to remove the residue H_2. After out-diffusion of H_2, the gratings were placed in a tube furnace (see Figure 4.10) and the thermal annealing procedure was commenced, where the gratings were subjected to a continuous ramping rate of 3 °C/min starting from room temperature (25 °C) until 550 °C. Recording of the transmission spectra was carried out on a one minute interval basis. As discussed in Chapter 4, the thermal decay at each annealing temperature experienced by the grating was represented using *NICC*, η, since *ICC* depicts the grating strength and is associated with the UV-induced refractive index change.

To verify the accuracy of the experiment, a separate stepwise annealing process was also carried out and a detailed set of data was obtained. This particular experiment was conducted under similar conditions to the continuous annealing process initiating from 25 ˚C followed by 125 °C, 225 °C, 325 °C and 425 °C in a stepwise process. With the aid of an inbuilt program in the furnace, the temperature was dwelled on for a time duration of 2 hours at each temperature. Afterwards, these treated gratings which underwent the stepwise annealing process were subjected to an isothermal annealing procedure for 8 hours at 200 ˚C to explore their thermal stability. This procedure was repeated at 300 ˚C and 400 ˚ C.

Figure 5.1 illustrates the growth of the index change of H_2 loaded Ge/B co-doped photosensitive fibre using an ArF excimer laser. A ~99.98 % grating reflectivity with an index change of ~1.3×10^{-4} is achieved within ~96 s. Figure 5.2 indicates the transmission spectrum of the grating produced.

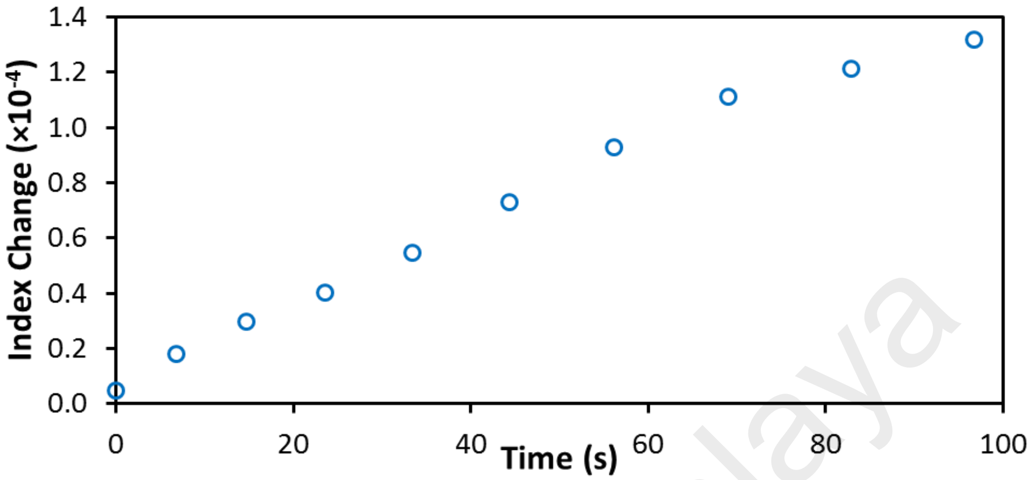

Figure 5.1: Rise of the refractive index change with increasing time during grating fabrication.

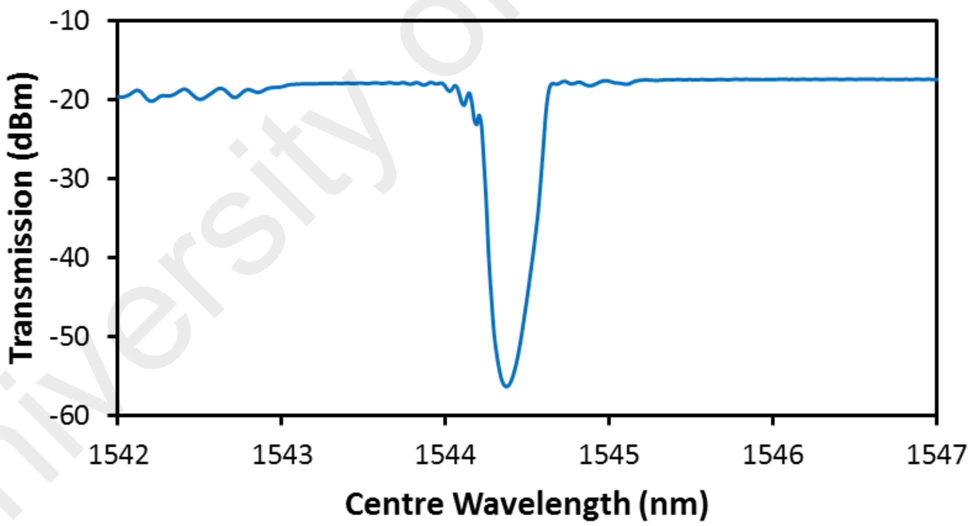

Figure 5.2: Transmission spectrum of the 10 mm long FBG inscribed in PS 1250/1500 fibre.

It is presumed that the activation energy of the thermodynamically unstable traps is broadly distributed when predicting the operational lifetime of the grating. Grating fabrication is responsible for this effect. The experimental support proving this can be found in (Pal, Mandal, Sun, & Grattan, 2003). Hence, the degree of ageing of an FBG at any particular time (t) and temperature (T) is ascertained with reference to an ageing parameter also acknowledged as the demarcation energy (E_d) (Erdogan et al. 1994) which is given by Eq. (4.3). The v value denotes the frequency term obtained through an iterative process where sets of data acquired at different temperatures are fitted.

The ageing curves for the data acquired during the two types of annealing processes are illustrated in Figure 5.3. A gradual decay until ~1.2 eV is observed for the FBG during the continuous annealing procedure. Nevertheless, a significant deviation in the general thermal decay behaviour is noticed past this point, where the *NICC* denotes a rise until ~1.4 eV. Therefore, a stepwise annealing procedure was conducted owing to this unpredicted observation, to yield more control over the annealing process. The grating reflectivity was also closely observed. Based on the results obtained from this experiment at four divergent temperatures of 125 °C, 225 °C, 325 °C and 425 °C, an increase in the *NICC* is again evident at ~1.2 eV. For the stepwise annealing procedure, the *NICC* achieves its peak at ~1.4 eV. This phenomenon corresponding to significant growth in the grating reflectivity, alluded to as the thermally induced reversible effect, possesses numerous advantages.

During the thermal annealing process, comprehensive information about the characteristic behaviour of the FBG can be acquired from the transmission spectra. This is due to the fact that a complete erasure of the seed grating does not take place during annealing, thereby allowing continuous observation of the Bragg transmission dip from the spectra. Figure 5.3 shows a plot of the *NICC* curves of both stepwise and continuous annealing processes in an overlaid graph. According to the plot, it is observed that the curves completely overlap over the full range of temperature. Hence, it is realised that regardless of the annealing approach, a similar characteristic curve is achieved for both annealing techniques when examined in the E_d domain. Thus, this method is beneficial in the prediction of the grating evolution when subjected to thermal annealing. Moreover, since it provides information for both continuous and stepwise annealing approaches, it can be incorporated as a grating characterisation technique in a user friendly manner.

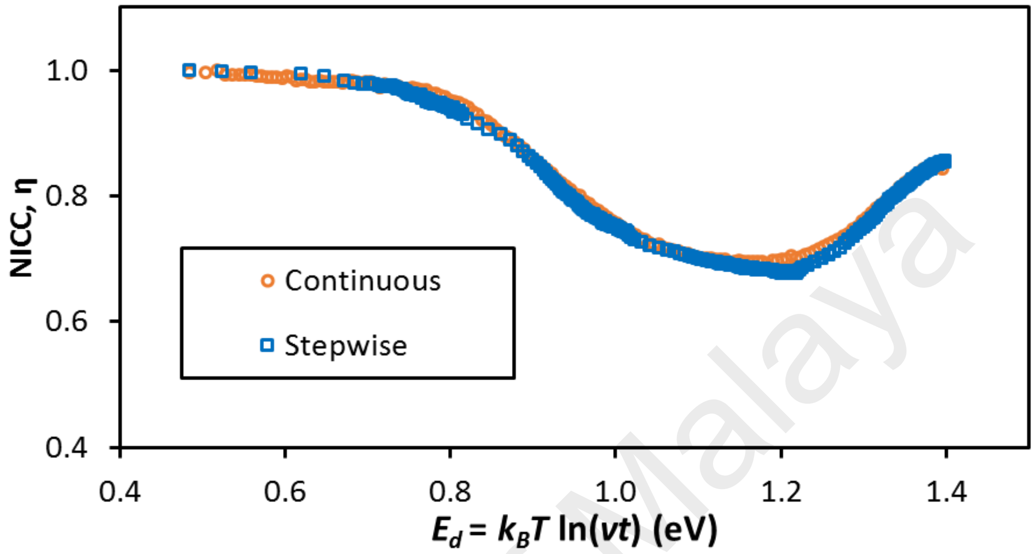

Figure 5.3: Accelerated ageing curves of continuous and stepwise thermal annealing processes plotted on an overlaid graph.

Figure 5.4 and 5.5 present the shift in centre wavelength during continuous and stepwise annealing procedures respectively.

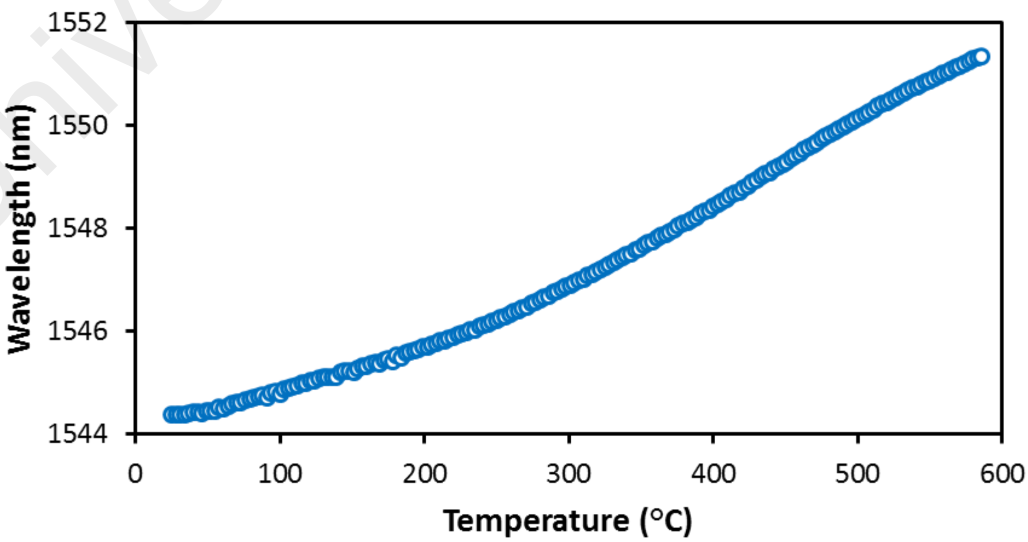

Figure 5.4: Progression of the centre wavelength during the continuous thermal annealing process.

An overall shift of ~7 nm is observed in the scenario of the continuous annealing approach and ~5 nm is noticed for the stepwise annealing procedure under different annealing time intervals.

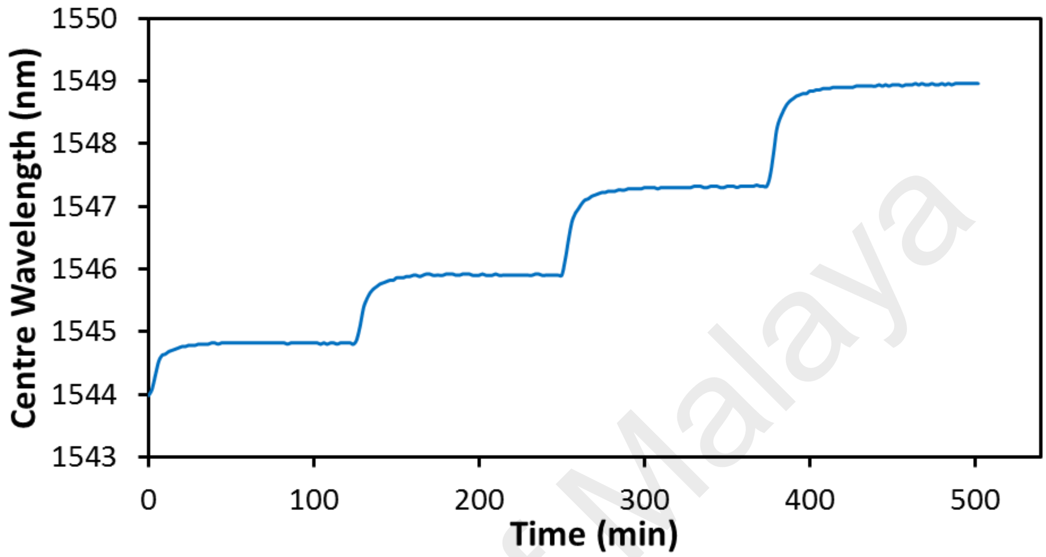

Figure 5.5: Progression of the centre wavelength during the stepwise thermal annealing process.

Figure 5.6 indicates the variation in the grating reflectivity observed during the continuous annealing process at temperatures before (375 ˚C) and after (485 ˚C) the temperature at which the thermally induced reversible effect takes place. Evidently, a prominent increase in the grating reflectivity is observed for the latter temperature.

The thermal decay behaviour of the 10 mm long grating at 125 °C, 225 °C, 325 °C and 425 °C ranging over a time duration of 2 hours at each specific temperature is shown in Figure 5.7. This thorough study is helpful in predicting the thermal stability of the grating. Thermal degradation at each temperature is calculated based on its initial grating strength. At the temperatures of 125 °C, 225 °C and 325 °C, a fast degradation followed by a substantial slow degradation is observed resulting in an overall decay of 7 %, 20 % and 6 %, respectively. Nevertheless, a noticeable increase in the *NICC* by an amount of ~18 %

owing to the thermally induced reversible effect is observed at 425 °C. When compared to the initial grating strength prior to the initiation of the annealing procedure, it is also evident that the grating strength has reduced only by 15 %. Thermal decay characteristics of the FBG demonstrated in Figure 5.7 are examined in terms of *NICC* due to its correlation with Δn_{mod}.

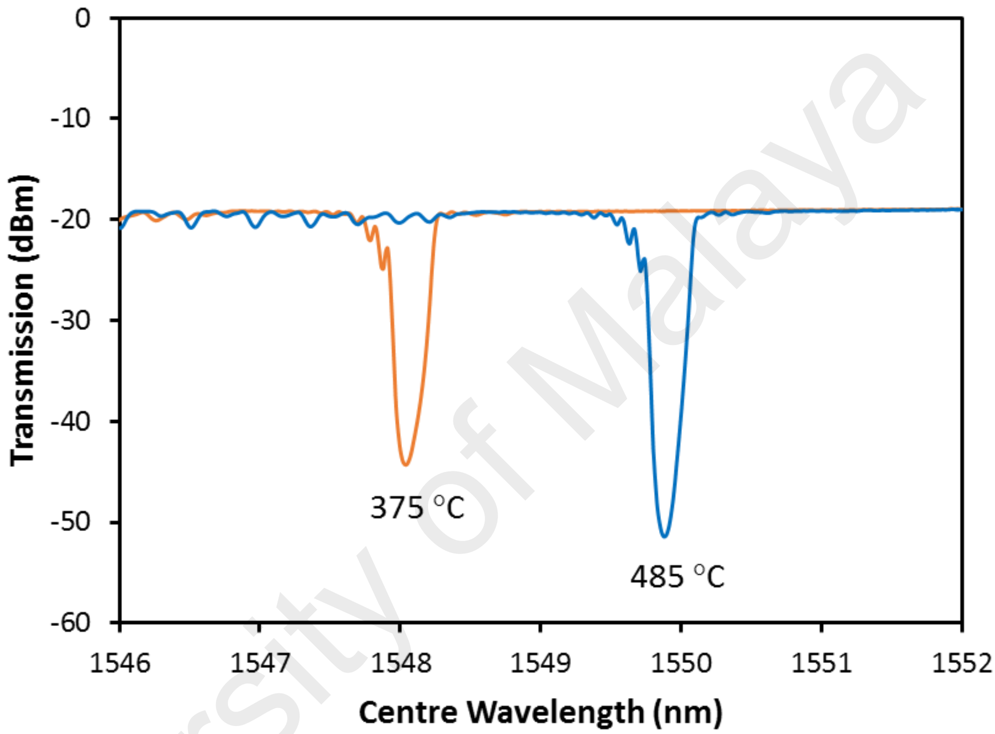

Figure 5.6: Difference in grating reflectivity at 375 °C and 485 °C during continuous annealing.

In Figure 5.3, the best fit value for v was found to be 2.5×10^{6}, in the fitting of step-wise and continuous annealing curves. By fitting the data of the accelerated ageing tests at 125 °C, 225 °C and 325 °C (Figure 5.7) to a single ageing curve (Erdogan et al., 1994; Kannan et al., 1997; Pal et al., 2003), this value is acquired. According to Hidayat et al. (2001) and Razafimahatratra et al. (2000), the factors such as the processing and the type of the grating used are responsible for the variation in the grating reflectivity caused by the temperature induced reversible and irreversible changes. A reversible temperature induced rise in the reflectivity of a pre-annealed type I grating has been recorded. Moreover, a strategy for extrapolation in accelerated testing based on a step stress experiment has been proposed by LuValle, Copeland, Kannan, Judkins, and Lemaire (1998) to decrease the influence of large *v* values compared to the estimated ones. Furthermore, a recent investigation of Poumellec and Lancry (2015) has suggested a framework based on dispersed activated energy of a physico-chemical reaction, to model thermally activated procedures for the creation or erasure of species. These species are particularly related to the UV-induced index changes in optical fibres. The framework gives details about the entire time behaviour and permits the annealing conditions for elongated lifetimes to be deduced. Hence, these highly complex phenomena related to grating degradation complicate precise computation of the grating stability.

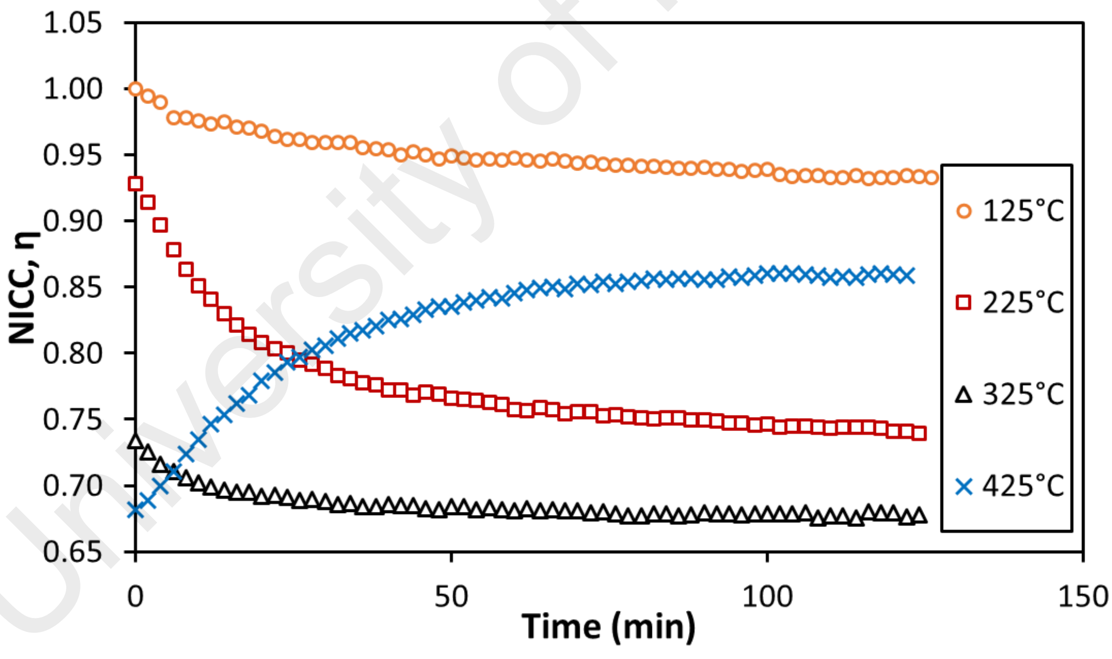

Figure 5.7: Thermal degradation of the grating with time in terms of *NICC* at different temperatures of 125°C, 225°C, 325°C and 425°C.

Figure 5.8 demonstrates the accelerated ageing experiments conducted on the treated FBG at 200 °C, 300 °C and 400 °C, after being subjected to the previously discussed annealing processes. The temperature was maintained constant for 8 hours at each temperature. Based on Figure 5.8, a decay of the grating strength by an amount of ~1 % and ~1.5 % is observed at 200 °C and 300 °C respectively. At 400 °C, an overall degradation of ~6 % is evident over the time duration of 8 hours. This suggests the high durability of the treated FBG. Additionally, the decay of *NICC* present at the initial phase of the annealing process can be attributed to several factors for instance, the initial ramping rate (10 ˚C/min) and the temperature stabilisation period before being subjected to the fixed temperatures at 200 °C, 300 °C and 400 °C.

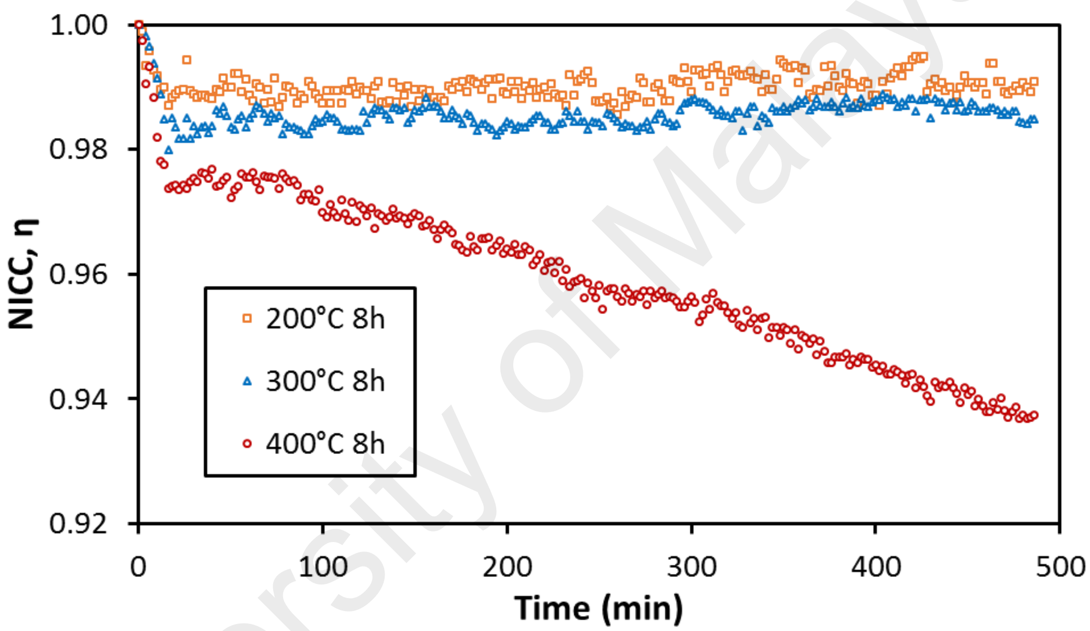

Figure 5.8: Accelerated ageing curves at 200 °C, 300 °C and 400 °C for the treated grating.

The data of Figure 5.8 were fitted with the ageing curve model (Erdogan et al., 1994) described by Eq. (4.4) to evaluate the long-term stability of the grating. E_d was predicted using a single value of the estimated frequency, v on the basis of the ageing curve approach. Afterwards, the grating decay was anticipated depending on the best fit to the single ageing curve (Erdogan et al., 1994; Kannan et al., 1997). When compared to the power-law approach, the ageing curve approach is believed to be more universal (Kannan et al., 1997).

The anticipated decay characteristics of a 10 mm long grating at three different temperatures of 200 °C, 300 °C and 400 °C simulated over a time duration of a thousand years is shown in Figure 5.9. Within a time interval of a thousand years, a ~1 % and ~2 % deterioration of the grating strength at 200 °C and 300 °C, respectively are observed. However, the grating strength gently decays to a complete zero at 400 °C. In general, a telecommunication grating consisting of a maximum degradation below 2 % for a time duration of at least 20 years at an operating temperature ranging from -20 °C to 70 °C is required (Chen & Herman, 2003). The FBG whose decay characteristic is illustrated in Figure 5.9 is capable of withstanding temperatures up to 300 ˚C whilst exhibiting a decay of ~2 % over a 1000 years. This is 50 times higher than the specified time period and ~4 times higher than the necessary operating temperature limit. In addition, the comparatively low percentage thermal degradation at each temperature for an FBG with a grating length as short as 10 mm, is also considered as a significant achievement.

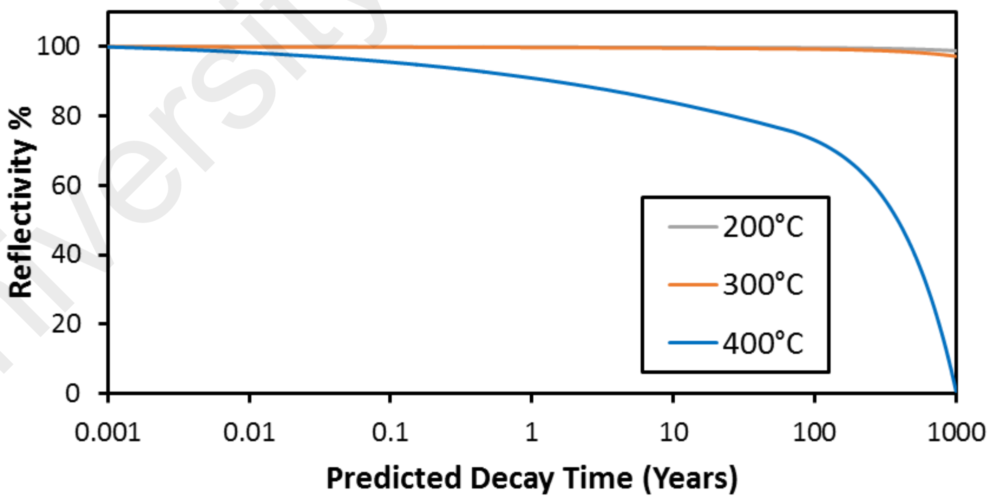

Figure 5.9: Predicted decay time for the treated FBG at 200 °C, 300 °C and 400 °C.

5.3.1 Effect of temperature ramping rate

Over the past few years, some studies have demonstrated the effect of using different temperature ramping rates on different types of fibres during various experiments when exploring the thermal decay characteristics of gratings. Rathje et al. (2000) has investigated the effect of temperature ramp speeds on the survival of the grating of both deuterium (D_2) loaded and non-loaded 15 mol% Ge-doped photosensitive fibre. According to the study three similar gratings have been annealed at three different ramping speeds of 0.25, 0.025 and 0.0036 K/s. The analysis of the normalised thermal degradation of the grating strength, κL has indicated that all three gratings possess a similar shape of thermal decay curves but are lengthened along the temperature axis indicating that the FBG experiencing the fastest heating rate exhibits the maximum surviving temperature. Afterwards, an ageing curve has been plotted and its reliability obtained from raw data has been tested by performing a separate experiment. The results achieved have indicated that the actual and the predicted decay curves exhibit good agreement with each other. Differentiating the ageing curve has provided sufficient information on the underlying energy distribution. A similar type of experiment has been conducted using gratings inscribed in D_2 loaded fibre and the results obtained have indicated two energy distributions showing the involvement of two different defects.

The study of Violakis, Limberger, Mashinsky, and Dianov (2011) has revealed the thermal stability of H_2 loaded and non-loaded Bi-Al-SiO_2 and SMF-28 fibres through continuous isochronal thermal annealing procedure. Three varying ramp rates of 0.25, 0.025 and 0.0038 K/s have been used during the experiment on three similar FBGs in each type of fibre. The fastest and slowest heating rates have been constrained by the specifications of the furnace and some practical concerns such as the complete run time (< 3 days). Motivation for using the three different ramp rates is to be able to include two orders of magnitude of ramp rate over the range 0.25 to 0.0038 K/s. The resulting spectra have been analysed in a similar way to that suggested by Rathje et al. (2000) when determining the thermal sustainability of the FBGs. The refractive index changes and the thermal decay parameters for each heating rate have also been illustrated.

The study of temperature ramping rate is not limited to the analysis of thermal decay characteristics. Some research studies have investigated the role of different thermal ramping rates during thermal regeneration of FBGs. As discussed in Chapter 4, Bueno et al. (2013) has managed to achieve fast regeneration of Bragg gratings. A RFBG with 1.6 dB reflectivity has been achieved within a time span of 10 min and by adjusting the temperature of the oven, RFBGs exhibiting different amounts of losses over various time spans have also been obtained. In addition, Lai, Gunawardena, et al. (2015) has demonstrated the time consumed by three distinct types of gratings in different fibres namely, PS 1250/1500, SM 1500 and ZWP-SMF for grating regeneration under different heating rates by direct CO_2 laser annealing. According to this study, PS 1250/1500 fibre has appeared to produce the optimum result of the three types of fibres examined.

5.3.2 Thermal decay comparison of different gratings

Figure 5.10 shows the decay characteristics of PS 1250/1500, SM 1500 and ZWPF at three different annealing rates of 3 °C/min, 6 °C/min and 9 °C/min. In Figure 5.10(a), a gradual decay is observed until 425 °C in PS 1250/1500 which follows the usual temperature decay behaviour of a grating. However, subsequently an increase in the *NICC* is observed in the region of 425-550 °C depending on the ramping rate. This phenomenon known as the thermally induced reversible effect has been observed in PS 1250/1500 gratings during both stepwise and continuous annealing processes as discussed in Chapter 5.3. Afterwards, a rapid thermal decay can be observed until the grating completely vanishes, commencing the grating regeneration process.

Nevertheless, when the annealing temperature is further increased the RFBG initiates its decaying process in the region of 900-950 °C. It is also noticed that gratings inscribed in the PS 1250/1500 have the lowest value of regeneration temperature between the three fibres investigated. The existence of the boron dopant reduces the glass transition temperature of the fibre material which permits stress relaxation to occur and the glass structure to be rearranged at a lower temperature (Lai, Gunawardena, et al., 2015). A slight increase in the *NICC* in the region of ~350 °C is observed in the case of the SM 1500. However, it is less significant compared to the phenomenon present in Figure 5.10(a). Regeneration characteristics in SM 1500 gratings were observed at 800 °C, 838 °C and 860 °C for temperature ramping rates of 3 °C/min, 6 °C/min and 9 °C/min respectively. When compared with PS 1250/1500 and OFS zero water peak fibre, SM 1500 exhibits the highest *NICC* during regeneration especially when the experiment was conducted at a ramping rate of 3 °C/min. The presence of the thermally induced reversible effect can be considered negligible in ZWPF although grating regeneration can still be clearly observed in 950-1015 °C range which subsequently decays to a complete zero with increasing temperature.

Furthermore, according to Figure 5.10 it is also noticed that with increasing annealing rate the temperature at which the grating regeneration occurs gradually increases. This condition is visible in the gratings inscribed in all three types of fibre. In addition, it is also found that H_2 loading plays a vital role in increasing the possibility of attaining thermal regeneration (Canning et al., 2010).

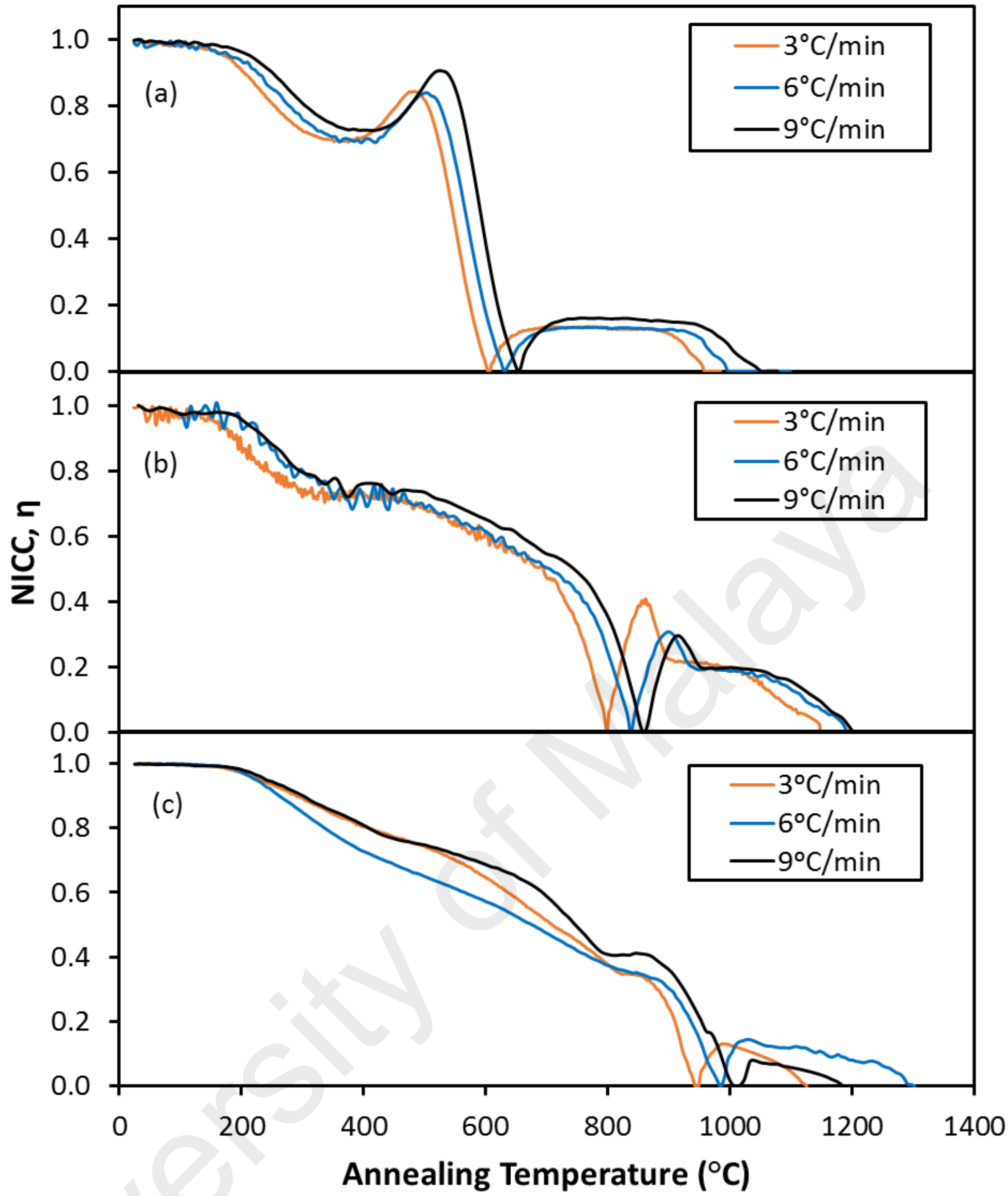

Figure 5.10: Thermal decay characteristics of (a) PS 1250/1500 (b) SM 1500 and (c) ZWPF at temperature ramping rates of 3 °C/min, 6 °C/min and 9 °C/min.

The degree of ageing of a particular grating at a specific time (t) and temperature (T) is realised by the demarcation energy, (E_d) (Erdogan et al., 1994) also known as the ageing parameter (refer to Eq. (4.3)). Figure 5.11 illustrates the accelerated ageing curves of the three types of fibre at three different temperature ramping rates. When plotted on an overlaid graph in the demarcation energy (E_d) domain, each type of grating namely, PS 1250/1500, SM 1500 and ZWPF indicate a common regeneration point regardless of the difference in the temperature ramping rates. For PS 1250/1500 this point occurs at ~1.46 eV and it is clearly noticed that a higher ramping rate results in a higher *NICC* of 0.16. In the case of SM 1500 and ZWPF, the regeneration points are achieved at 1.57 and 1.96 eV respectively. The calculated v value for PS 1250/1500, SM 1500 and zero water peak gratings are 2.5×10^{6} Hz, 2×10^{4} Hz and 1×10^{5} Hz respectively. Representing the thermal degradation of the FBGs in the E_d domain provides the opportunity of projecting the decay of an FBG for any amalgamation of time and temperature.

Figure 5.12 indicates transmission spectra of the three types of fibre and their respective centre wavelengths obtained during the grating regeneration procedure at a temperature ramping rate of 9 °C/min. Regeneration in SM 1500 occurs at a much higher wavelength/temperature compared to PS 1250/1500 and ZWPF. Comparatively, SM 1500 exhibits a much higher maximum grating reflectivity of ~6.3 dB during regeneration followed by PS 1250/1500 and lastly ZWPF.

This is possibly related to the thermal sensitivity and the original Bragg wavelength. Based on the observed results, grating regeneration of ZWPF occurs at the highest temperature in comparison to the rest of the gratings and results in a grating reflectivity of approximately 1 dB.

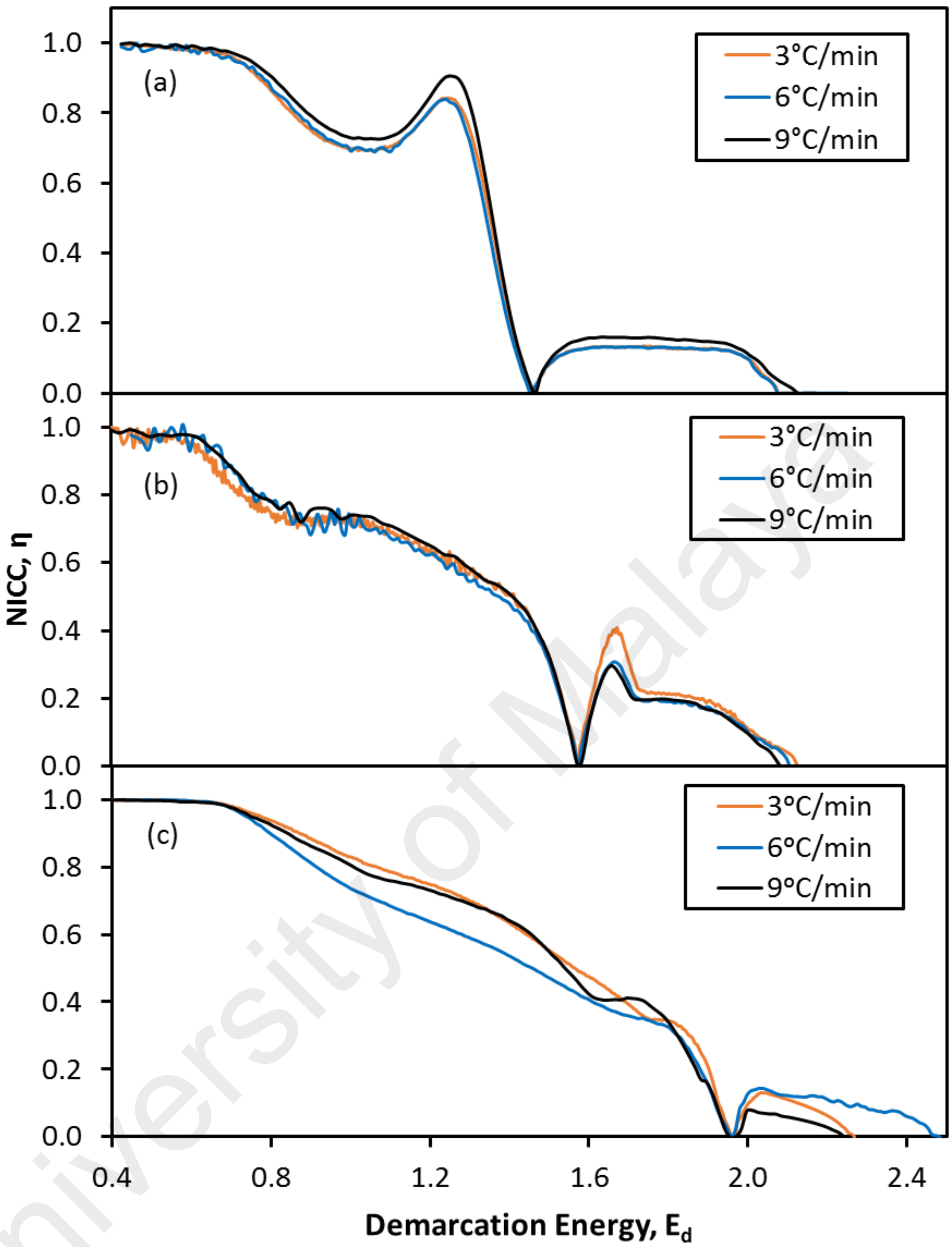

Figure 5.11: Accelerated ageing curves of (a) PS 1250/1500 (b) SM 1500 and (c) OFS ZWPF at temperature ramping rates of 3 °C/min, 6 °C/min and 9 °C/min.

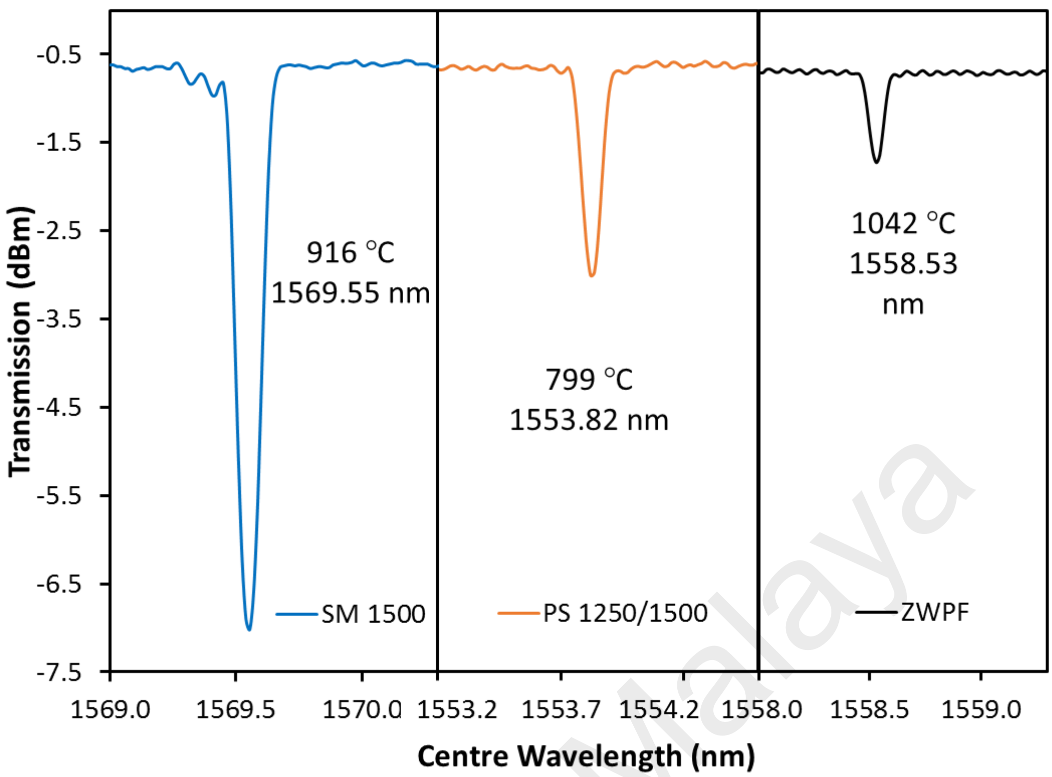

Figure 5.12: Segments of transmission spectra indicating the maximum grating reflectivity of three regenerated gratings in PS 1250/1500, SM 1500 and ZWPF at 9 °C/min ramping rate.

5.4 Summary

This chapter included a comprehensive investigation of a thermally enduring fibre Bragg grating which possesses the capability of functioning for a thousand years at 300 ˚C with a predicted thermal decay of less than 2 %. This specific FBG was inscribed in a Ge/B co-doped silica fibre with a short grating length of 10 mm. Both stepwise and continuous annealing processes produced gratings with similar decay behaviour when characterised in the demarcation energy, E_d domain. During thermal annealing, a considerable growth in the grating reflectivity was observed referred to as the thermally induced reversible effect. The transmission spectra provide comprehensive information about the progression of the FBG since the seed grating does not undergo complete erasure during the thermal annealing process.

In addition, the thermal decay behaviour of gratings written in three distinct types of H_2 loaded fibre under three different ramping rates of 3 °C/min, 6 °C/min and 9 °C/min were investigated. The ageing characteristics were explored and a characterisation technique for the thermal decay of a specific grating in the demarcation energy domain was proposed with minimum reliance on the temperature ramping rate.

CHAPTER 6: CONCLUSION AND FUTURE DIRECTION

This chapter concludes the thesis which deals with various techniques for characterisation and realisation of novel fibre Bragg gratings (FBGs) both in theoretical and experimental point of views. It summarises the results and findings of this research study and proposes a direction for future research to exploit the key findings of the current investigation.

6.1 Conclusion

The research contribution of this thesis has concentrated on the photosensitivity, grating strength and thermal endurance of fibre Bragg gratings (FBGs). The proposed Ga-doped optical fibre demonstrates high photosensitivity capabilities and is more photosensitive compared to the generally used Ge-doped fibre especially at low UV fluence levels when irradiated with 193 nm ArF excimer laser at both H_2 loaded and H_2 free conditions. The enhancement in photosensitivity to the ArF excimer laser is due to the high absorbance at 193 nm. Since Ga-doped fibre produces high index changes at low UV fluence levels in the prescence of H_2, it can be considered as an excellent candidate for efficient FBG production with minimum consumption of UV fluence.

A mathematical model was proposed to characterise the growth of refractive index change in fibre during grating fabrication. Both Δn_{ave} and Δn_{mod} were determined from the recorded transmission spectra and were incorporated in the generation of the local refractive index changes, Δn_{max} and Δn_{min}. A single characteristic function, $\Delta n[F]$ was used to characterise the curves of Δn_{max} and Δn_{min}. A gradual decrease in the grating visibility, v_g was observed during the FBG inscription process. The curve-matching technique was used to measure the interference visibility, v_i with the aid of Δn_{max} and Δn_{min} curves. This simple technique serves as a convenient tool for characterisation of the grating inscription setup especially when determining the interference and grating visibilities.

The bent-spectral analysis method was conducted in two stages, where spectral properties of the FBGs were analysed at each stage which assisted in deducing the grating visibility values under applied UV fluence and bending conditions. Measurements of the grating visibility after grating inscription and with decreasing bending radius were compared by representing the two functions on an overlaid graph. The experiment was repeated for a wide range of visibility values to verify the validity of the results. The accuracy of these results was confirmed by investigating the cross correlation coefficient of the functions. Interference and grating visibilities are two parameters which influence the grating strength. Therefore, the importance in calculating these two parameters together with the relative ease of use and cost effectiveness offered by this technique makes it more appealing to be used in practical applications.

In the exploration of thermal stability of Bragg gratings, grating regeneration characteristics were observed in Ga-doped optical fibres. These regenerated fibre Bragg gratings (RFBGs) are suitable for measuring temperature even at high temperature range. The grating regeneration results in an increase of the grating reflectivity at 720 °C after being initially bleached. Temperature sensitivities of 15.2 pm/°C and 15.0 pm/°C were attained during temperature calibration for the respective heating and cooling processes. These findings of RFBGs open up an entirely new area of research in designing temperature sensors using new glass compositions capable of withstanding high temperatures.

In addition, with the use of a new annealing treatment, a thermal enduring FBG sensor was fabricated based on thermally induced reversible effect, which is capable of operating for a thousand years with a predicted thermal decay of less than 2 % at 300 ˚C. The FBG consisting of a grating length as short as 10 mm is inscribed in Germanium/Boron co-doped photosensitive silica core fibre. A similar trend of progression during both stepwise and continuous annealing procedures was observed for the gratings when characterised with respect to the demarcation energy E_d. This permits reliable predictions to be made on the thermal decay characteristics of the respective gratings. Since the process does not involve complete erasure of the seed grating (SG) as in the case of grating regeneration, it provides the possibility of observing the grating decay behaviour through monitoring of the transmission spectra and enabling detailed information to be obtained on the progression of the grating. The predicted thermal degradation of the grating is less than 2 % for a thousand years and maintains a grating reflectivity of 98 % at 300 ˚C. This grating with prolonged thermal endurance gives rise to a new sector of research in the investigation of durable fibre grating sensors suitable for applications conducted in the range of 200 - 400 ˚C.

The thermal degradation of gratings fabricated in three different types of H_2 loaded fibres were explored under three different temperature ramping rates of 3 °C/min, 6 °C/min and 9 °C/min. The thermally induced reversible effect was prominent in PS 1250/1500 gratings. The ageing characteristics were explored in the E_d domain and a characterising technique which can be used to predict the thermal degradation of a particular FBG with minimum dependence on the thermal annealing rate was proposed.

6.2 Future Direction

As well as the interest of producing photosensitive fibre with regeneration capabilities, Ga-doping can also be beneficial in the production of efficient and high power optical amplifiers and lasers, because it possesses index raising capabilities and the added benefit of being used as a substitute for Aluminium (Al) when co-doping with rare-earth materials. In addition, gratings can be efficiently inscribed in these rare-earth doped fibres followed by thermal regeneration to produce efficient fibre lasers or distributed Bragg reflectors (DBRs) which can withstand high temperatures. Also, it is believed that Ga-doped fibre at communication transmission bands can be accommodated as an alternative to germanosilicate fibre for similar applications.

In the characterisation of the grating strength, the measurement results of interference and grating visibilities can be used to obtain information about the coherence properties of the laser used which will be beneficial in optimising the performance of the grating inscription system. Since both the curve-matching technique and the bent-spectral analysis technique use only the existing components and equipment in the grating inscription system, additional peripheral tools will not be required for this characterisation tests making them cost-effective characterisation tools suitable for both the manufacturing industry and academic research of FBGs.

The grating with prolonged thermal endurance fabricated based on the thermally induced reversible effect can be successfully used as a temperature sensor at elevated temperatures due to its enhanced temperature response which does not involve complete grating regeneration. These gratings can also be accommodated in a vast number of applications where extended grating lifetime is a priority. Moreover, the study conducted to analyse the effect of annealing at various temperature ramping rates can be further extended to few-mode and multi-mode fibre where a comprehensive investigation can be carried out in the E_d domain. Optical fibres have revolutionised the telecommunication and sensing industries and FBGs are considered to be prime components of the optical fibre technology. Hence, further research needs to be carried out to harness each and every aspect of Bragg gratings.

REFERENCES

Aarts, R. M., Irwan, R., & Janssen, A. J. (2002). Efficient tracking of the cross-correlation coefficient. *IEEE Transactions on Speech and Audio Processing*, *10*(6), 391-402.

Albert, J., Hill, K. O., Johnson, D. C., Bilodeau, F., & Rooks, M. J. (1996). Moire phase masks for automatic pure apodisation of fibre Bragg gratings.*Electronics Letters*, *32*(24), 2260-2261.

Albert, J., Theriault, S., Bilodeau, F., Johnson, D. C., Hill, K. O., Sixt, P., & Rooks, M. J. (1996). Minimization of phase errors in long fiber Bragg grating phase masks made using electron beam lithography. *IEEE Photonics Technology Letters*, *8*(10), 1334-1336.

Albert, J., Hill, K. O., Johnson, D. C., Bilodeau, F., Mihailov, S. J., Borrelli, N. F., & Amin, J. (1999). Bragg gratings in defect-free germanium-doped optical fibers. *Optics letters*, *24*(18), 1266-1268.

Albert, J., Hill, K. O., Malo, B., Theriault, S., Bilodeau, F., Johnson, D. C., & Erickson, L. E. (1995). Apodisation of the spectral response of fibre Bragg gratings using a phase mask with variable diffraction efficiency. *Electronics Letters*, *31*(3), 222-223.

Allard, L. B., Albert, J., Brebner, J. L., & Atkins, G. R. (1997). Photoinduced optical absorption and 400-nm luminescence in low-germanium-content optical fiber preforms irradiated with ArF and KrF excimer-laser light. *Optics letters*, *22*(11), 819-821.

Anderson, D. Z., Mizrahi, V., Erdogan, T., & White, A. E. (1993a). Production of in-fibre gratings using a diffractive optical element. *Electronics Letters*, *29*(6), 566-568.

Anderson, D. Z., Mizrahi, V., Erdogan, T., & White, A. E. (1993b, February). Phase-mask method for volume manufacturing of fiber phase gratings. In*Optical Fiber Communication Conference* (p. PD16). Optical Society of America.

Antipov, S., Ams, M., Williams, R. J., Magi, E., Withford, M. J., & Fuerbach, A. (2016). Direct infrared femtosecond laser inscription of chirped fiber Bragg gratings. *Optics express*, *24*(1), 30-40.

Archambault, J. L. (1994). *Photorefractive gratings in optical fibres* (Doctoral Thesis, Southampton University, United Kingdom).

Archambault, J. L., Reekie, L., & Russell, P. S. J. (1993a). 100% reflectivity Bragg reflectors produced in optical fibres by single excimer laser pulses.*Electronics Letters, 29*(5), 453-455.

Archambault, J. L., Reekie, L., & Russell, P. S. J. (1993b). High reflectivity and narrow bandwidth fibre gratings written by single excimer pulse.*Electronics letters*, *29*(1), 28-29.

Åslund, M., & Canning, J. (2000). Annealing properties of gratings written into UV-presensitized hydrogen-outdiffused optical fiber. *Optics letters*, *25*(10), 692-694.

Åslund, M., Canning, J., & Yoffe, G. (1999). Locking in photosensitivity within optical fiber and planar waveguides by ultraviolet preexposure. *Opt. Lett*, *24*(24), 1826-1828.

Atkins, R. M., & Mizrahi, V. (1992). Observations of changes in UV absorption bands of singlemode germanosilicate core optical fibres on writing and thermally erasing refractive index gratings. *Electronics Letters*, *28*(18), 1743-1744.

Atkins, R. M., Lemaire, P. J., Erdogan, T., & Mizrahi, V. (1993). Mechanisms of enhanced UV photosensitivity via hydrogen loading in germanosilicate glasses. *Electronics Letters*, *29*(14), 1234-1235.

Atkins, R. M., Mizrahi, V., & Erdogan, T. (1993). 248 nm induced vacuum UV spectral changes in optical fibre preform cores: support for a colour centre model of photosensitivity. *Electronics Letters*, *29*(4), 385-387.

Baker, S. R., Rourke, H. N., Baker, V., & Goodchild, D. (1997). Thermal decay of fiber Bragg gratings written in boron and germanium codoped silica fiber. *Journal of Lightwave Technology*, *15*(8), 1470-1477.

Ball, G. A., & Morey, W. W. (1991). Efficient integrated Nd/sup 3+/fiber laser.*IEEE photonics technology letters*, *3*(12), 1077-1078.

Ball, G. A., Morey, W. W., & Glenn, W. H. (1991). Standing-wave monomode erbium fiber laser. *IEEE Photonics Technology Letters*, *3*, 613-615.

Ball, G. A., & Morey, W. W. (1992). Continuously tuneable single-mode erbium fiber laser. *Optics letters*, *17*(6), 420-422.

Bandyopadhyay, S., Canning, J., Biswas, P., Stevenson, M., & Dasgupta, K. (2011). A study of regenerated gratings produced in germanosilicate fibers by high temperature annealing. *Optics express*, *19*(2), 1198-1206.

Bandyopadhyay, S., Canning, J., Stevenson, M., & Cook, K. (2008). Ultrahigh-temperature regenerated gratings in boron-codoped germanosilicate optical fiber using 193 nm. *Opt. Lett*, *33*(16), 1917-1919.

Barsanti, S., Cannas, M., & Bicchi, P. (2007). Gallium doped SiO 2: Towards a new luminescent material. *Journal of Non-Crystalline Solids*, *353*(5), 679-683.

Bazylenko, M. V., Moss, D., & Canning, J. (1998). Complex photosensitivity observed in germanosilica planar waveguides. *Optics letters*, *23*(9), 697-699.

Bernardin, J. P., & Lawandy, N. M. (1990). Dynamics of the formation of Bragg gratings in germanosilicate optical fibers. *Optics communications*, *79*(3-4), 194-199.

Bilodeau, F., Hibino, Y., Abe, M., Malo, B., Albert, J., Kawachi, M., ... & Hill, K. O. (1993). Photosensitization of optical fiber and silica-on-silicon/silica waveguides. *Optics Letters*, *18*(12), 953-955.

Brambilla, G., & Pruneri, V. (2001). Enhanced photorefractivity in tin-doped silica optical fibers (review). *Institute of Electrical and Electronics Engineers: Journal of Selected Topics in Quantum Electronics*, *7*(3), 403-408.

Brambilla, G., Pruneri, V., & Reekie, L. (2000). Photorefractive index gratings in SnO2: SiO2 optical fibres. *Appl. Phys. Lett*, *76*(7), 807.

Brambilla, G., Pruneri, V., Reekie, L., & Payne, D. N. (1999). Enhanced photosensitivity in germanosilicate fibers exposed to CO 2 laser radiation.*Optics letters*, *24*(15), 1023-1025.

Bueno, A., Kinet, D., Mégret, P., & Caucheteur, C. (2013). Fast thermal regeneration of fiber Bragg gratings. *Optics letters*, *38*(20), 4178-4181.

Butov, O. V., Dianov, E. M., & Golant, K. M. (2006). Nitrogen-doped silica-core fibres for Bragg grating sensors operating at elevated temperatures.*Measurement science and technology*, *17*(5), 975.

Byron, K. C., Sugden, K., Bricheno, T., & Bennion, I. (1993). Fabrication of chirped Bragg gratings in photosensitive fibre. *Electronics letters*, *29*(18), 1659-1660.

Callister, W. D., & Rethwisch, D. G. (2008). *Fundamentals of materials science and engineering: an integrated approach*. Wiley.

Camlibel, I., Pinnow, D. A., & Dabby, F. W. (1975). Optical aging characteristics of borosilicate clad fused silica core fiber optical waveguides. *Applied Physics Letters*, *26*(4), 185-187.

Canning, J. (2008). Fibre gratings and devices for sensors and lasers. *Laser & Photonics Reviews*, *2*(4), 275-289.

Canning, J., & Åslund, M. (1999). Correlation of ultraviolet-induced stress changes and negative index growth in type IIa germanosilicate waveguide gratings. *Optics letters*, *24*(7), 463-465.

Canning, J., & Sceats, M. G. (1994). Pi-phase-shifted periodic distributed structures in optical fibres by UV post-processing. *Electronics Letters*, *30*, 1344-1345.

Canning, J., Cook, K., Åslund, M., Stevenson, M., Biswas, P., & Bandyopadhyay, S. (2010). *Regenerated fibre Bragg gratings*. INTECH Open Access Publisher.

Caucheteur, C., Wuilpart, M., Chen, C., Megret, P., & Albert, J. (2009, January). Multi-point in-line refractometry using tilted fiber Bragg gratings. In*2009 IEEE/LEOS Winter Topicals Meeting Series*.

Chen, K. P., & Herman, P. R. (2003). Photosensitization of standard fibers with deep UV laser radiation. *Journal of lightwave technology*, *21*(9), 1958-1968.

Chen, K. P., Herman, P. R., Taylor, R., & Hnatovsky, C. (2003). Vacuum-ultraviolet laser-induced refractive-index change and birefringence in standard optical fibers. *Journal of lightwave technology*, *21*(9), 1969-1977.

Cheong, Y. K., Chong, W. Y., Chong, S. S., Lim, K. S., & Ahmad, H. (2014). Regenerated Type-IIa Fibre Bragg Grating from a Ge–B codoped fibre via thermal activation. *Optics & Laser Technology*, *62*, 69-72.

Chiang, K. S., Sceats, M. G., & Wong, D. (1993). Ultraviolet photolytic-induced changes in optical fibers: the thermal expansion coefficient. *Optics letters*, *18*(12), 965-967.

Cole, M. J., Loh, W. H., Laming, R. I., Zervas, M. N., & Barcelos, S. (1995). Moving fibre/phase-mask-scanning beam technique for enhanced flexibility in producing fibre gratings with uniform phase-mask. *Electronics Letters-IEE*, *31*, 1488-1490.

Cook, K., Shao, L. Y., & Canning, J. (2012). Regeneration and helium: regenerating Bragg gratings in helium-loaded germanosilicate optical fibre.*Optical Materials Express*, *2*(12), 1733-1742.

Cortes, P. Y., Ouellette, F., & LaRochelle, S. (1998). Intrinsic apodisation of Bragg gratings written using UV-pulse interferometry. *Electronics Letters*, *34*(4), 396-397.

D'Amato, F. X., & Dunphy, J. R. (1992, November). Tuneable semiconductor laser sources using fiber Bragg gratings. In *LEOS'92, Conference Proceedings. IEEE Lasers and Electro-Optics Society, 1992 Annual Meeting*(pp. 343-344). IEEE.

Davis, D. D., Gaylord, T. K., Glytsis, E. N., & Mettler, S. C. (1999). Very-high-temperature stable CO 2-laser-induced long-period fibre gratings.*Electronics Letters*, *35*(9), 740-742.

Davis, K. M., & Tomozawa, M. (1995). Water diffusion into silica glass: structural changes in silica glass and their effect on water solubility and diffusivity. *Journal of Non-Crystalline Solids*, *185*(3), 203-220.

Dianov, E. M., Golant, K. M., Khrapko, R. R., Kurkov, A. S., & Tomashuk, A. L. (1995). Low-hydrogen silicon oxynitride optical fibers prepared by SPCVD. *Journal of lightwave technology*, *13*(7), 1471-1474.

Dianov, E. M., Golant, K. M., Khrapko, R. R., Kurkov, A. S., Leconte, B., Douay, M., ... & Niay, P. (1997, February). Grating formation in a germanium free silicon oxynitride fibre. In *Optical Fibre Gratings (Digest No. 1997/037), IEE Colloquium on* (pp. 4-1). IET.

Dianov, E. M., Golant, K. M., Mashinsky, V. M., Medvedkov, O. I., Nikolin, I. V., Sazhin, O. D., & Vasiliev, S. A. (1997). Highly photosensitive nitrogen-doped germanosilicate fibre for index grating writing. *Electronics Letters*, *33*(15), 1334-1335.

Dianov, E. M., Karpov, V. I., Grekov, M. V., Golant, K. M., Vasiliev, S. A., Medvedkov, O. I., & Khrapko, R. R. (1997, January). Thermo-induced long-period fibre gratings. In *IEE conference publication* (Vol. 2, pp. 53-56). Institution of Electrical Engineers.

Dianov, E. M., Plotnichenko, V. G., Koltashev, V. V., Pyrkov, Y. N., Ky, N. H., Limberger, H. G., & Salathe, R. P. (1997). UV-irradiation-induced structural transformation of germanoscilicate glass fiber. *Optics letters*, *22*(23), 1754-1756.

Dong, L., & Liu, W. F. (1997). Thermal decay of fiber Bragg gratings of positive and negative index changes formed at 193 nm in a boron-codoped germanosilicate fiber. *Applied optics*, *36*(31), 8222-8226.

Dong, L., Archambault, J. L., Reekie, L., Russell, P. S. J., & Payne, D. N. (1995). Photoinduced absorption change in germanosilicate preforms: evidence for the color-center model of photosensitivity. *Applied optics*, *34*(18), 3436-3440.

Dong, L., Cruz, J. L., Reekie, L., Xu, M. G., & Payne, D. N. (1995). Enhanced photosensitivity in tin-codoped germanosilicate optical fibers.*IEEE Photonics Technology Letters*, *7*(9), 1048-1050.

Dong, L., Cruz, J. L., Tucknott, J. A., Reekie, L., & Payne, D. N. (1995). Strong photosensitive gratings in tin-doped phosphosilicate optical fibers.*Optics letters*, *20*(19), 1982-1984.

Dong, L., Liu, W. F., & Reekie, L. (1996). Negative-index gratings formed by a 193-nm excimer laser. *Optics letters*, *21*(24), 2032-2034.

Dong, L., Pinkstone, J., Russell, P. S. J., & Payne, D. N. (1994). Ultraviolet absorption in modified chemical vapor deposition preforms. *JOSA B*, *11*(10), 2106-2111.

Douay, M., Fertein, E., Xie, W. X., Bernage, P., Niay, P., Bayon, J. F., & Georges, T. (1993). Thermal hysteresis of Bragg wavelengths of intra-core fiber gratings. *IEEE photonics technology letters*, *5*(11), 1331-1334.

Dürr, F., Limberger, H. G., Salathé, R. P., Vasiliev, S. A., Medvedkov, O. I., Bozhkov, A. S., & Dianov, E. M. (2005). Annealing-induced stress changes in UV-irradiated germanium-doped fibers. In *BGPP'2005, Bragg Gratings, Photosensitivity, and Poling in Glass Waveguides: OSA Topical Meeting*.

Dyer, P. E., Farley, R. J., & Giedl, R. (1995). Analysis of grating formation with excimer laser irradiated phase-masks. *Optics communications*, *115*(3), 327-334.

Eggleton, B. J., Ahmed, K. A., Liu, H. F., Krug, P. A., & Poladian, L. (1994). Experimental demonstration of compression of dispersed optical pulses by reflection from self-chirped optical fiber Bragg gratings. *Optics letters*, *19*(12), 877-879.

Erdogan, T. (1997). Fiber grating spectra. *Journal of lightwave technology*, *15*(8), 1277-1294.

Erdogan, T., Mizrahi, V., Lemaire, P. J., & Monroe, D. (1994). Decay of ultraviolet-induced fiber Bragg gratings. *Journal of Applied Physics*, *76*(1), 73-80.

Farries, M. C., Radgale, C., & Reid, D. C. J. (1992). Broadband chirped fibre Bragg filters for pump rejection and recycling in erbium doped fibre amplifiers. *Electronics letters*, *28*(5), 487-489.

Fiori, C., & Devine, R. A. B. (1985). Ultraviolet irradiation induced compaction and photoetching in amorphous, thermal SiO 2. In *MRS Proceedings* (Vol. 61, p. 187). Cambridge University Press.

Fokine, M. (2002). *Photosensitivity, chemical composition gratings and optical fiber based components* (Doctoral Thesis, Royal Institute of Technology, Stockholm, Sweden). Retrieved from http://www.diva-portal.org/smash/get/diva2:9235/FULLTEXT01.pdf

Fokine, M. (2004). Underlying mechanisms, applications, and limitations of chemical composition gratings in silica based fibers. *Journal of non-crystalline solids*, *349*, 98-104.

Fokine, M., Sahlgren, B. E., & Stubbe, R. (1996, December). High temperature resistant Bragg gratings fabricated in silica optical fibres. In*Proc. Australian Conf. on Optical Fibre Technology (ACOFT)*.

Fonjallaz, P. Y., Cochet, F., Leuenberger, B., Limberger, H. G., & Salathé, R. P. (1995). Tension increase correlated to refractive-index change in fibers containing UV-written Bragg gratings. *Optics letters*, *20*(11), 1346-1348.

Fujimaki, M., Watanabe, T., Katoh, T., Kasahara, T., Miyazaki, N., Ohki, Y., & Nishikawa, H. (1998). Structures and generation mechanisms of paramagnetic centers and absorption bands responsible for Ge-doped SiO 2 optical-fiber gratings. *Physical Review B*, *57*(7), 3920.

Ghosh, S., Das, S., Paul, M. C., Dasgupta, K., Bohra, D., Chaudhary, H. S., ... & Vaijapurkar, S. G. (2011). Evaluation of the performance of high phosphorous with germanium codoped multimode optical fiber for use as a radiation sensor at low dose rates. *Applied Optics*, *50*(25), E80-E85.

Gnusin, P. I., Vasil'ev, S. A., Medvedkov, O. I., & Dianov, E. M. (2010). Reversible changes in the reflectivity of different types of fibre Bragg gratings. *Quantum Electronics*, *40*(10), 879-886.

Grand, G., Jadot, J. P., Denis, H., Valette, S., Fournier, A., & Grouillet, A. M. (1990). Low-loss PECVD silica channel waveguides for optical communications. *Electronics letters*, *26*(25), 2135-2137.

Grattan, K. T. V., & Meggitt, B. T. (Eds.). (2000). *Optical fiber sensor technology: Advanced applications :* Kluwer Academic. Dordrecht.

Groothoff, N., & Canning, J. (2004). Enhanced type IIA gratings for high-temperature operation. *Optics letters*, *29*(20), 2360-2362.

Grubsky, V., Starodubov, D. S., & Feinberg, J. (1999a). Photochemical reaction of hydrogen with germanosilicate glass initiated by 3.4–5.4-eV ultraviolet light. *Optics letters*, *24*(11), 729-731.

Grubsky, V., Starodubov, D. S., & Feinberg, J. (1999b, February). Effect of molecular water on thermal stability of gratings in hydrogen-loaded optical fibers. In *Optical Fiber Communication Conference, 1999, and the International Conference on Integrated Optics and Optical Fiber Communication. OFC/IOOC'99. Technical Digest* (Vol. 3, pp. 53-55). IEEE.

Hand, D. P., & Russell, P. S. J. (1990). Photoinduced refractive-index changes in germanosilicate fibers. *Optics letters*, *15*(2), 102-104.

Harwig, T., & Kellendonk, F. (1978). Some observations on the photoluminescence of doped β-galliumsesquioxide. *Journal of Solid State Chemistry*, *24*(3), 255-263.

Herbst, L., & Govorkov, S. V. (2003, April). Excimer laser application: writing of fiber Bragg gratings. In *Photonics Fabrication Europe* (pp. 35-42). International Society for Optics and Photonics.

Hidayat, A., Wang, Q., Niay, P., Douay, M., Poumellec, B., Kherbouche, F., & Riant, I. (2001). Temperature-induced reversible changes in the spectral characteristics of fiber Bragg gratings. *Applied optics*, *40*(16), 2632-2642.

Hill, K. O., & Meltz, G. (1997). Fiber Bragg grating technology fundamentals and overview. *Journal of lightwave technology*, *15*(8), 1263-1276.

Hill, K. O., Bilodeau, F., Malo, B., & Johnson, D. C. (1991). Birefringent photosensitivity in monomode optical fibre: application to external writing of rocking filters. *Electronics Letters*, *27*(17), 1548-1550.

Hill, K. O., Fujii, Y., Johnson, D. C., & Kawasaki, B. S. (1978). Photosensitivity in optical fiber waveguides: Application to reflection filter fabrication. *Applied Physics Letters, 32*(10), 647-649.

Hill, K. O., Malo, B., Bilodeau, F., Johnson, D. C., & Albert, J. (1993). Bragg gratings fabricated in monomode photosensitive optical fiber by UV exposure through a phase mask. *Applied Physics Letters*, *62*(10), 1035-1037.

Hill, K. O., Malo, B., Vineberg, K. A., Bilodeau, F., Johnson, D. C., & Skinner, I. (1990). Efficient mode conversion in telecommunication fibre using externally written gratings. *Electronics Letters*, *26*(16), 1270-1272.

Hill, K. O., Takiguchi, K., Bilodeau, F., Malo, B., Kitagawa, T., Thériault, S., ... & Albert, J. (1994). Chirped in-fiber Bragg gratings for compensation of optical-fiber dispersion. *Optics letters*, *19*(17), 1314-1316.

Hosono, H., Abe, Y., Kinser, D. L., Weeks, R. A., Muta, K., & Kawazoe, H. (1992). Nature and origin of the 5-eV band in SiO 2: GeO 2 glasses. *Physical Review B*, *46*(18), 11445.

Hosono, H., Mizuguchi, M., Kawazoe, H., & Nishii, J. (1996). Correlation between Ge E′ Centers and Optical Absorption Bands in SiO2: GeO2 Glasses. *Japanese journal of applied physics*, *35*(2B), L234.

Huebner, J., Svalgaard, M., Gruener-Nielsen, L., & Kristensen, M. (1997, January). Phenomenological model of UV-induced Bragg grating growth in germanosilicate fibers. In *Photonics West'97* (pp. 11-21). International Society for Optics and Photonics.

Iadicicco, A., Campopiano, S., Paladino, D., Cutolo, A., & Cusano, A. (2007). Micro-structured fiber Bragg gratings: optimization of the fabrication process. *Optics express*, *15*(23), 15011-15021.

Islam, M. R., Gunawardena, D. S., Lee, Y. S., Lim, K. S., Yang, H. Z., & Ahmad, H. (2016). Fabrication and characterization of laser-ablated cladding resonances of two different-diameter photosensitive optical fibers. *Sensors and Actuators A: Physical*, *243*, 111-116.

Ivanov, O. V. (2004). Near-field effects in fabrication of fiber Bragg gratings using phase masks. *Optics communications*, *229*(1), 167-172.

James, S. W., & Tatam, R. P. (2003). Optical fibre long-period grating sensors: characteristics and application. *Measurement science and technology*, *14*(5), R49.

Kajihara, K., Ikuta, Y., Oto, M., Hirano, M., Skuja, L., & Hosono, H. (2004). UV–VUV laser induced phenomena in SiO 2 glass. *Nuclear Instruments and Methods in Physics Research Section B: Beam Interactions with Materials and Atoms*, *218*, 323-331.

Kannan, S., & Lemaire, P. J. Thermal reliability of Bragg gratings written in hydrogen-sensitized fibers. In *Optical Fiber Communications, 1996. OFC'96*(pp. 84-85). IEEE.

Kannan, S., Guo, J. Z., & Lemaire, P. J. (1997). Thermal stability analysis of UV-induced fiber Bragg gratings. *Journal of lightwave technology*, *15*(8), 1478-1483.

Karpov, V. I., Grekov, M. V., Dianov, E. M., Golant, K. M., & Khrapko, R. R. (1998). Utlra-Thermostable Long-Period Gratings Written in Nitrogen-Doped Silica Fibers. In *MRS Proceedings* (Vol. 531, p. 391). Cambridge University Press.

Kashyap, R. (1999). *Fiber bragg gratings*. Academic press.

Kashyap, R., Armitage, J. R., Wyatt, R., Davey, S. T., & Williams, D. L. (1990). All-fibre narrowband reflection gratings at 1500 nm. *Electronics Letters*, *26*(11), 730-732.

Kashyap, R., McKee, P. F., Campbell, R. J., & Williams, D. L. (1994). Novel method of producing all fibre photoinduced chirped gratings. *Electronics letters*, *30*(12), 996-998.

Kersey, A. D., Davis, M. A., Patrick, H. J., LeBlanc, M., Koo, K. P., Askins, C. G., ... & Friebele, E. J. (1997). Fiber grating sensors. *Journal of lightwave technology*, *15*(8), 1442-1463.

Kim, C. S., Han, Y., Lee, B. H., Han, W. T., Paek, U. C., & Chung, Y. (2000). Induction of the refractive index change in B-doped optical fibers through relaxation of the mechanical stress. *Optics Communications*, *185*(4), 337-342.

Kim, J. M., Oh, K., Park, T. S., Kim, C. S., & Jeong, K. (2000). Suppression of cladding-mode coupling loss in fiber Bragg gratings by independent control of refractive index and photosensitive profiles in a single-mode optical fiber.*IEEE Photonics Technology Letters*, *12*(11), 1504-1506.

Kim, N. H., Kim, H. W., & Lee, C. (2004). Amorphous gallium oxide nanowires synthesized by metalorganic chemical vapor deposition. *Materials Science and Engineering: B*, *111*(2), 131-134.

Kirchof, J., Unger, S., Pissler, H. J., & Knappe, B. (1995, February). Hydrogen-induced hydroxyl profiles in doped silica layers. In *Optical Fiber Communication Conference* (p. WP9). Optical Society of America.

Kogelnik, H., & Shank, C. V. (1972). Coupled-wave theory of distributed feedback lasers. *Journal of applied physics*, *43*(5), 2327-2335.

Kohnke, G. E., Nightingale, D. W., Wigley, P. G., & Pollock, C. R. (1999, February). Photosensitization of optical fiber by UV exposure of hydrogen loaded fiber. In *Optical Fiber Communication Conference* (p. PD20). Optical Society of America.

Ky, N. H., Limberger, H. G., Salathé, R. P., Cochet, F., & Dong, L. (2003). UV-irradiation induced stress and index changes during the growth of type-I and type-IIA fiber gratings. *Optics Communications*, *225*(4), 313-318.

Ky, N. H., Limberger, H. G., Salathé, R. P., Cochet, F., & Dong, L. (1998). Effects of drawing tension on the photosensitivity of Sn–Ge-and B–Ge-codoped core fibers. *Optics letters*, *23*(17), 1402-1404.

Laffont, G., Cotillard, R., & Ferdinand, P. (2013). Multiplexed regenerated fiber Bragg gratings for high-temperature measurement. *Measurement Science and Technology*, *24*(9), 094010.

Lai, M. H., Gunawardena, D. S., Lim, K. S., Yang, H. Z., & Ahmad, H. (2015). Observation of grating regeneration by direct CO_2 laser annealing.*Optics express*, *23*(1), 452-463.

Lai, M. H., Lim, K. S., Gunawardena, D. S., Yang, H. Z., Chong, W. Y., & Ahmad, H. (2015). Thermal stress modification in regenerated fiber Bragg grating via manipulation of glass transition temperature based on CO_2-laser annealing. *Optics letters*, *40*(5), 748-751.

Lancry, M., & Poumellec, B. (2013). UV laser processing and multiphoton absorption processes in optical telecommunication fiber materials. *Physics Reports*, *523*(4), 207-229.

Lancry, M., Poumellec, B., Costes, S., & Magné, J. (2014). Reliable Lifetime Prediction for Passivated Fiber Bragg Gratings for Telecommunication Applications. *Fibers*, *2*(1), 92-107.

Leconte, B., Xie, W. X., Douay, M., Bernage, P., Niay, P., Bayon, J. F., ... & Poignant, H. (1997). Analysis of color-center-related contribution to Bragg grating formation in Ge: SiO 2 fiber based on a local Kramers–Kronig transformation of excess loss spectra. *Applied optics*, *36*(24), 5923-5930.

Lemaire, P. J., Atkins, R. M., Mizrahi, V., & Reed, W. A. (1993). High pressure H2 loading as a technique for achieving ultrahigh UV photosensitivity and thermal sensitivity in GeO2 doped optical fibres.*Electronics Letters*, *29*(13), 1191-1193.

Leviton, D. B., & Frey, B. J. (2006, June). Temperature-dependent absolute refractive index measurements of synthetic fused silica. In *SPIE Astronomical Telescopes+ Instrumentation* (pp. 62732K-62732K). International Society for Optics and Photonics.

Liberman, V., Bloomstein, T. M., Rothschild, M., Sedlacek, J. H. C., Uttaro, R. S., Bates, A. K., ... & Orvek, K. (1999). Materials issues for optical components and photomasks in 157 nm lithography. *Journal of Vacuum Science & Technology B*, *17*(6), 3273-3279.

Lim, K. S., Gunawardena, D. S., Lai, M. H., Islam, M. R., Yang, H. Z., Qiao, X., ... & Ahmad, H. (2015). Characterization of phasemask interference visibility and the evolution of grating visibility during grating formation. *Measurement*, *64*, 163-167.

Lim, K. S., Yang, H. Z., Becir, A., Lai, M. H., Ali, M. M., Qiao, X., & Ahmad, H. (2013). Spectral analysis of bent fiber Bragg gratings: theory and experiment. *Optics letters*, *38*(21), 4409-4412.

Limberger, H. G., Fonjallaz, P. Y., Lambelet, P., Salathe, R. P., Zimmer, C., & Gilgen, H. H. (1993, December). Optical low-coherence reflectometry (OLCR) characterization of efficient Bragg gratings in optical fiber. In *Optics Quebec* (pp. 272-283). International Society for Optics and Photonics.

Limberger, H. G., Fonjallaz, P. Y., Salathé, R. P., & Cochet, F. (1996). Compaction-and photoelastic-induced index changes in fiber Bragg gratings.*Applied Physics Letters*, *68*(22), 3069-3071.

Lindner, E., Chojetzki, C., Brückner, S., Becker, M., Rothhardt, M., & Bartelt, H. (2009). Thermal regeneration of fiber Bragg gratings in photosensitive fibers. *Optics express*, *17*(15), 12523-12531.

Long, X. C., & Brueck, S. R. J. (1999a). Composition dependence of the photoinduced refractive-index change in lead silicate glasses. *Optics letters*, *24*(16), 1136-1138.

Long, X. C., & Brueck, S. R. J. (1999b). Large photosensitivity in lead–silicate glasses. *Applied physics letters*, *74*(15), 2110-2112.

LuValle, M. J., Copeland, L. R., Kannan, S., Judkins, J. B., & Lemaire, P. J. (1998). A strategy for extrapolation in accelerated testing. *Bell Labs technical journal*, *3*(3), 139-147.

Malo, B., Hill, K. O., Bilodeau, F., Johnson, D. C., & Albert, J. (1993). Point-by-point fabrication of micro-Bragg gratings in photosensitive fibre using single excimer pulse refractive index modification techniques. *Electronics Letters*, *29*(18), 1668-1669.

Marcuse, D. (1976). Curvature loss formula for optical fibers. *JOSA*, *66*(3), 216-220.

Markowski, K., Jedrzejewski, K., & Osuch, T. (2016). Numerical analysis of double chirp effect in tapered and linearly chirped fiber Bragg gratings. *Applied Optics*, *55*(17), 4505-4513.

Martin, J., Lauzon, J., Thibault, S., & Ouellette, F. (1994, February). Novel Writing Technique of Long and Highly Reflective In-fiber Bragg Gratings and Investigation of the Linearly Chirped Component. In *Optical Fiber Communication Conference* (p. PD29). Optical Society of America.

Matsuhara, M., & Hill, K. O. (1974). Optical-waveguide band-rejection filters: design. *Applied Optics*, *13*(12), 2886-2888.

Medvedkov, O. I., Vasiliev, S. A., Gnusin, P. I., & Dianov, E. M. (2012). Photosensitivity of optical fibers with extremely high germanium concentration. *Optical Materials Express*, *2*(11), 1478-1489.

Meltz, G., & Morey, W. W. (1991, December). Bragg grating formation and germanosilicate fiber photosensitivity. In *International Workshop on Photoinduced Self-Organization Effects in Op* (pp. 185-199). International Society for Optics and Photonics.

Meltz, G., Morey, W., & Glenn, W. H. (1989). Formation of Bragg gratings in optical fibers by a transverse holographic method. *Optics letters*, *14*(15), 823-825.

Mihailov, S. J., & Gower, M. C. (1994). Recording of efficient high-order Bragg reflectors in optical fibres by mask image projection and single pulse exposure with an excimer laser. *Electronics Letters-IEE, 30*(9), 707-707.

Mizuguchi, M., Skuja, L., Hosono, H., & Ogawa, T. (1999a). Photochemical processes induced by 157-nm light in H 2-impregnated glassy SiO 2: OH.*Optics letters*, *24*(13), 863-865.

Mizuguchi, M., Skuja, L., Hosono, H., & Ogawa, T. (1999b). F-doped and H-2-impregnated synthetic SiO2 glasses for 157 nm optics. *Journal of Vacuum Science & Technology B*, *17*(6), 3280-3284.

Morey, W. W., Dunphy, J. R., & Meltz, G. (1992, January). Multiplexing fiber Bragg grating sensors. In *Distributed and Multiplexed Fiber Optic Sensors*(pp. 216-224). International Society for Optics and Photonics.

Nand, A. (2007). *Intragrating sensing using chirped optical fibre Bragg gratings* (Doctoral Thesis, Victoria University, Australia). Retrieved from http://vuir.vu.edu.au/1499/1/Nand.pdf

Niay, P., Bernage, P., Legoubin, S., Douay, M., Xie, W. X., Bayon, J. F., ... & Poumellec, B. (1994). Behaviour of spectral transmissions of Bragg gratings written in germania-doped fibres: writing and erasing experiments using pulsed or cw uv exposure. *Optics Communications*, *113*(1), 176-192.

Nishii, J., Fukumi, K., Yamanaka, H., Kawamura, K. I., Hosono, H., & Kawazoe, H. (1995). Photochemical reactions in GeO 2-SiO 2 glasses induced by ultraviolet irradiation: comparison between Hg lamp and excimer laser. *Physical Review B*, *52*(3), 1661.

Ojovan, M. I. (2009). Viscosity and glass transition in amorphous oxides.*Advances in Condensed Matter Physics*, *2008*.

Othonos, A. (1997). Fiber bragg gratings. *Review of scientific instruments*,*68*(12), 4309-4341.

Othonos, A., & Kalli, K. (1999). *Fiber Bragg gratings: fundamentals and applications in telecommunications and sensing*. Artech House.

Othonos, A., & Lee, X. (1995). Novel and improved methods of writing Bragg gratings with phase-masks. *IEEE Photonics Technology Letters*, *7*(10), 1183-1185.

Othonos, A., Alavie, A. T., Melle, S., & Karr, S. E. (1993). Fiber Bragg grating laser sensor. *Optical Engineering*, *32*(11), 2841-2846.

Pal, S. (2006). Characterisation of thermal (in) stability and temperature-dependence of type-I and type-IIA Bragg gratings written in B–Ge co-doped fiber. *Optics communications*, *262*(1), 68-76.

Pal, S., Mandal, J., Sun, T., & Grattan, K. T. (2003). Analysis of thermal decay and prediction of operational lifetime for a type I boron-germanium codoped fiber Bragg grating. *Applied optics*, *42*(12), 2188-2197.

Pilla, P., Iadicicco, A., Contessa, L., Campopiano, S., Cusano, A., Cutolo, A., & Giordano, M. (2005, May). Long period gratings coated with syndiotactic polystirene as highly sensitive chemical sensors. In *Bruges, Belgium-Deadline Past* (pp. 483-486). International Society for Optics and Photonics.

Poignant, H., Bayon, J. F., Delevaque, E., Monerie, M., Mellot, J. L., Grot, D., ... & Douay, M. (1997, February). Influence of H 2 loading on the kinetics of Type IIA fibre Bragg grating photoinscription. In *Optical Fibre Gratings (Digest No. 1997/037), IEE Colloquium on* (pp. 2-1). IET.

Poumellec, B. (1998). Links between writing and erasure (or stability) of Bragg gratings in disordered media. *Journal of non-crystalline solids*, *239*(1), 108-115.

Poumellec, B., & Lancry, M. (2015). Kinetics of thermally activated physical processes in disordered media. *Fibers*, *3*(3), 206-252.

Prohaska, J. D., Snitzer, E., Rishton, S., & Boegli, V. (1993). Magnification of mask fabricated fibre Bragg gratings. *Electronics Letters*, *29*(18), 1614-1615.

Raine, K. W., Feced, R., Kanellopoulos, S. E., & Handerek, V. A. (1999). Measurement of axial stress at high spatial resolution in ultraviolet-exposed fibers. *Applied optics*, *38*(7), 1086-1095.

Ramecourt, D., Niay, P., Bernage, P., Riant, I., & Douay, M. (1999). Growth of strength of Bragg gratings written in H 2 loaded telecommunication fibre during cw UV post-exposure. *Electronics Letters*, *35*(4), 329-331.

Rathje, J., Kristensen, M., & Pedersen, J. E. (2000). Continuous anneal method for characterizing the thermal stability of ultraviolet Bragg gratings. *Journal of Applied Physics*, *88*(2), 1050-1055.

Razafimahatratra, D., Niay, P., Douay, M., Poumellec, B., & Riant, I. (2000). Comparison of isochronal and isothermal decays of Bragg gratings written through continuous-wave exposure of an unloaded germanosilicate fiber. *Applied optics*, *39*(12), 1924-1933.

Riant, I. (2002). UV-photoinduced fibre gratings for gain equalisation. *Optical Fiber Technology*, *8*(3), 171-194.

Rowe, C. J., Bennion, I., & Reid, D. C. J. (1987). High-reflectivity surface-relief gratings in single-mode optical fibres. *IEE Proceedings J-Optoelectronics*, *3*(134), 197-202.

Saito, K., & Ikushima, A. J. (2002). Effects of fluorine on structure, structural relaxation, and absorption edge in silica glass. *Journal of applied physics*, *91*(8), 4886-4890.

Salik, E., Starodubov, D. S., Grubsky, V., & Feinberg, J. (1999, February). Thermally stable gratings in optical fibers without temperature annealing. In*Optical Fiber Communication Conference* (p. ThD3). Optical Society of America.

Sang, X., Chu, P. L., Yu, C., & Lai, R. (2006). Growth dynamics of Bragg gratings in multimode optical fibre. *Optics communications*, *260*(1), 131-135.

Shen, Y., Xia, J., Sun, T., & Grattan, K. T. (2004). Photosensitive indium-doped germano-silica fiber for strong FBGs with high temperature sustainability. *IEEE Photonics Technology Letters*, *16*(5), 1319-1321.

Simmons, K. D., Griscom, D. L., LaRochelle, S., Mizrahi, V., & Stegeman, G. I. (1991). Correlation of defect centers with a wavelength-dependent photosensitive response in germania-doped silica optical fibers. *Optics letters*, *16*(3), 141-143.

Singh, N., Jain, S. C., & Aggarwal, A. K. (2002, February). Fabrication of In-Fiber Bragg Gratings using phase mask technique. In *National conference on Advances in contemporary physics and energy* (pp. 172-173).

Skuja, L. N., Trukhin, A. N., & Plaudis, A. E. (1984). Luminescence in Germanium-Doped Glassy SiO2. *physica status solidi (a)*, *84*(2), K153-K157.

Smietana, M., Korwin-Pawlowski, M. L., Bock, W. J., Pickrell, G. R., & Szmidt, J. (2008). Refractive index sensing of fiber optic long-period grating structures coated with a plasma deposited diamond-like carbon thin film.*Measurement Science and Technology*, *19*(8), 085301.

Starodubov, D. S., Grubsky, V., Feinberg, J., Kobrin, B., & Juma, S. (1997). Bragg grating fabrication in germanosilicate fibers by use of near-UV light: a new pathway for refractive-index changes. *Optics letters*, *22*(14), 1086-1088.

Stepanov, D. Y., Canning, J., & Brodzeli, Z. (1999, November). Real-time characterisation of fibre grating Fabry-Perots and phase-shifted gratings with 100 kHz resolution. In *Technical Digest-Symposium on Optical Fiber Measurements, 1998* (Vol. 930, p. 149). DIANE Publishing.

Stephens, T., Krug, P. A., Brodzeli, Z., Dhosi, G., Ouellette, F., & Poladian, L. (1996). 257 km transmission at 10 Gbit/s in non-dispersion-shifted fibre using an unchirped fibre Bragg grating dispersion compensator. *Electronics Letters*, *32*(17), 1599-1601.

Storøy, H., Engan, H. E., Sahlgren, B., & Stubbe, R. (1997). Position weighting of fiber Bragg gratings for bandpass filtering. *Optics letters*, *22*(11), 784-786.

Sugden, K., Bennion, I., Molony, A., & Copner, N. J. (1994). Chirped gratings produced in photosensitive optical fibres by fibre deformation during exposure. *Electronics letters*, *30*(5), 440-442.

Sun, J., Li, Y., & Liu, D. (2005). Widely tunable long-period fiber gratings with interpolymers as sensitivity-enhanced materials. *Optics communications*, *249*(1), 193-200.

Takahashi, M., Fujiwara, T., Kawachi, T., & Ikushima, A. J. (1997). Defect formation in GeO2-SiO2 glass by poling with ArF laser excitation. *Applied physics letters*, *71*, 993-995.

Thompson, A. C., Cadusch, P. J., Robertson, D. F., Stoddart, P. R., & Wade, S. A. (2012). Origins of spectral changes in fiber Bragg gratings due to macrobending. *Journal of Lightwave Technology*, *30*(22), 3500-3511.

Tomozawa, M., Kim, D. L., & Lou, V. (2001). Preparation of high purity, low water content fused silica glass. *Journal of non-crystalline solids*, *296*(1), 102-106.

Townsend, J. E., Poole, S. B., & Payne, D. (1987). Solution-doping technique for fabrication of rare-earth-doped optical fibres. *Electronics Letters*, *7*(23), 329-331.

Trpkovski, S., Kitcher, D. J., Baxter, G. W., Collins, S. F., & Wade, S. A. (2005). High-temperature-resistant chemical composition Bragg gratings in Er 3+-doped optical fiber. *Optics letters*, *30*(6), 607-609.

Tsai, T. E., Williams, G. M., & Friebele, E. J. (1998). Uniform component of index structure induced in Ge-SiO2 fibers by spatially modulated ultraviolet light. *Applied physics letters*, *72*(25), 3243-3245.

Vengsarkar, A. M., Lemaire, P. J., Judkins, J. B., Bhatia, V., Erdogan, T., & Sipe, J. E. (1996). Long-period fiber gratings as band-rejection filters. *Journal of lightwave technology*, *14*(1), 58-65.

Violakis, G., Limberger, H. G., Mashinsky, V. M., & Dianov, E. M. (2011). Fabrication and thermal decay of fiber Bragg gratings in pristine and H 2-loaded Bi-Al co-doped optical fibers. *Optics express*, *19*(26), B350-B356.

Wade, S. A., Robertson, D. F., Thompson, A. C., & Stoddart, P. R. (2011). Changes in spectral properties of fibre Bragg gratings owing to bending.*Electronics Letters*, *47*(9), 558-559.

Wang, T., Shao, L. Y., Canning, J., & Cook, K. (2013). Regeneration of fiber Bragg gratings under strain. *Applied optics*, *52*(10), 2080-2085.

Wang, Y., Phillips, L., Yelleswarapu, C., George, T., Sharma, A., Burgett, S., & Ruffin, P. (1999). Enhanced growth rate for Bragg grating formation in optical fibers with titania-doped outer cladding. *Optics communications*, *163*(4), 185-188.

Williams, D. L., & Smith, R. P. (1995). Accelerated lifetime tests on UV written intra-core gratings in boron germania codoped silica fibre. *Electronics Letters*, *31*(24), 2120-2121.

Williams, D. L., Ainslie, B. J., Armitage, J. R., Kashyap, R., & Campbell, R. (1993). Enhanced UV photosensitivity in boron codoped germanosilicate fibres. *Electronics Letters*, *29*(1), 45-47.

Williams, D. L., Davey, S. T., Kashyap, R., Armitage, J. R., & Ainslie, B. J. (1992). Direct observation of UV induced bleaching of 240 nm absorption band in photosensitive germanosilicate glass fibres. *Electronics Letters*, *28*, 369-371.

Wong, D., Poole, S. B., & Sceats, M. G. (1992). Stress-birefringence reduction in elliptical-core fibers under ultraviolet irradiation. *Optics letters*, *17*(24), 1773-1775.

Xie, W. X., Niay, P., Bernage, P., Douay, M., Bayon, J. F., Georges, T., ... & Poumellec, B. (1993). Experimental evidence of two types of photorefractive effects occuring during photoinscriptions of Bragg gratings within germanosilicate fibres. *Optics communications*, *104*(1-3), 185-195.

Yablon, A. D. (2004). Optical and mechanical effects of frozen-in stresses and strains in optical fibers. *IEEE Journal of Selected Topics in Quantum Electronics*, *10*(2), 300-311.

Yablon, A. D., Yan, M. F., Wisk, P., DiMarcello, F. V., Fleming, J. W., Reed, W. A., ... & Lines, M. E. (2003, March). Anomalous refractive index changes in optical fibers resulting from frozen-in viscoelastic strain. In *Optical Fiber Communication Conference* (p. PD06). Optical Society of America.

Yang, H. Z., Qiao, X. G., Das, S., & Paul, M. C. (2014). Thermal regenerated grating operation at temperatures up to 1400° C using new class of multimaterial glass-based photosensitive fiber. *Optics letters*, *39*(22), 6438-6441.

Yariv, A. (1973). Coupled-mode theory for guided-wave optics. *IEEE Journal of Quantum Electronics*, *9*(9), 919-933.

Yoffe, G. W., Krug, P. A., Ouellette, F., & Thorncraft, D. A. (1995). Passive temperature-compensating package for optical fiber gratings. *Applied Optics*, *34*(30), 6859-6861.

Zhang, B., & Kahrizi, M. (2007). High-temperature resistance fiber Bragg grating temperature sensor fabrication. *IEEE Sensors Journal*, *7*(4), 586-591.

Zhang, J., Herman, P. R., Lauer, C., Chen, K. P., & Wei, X. M. (2001, June). 157-nm laser-induced modification of fused-silica glasses. In *Photonics West 2001-LASE* (pp. 125-132). International Society for Optics and Photonics.

LIST OF PUBLICATIONS AND PAPERS PRESENTED

Thesis related publications by the author

1. Lim, K. S., **Gunawardena, D. S.,** Lai, M. H., Islam, M. R., Yang, H. Z., Qiao, X., ... & Ahmad, H. (2015). Characterization of phasemask interference visibility and the evolution of grating visibility during grating formation. *Measurement*, *64*, 163-167.

2. **Gunawardena, D. S.,** Lai, M. H., Lim, K. S., Ali, M. M., & Ahmad, H. (2015). Measurement of grating visibility of a fiber Bragg grating based on bent-spectral analysis. *Applied optics*, *54*(5), 1146-1151.

3. **Gunawardena, D. S.,** Mat-Sharif, K. A., Tamchek, N., Lai, M. H., Omar, N. Y., Emami, S. D., ... & Ahmad, H. (2015). Photosensitivity of gallium-doped silica core fiber to 193 nm ArF excimer laser. *Applied optics*, *54*(17), 5508-5512.

4. **Gunawardena, D. S.,** Mat-Sharif, K. A., Lai, M. H., Lim, K. S., Tamchek, N., Omar, N. Y., ... & Ahmad, H. (2016). Thermal Activation of Regenerated Grating in Hydrogenated Gallosilicate Fiber. *IEEE Sensors Journal*, *16*(6), 1659-1664.

5. **Gunawardena, D. S.,** Lai, M. H., Lim, K. S., Malekmohammadi, A., & Ahmad, H. (2016). Fabrication of thermal enduring FBG sensor based on thermal induced reversible effect. *Sensors and Actuators A: Physical*, *242*, 111-115.

6. **Gunawardena, D. S.,** Lai, M. H., Lim, K. S., & Ahmad, H. (2016). Impact of CO_2 Laser Pre-treatment on the Thermal Endurance of Bragg Gratings. *Journal of Optical Society Korea*, *20*(5), 575-578.

7. **Gunawardena, D. S.,** Lai, M. H., Lim, K. S., & Ahmad, H. (2016). Thermal Decay Analysis of Fiber Bragg Gratings using Demarcation Energy Approximation. *Optical Fiber Technology*, (Under Review).

Conference/Colloquium/Seminar contributions by the author

1. **Gunawardena, D. S.,** Lai, M. H., Lim, K. S., & Ahmad, H. (2015, February). Enhanced Photosensitivity in 248nm KrF and 193nm ArF Excimer Laser Irradiated Germanosilicate Fiber. In *International Conference on Technological Advances in Electrical, Electronics and Computer Engineering (ICTAEECE)*, Kuala Lumpur, Malaysia.

2. **Gunawardena, D. S.,** Lai, M. H., Lim, K. S., & Ahmad, H. (2015, November). Analysis of Thermal Decay Characteristics of UV-induced FBGs Pre-treated with CO_2 Laser. In *International OSA Network of Students Conference on Optics, Atoms and Laser Applications (IONS KOALA)*, Auckland, New Zealand.

3. **Gunawardena, D. S.,** (2016, April). Photosensitivity Enhancement and Characterising Grating Strength of Fiber Bragg Gratings. In *Finding Research Seminar*, Institute of Graduate Studies, University of Malaya, Kuala Lumpur, Malaysia.

4. **Gunawardena, D. S.,** (2016, March). Discovery of an Optical Fiber Sensor Durable for a 1000 Years. In *University of Malaya Three Minute Thesis Competition (UM3MT)*, University of Malaya, Kuala Lumpur, Malaysia.

5. **Gunawardena, D. S.,** (2016, March). Photosensitivity Enhancement and Characterising Grating Strength of Fiber Bragg Gratings. In *Candidature Defence Seminar*, Institute of Graduate Studies, University of Malaya, Kuala Lumpur, Malaysia.

6. **Gunawardena, D. S.,** (2015, February). Photosensitivity and Characterising Grating Strength of Fiber Bragg Gratings. In *Proposal Defence Seminar*, Institute of Graduate Studies, University of Malaya, Kuala Lumpur, Malaysia.

7. **Gunawardena, D. S.,** Lim, K. S., & Ahmad, H. (2015, June). Grating Visibility Measurement of a Fiber Bragg Grating using Bent Spectral Analysis. In *Annual physics colloquium*, University of Malaya, Kuala Lumpur, Malaysia.

8. Lai, M. H., **Gunawardena, D. S.,** Lim, K. S., & Ahmad, H. (2015, December). Cooling-Rate Induced Fiber Birefringence Variation in Regenerated High Birefringent Fiber. In 18^{th} *International Conference on Photonics (ICP 2015)*, Penang, Malaysia.

9. Lim, K. S., Lai, M. H., **Gunawardena, D. S.,** & Ahmad, H. (2015, November). Fabrication of regenerated grating using carbon dioxide laser. In *Workshop on Specialty Optical Fibers and their Applications*, Hong Kong (pp. WF4A-5). Optical Society of America.

Other related publications by the author during the candidature

1. Islam, M. R., **Gunawardena, D. S.,** Lee, Y. S., Lim, K. S., Yang, H. Z., & Ahmad, H. (2016). Fabrication and characterization of laser-ablated cladding resonances of two different-diameter photosensitive optical fibers. *Sensors and Actuators A: Physical*, *243*, 111-116.

2. Lai, M. H., **Gunawardena, D. S.,** Lim, K. S., Machavaram, V. R., Lee, S. H., Chong, W. Y., ... & Ahmad, H. (2016). Thermal activation of regenerated fiber Bragg grating in few mode fibers. *Optical Fiber Technology*, *28*, 7-10.

3. Lai, M. H., **Gunawardena, D. S.,** Lim, K. S., Yang, H. Z., & Ahmad, H. (2015). Observation of grating regeneration by direct CO_2 laser annealing. *Optics express*, *23*(1), 452-463.

4. Nazal, N. A. M., **Gunawardena, D. S.,** Zaini, M. K. A., Lim, K. S., Chong, W. Y., & Ahmad, H. (2016). Thermal properties of regenerated gratings in optical fibers of different core size. *Applied Optics*, (Under Review).

5. Lai, M. H., Lim, K. S., **Gunawardena, D. S.,** Lee, Y. S., & Ahmad, H. (2016). Review of CO2 laser applications in optical fiber components fabrication and treatment. *Infrared Physics and Technology*, (Under Review).

6. Lai, M. H., Lim, K. S., **Gunawardena, D. S.,** Yang, H. Z., Chong, W. Y., & Ahmad, H. (2015). Thermal stress modification in regenerated fiber Bragg grating via manipulation of glass transition temperature based on CO_2-laser annealing. *Optics letters*, *40*(5), 748-751.

7. Ali, M. M., Islam, R., Lim, K. S., **Gunawardena, D. S.,** Yang, H. Z., & Ahmad, H. (2015). PCF-Cavity FBG Fabry-Perot Resonator for Simultaneous Measurement of Pressure and Temperature. *IEEE Sensors Journal*, *15*(12), 6921-6925.

8. Lai, M. H., Lim, K. S., Islam, M. R., **Gunawardena, D. S.,** Yang, H. Z., & Ahmad, H. (2015). Effect of CO 2 Laser Annealing on Stress Applying Parts Contributing Toward Birefringence Modification in Regenerated Grating in Polarization Maintaining Fiber. *IEEE Photonics Journal*, *7*(5), 1-9.

9. Islam, M. R., Ali, M. M., Lai, M. H., Lim, K. S., **Gunawardena, D. S.,** Machavaram, V. R., & Ahmad, H. (2015). Wide-range in-fibre Fabry-Perot resonator for ultrasonic sensing. *IET Optoelectronics*, *9*(3), 136-140.

10. Yang, H. Z., Ali, M. M., Islam, M. R., Lim, K. S., **Gunawardena, D. S.,** & Ahmad, H. (2015). Cladless few mode fiber grating sensor for simultaneous refractive index and temperature measurement. *Sensors and Actuators A: Physical*, *228*, 62-68.

11. Liu, H., Yang, H. Z., Qiao, X. G., Hu, M. L., Feng, Z. Y., Wang, R., Rong, Q., **Gunawardena, D. S.,** Lim, K. S., & Ahmad, H. (2016). Strain measurement at high temperature environment based on Fabry-Perot interferometer cascaded fiber

regeneration grating. *Sensors and Actuator A: Physical*, *Sensors and Actuator A: Physical*, *248*, 199-205.

12. Yang, H. Z., Liu, H., Wang, Y., Qiao, X. G., Su, D., Li, L., Lim, K. S., **Gunawardena, D. S.,** & Ahmad, H. (2016). Strain measurement at temperatures up to 800 ˚C using regenerated gratings produced in the high Ge doped and B/Ge co-doped fibers. *IEEE Sensors Journal*, (Under Review).

Author's awards and honours during the candidature

1. **1st Runner Up** (Faculty Level) at the **3 minute thesis competition (UM3MT)** organised by the University of Malaya, Kuala Lumpur, Malaysia, 2016.

2. Awarded with a **conference travel grant** to attend International OSA Network of Students Conference on Optics, Atoms and Laser Applications **(IONS KOALA), Auckland, New Zealand**, 2015.

3. **Excellent paper award for the best presentation** at the 10th international conference on Technological Advances in Electrical, Electronics and Computer Engineering **(ICTAEECE)**, The International Institute of Engineers and Researchers, Kuala Lumpur, Malaysia, 2015.

4. Awarded with a **conference travel grant** to attend 10th international conference on Technological Advances in Electrical, Electronics and Computer Engineering **(ICTAEECE)**, The International Institute of Engineers and Researchers, Kuala Lumpur, Malaysia, 2015.

5. Selected for the **5th Summer School on Lasers and Laser Applications (SSOLLA 2014)** organised for young scientists from Asia by the Advanced Photonics Research Institute (APRI), Gwangju Institute of Science and Technology, **Gwangju, South Korea**, 2014.

6. Awarded with **IPPP grant** by University of Malaya to conduct Ph.D. research under the grant no. **PG004-2014A**.

7. Completely funded **Bright Sparks Scholarship** to conduct research throughout the Ph.D. candidature (2013-2016) at University of Malaya, Kuala Lumpur, Malaysia.